1999

Computational Approach for Determination of the Hydraulic Conductivity of Soils Using Continuous Intrusion Piezocone Penetration Test.

Chung Rak Song
Louisiana State University and Agricultural & Mechanical College

INFORMATION TO USERS

This manuscript has been reproduced from the microfilm master. UMI films the text directly from the original or copy submitted. Thus, some thesis and dissertation copies are in typewriter face, while others may be from any type of computer printer.

The quality of this reproduction is dependent upon the quality of the copy submitted. Broken or indistinct print, colored or poor quality illustrations and photographs, print bleedthrough, substandard margins, and improper alignment can adversely affect reproduction.

In the unlikely event that the author did not send UMI a complete manuscript and there are missing pages, these will be noted. Also, if unauthorized copyright material had to be removed, a note will indicate the deletion.

Oversize materials (e.g., maps, drawings, charts) are reproduced by sectioning the original, beginning at the upper left-hand corner and continuing from left to right in equal sections with small overlaps.

Photographs included in the original manuscript have been reproduced xerographically in this copy. Higher quality 6" x 9" black and white photographic prints are available for any photographs or illustrations appearing in this copy for an additional charge. Contact UMI directly to order.

Bell & Howell Information and Learning
300 North Zeeb Road, Ann Arbor, MI 48106-1346 USA
800-521-0600

COMPUTATIONAL APPROACH FOR DETERMINATION OF THE HYDRAULIC CONDUCTIVITY OF SOILS USING CONTINUOUS INTRUSION PIEZOCONE PENETRATION TEST

A Dissertation

Submitted to the Graduate Faculty of the
Louisiana State University and
Agricultural and Mechanical College
in partial fulfillment of the
requirements for the degree of
Doctor of Philosophy

in

The Department of Civil and Environmental Engineering

by

Chung Rak Song
B.S., Yonsei University, Korea, 1984
M.S., The University of Texas at Austin, 1986
December, 1999

UMI Number: 9960099

UMI Microform 9960099

Bell & Howell Information and Learning Company
300 North Zeeb Road
P.O. Box 1346
Ann Arbor, MI 48106-1346

Errata (June, 29, 2010)

p.1, end of line 9, The following should be added.

The development history of PCPT is well addressed by Kurup (1993) as follows.

P.1, beginning of line 10, " should be inserted.

P.1, end of line 19, " should be inserted.

p.11, line 1, "Levadous" should be corrected to "Levadoux".

P.11, line 5, "below" should be corrected to "below as addressed by Kurup (1993) and Abu-Farsakh (1998)"

p.31, line 3, "over consolidated" should be corrected to "overconsolidated".

p.32, line 4, "pressures" should be corrected to "pressure"

p.75, before line 5, the following sentence should be inserted.

Numerical formulation and FEM implementation are similar to Abu-Farsakh (1998) but modified to reflect AMCCM.

p.94, line 5, The following should be added.

The fundamental experimental procedure (Laboratory Experiments and Calibration Chamber Tests) is transferred from Kurup (1993) and de Lima (1990).

P.95, The title of Table 4.1.2 must be changed to "Fundamental properties of soil mixtures (Kurup, 1993)"

p.100, between line 2 and 3, the following should be added.

The fundamental procedure for sample preparation, slurry (re)consolidation, saturation process and general penetration is the same as that shown in Kurup (1993) and de Lima (1990), but quoted here for completeness.

p.113, line 14, "results" should be corrected to "result".

ACKNOWLEDGEMENTS

I would like to acknowledge my advisor Dr. George Z. Voyiadjis for his scientific guidance and friendship during the course of my work. I enjoyed his numerous discussions on the constitutive modeling of the material behavior and the microstructures. I also wish to express my sincere appreciation and gratitude to co-advisor Professor Mehmet T. Tumay, for his guidance and continued encouragement during this research. I also would like to thank my examining committee, Drs. Ernest Heymsfield, Robert Dorroh, and Andrzej Wojtanowicz for giving time and effort to this endeavor.

I would like to acknowledge the financial support provided to me through the Boyd Professorship of Dr. Voyiadjis, and the Department of Civil and Environmental Engineering. I also acknowledge the CALCHAS facilities provided for my experimental work through the Louisiana Transportation Research Center at LSU.

This work is also indebted to many good persons. Special thanks go to Dr. Soo Il Kim of Yonsei University, Korea, and Mr. Han Ki Shin of Baytech Korea for never ending encouragement and support. My appreciation also goes to Dr. M. Abu-Farsakh, Mr. D.K. Kim, Mr. B.S. Lim, and Dr. B. Deliktas for their help and good humor during this research

I would like to thanks to my parents Mr. Chong C. Song and Mrs Cho S. Song for their warm love and support. Lastly, I wish to express my deep appreciation to my wife Kyung, and my two sons Dong Hee and Dong Kwan, for their patience, support and love throughout this work. Their presence by my side has been a great joy. I dedicate this work to my wife, my two sons, and my parents.

TABLE OF CONTENTS

LIST OF TABLES

LIST OF FIGURES

ABSTRACT

In order to obtain the hydraulic conductivity or the coefficient of consolidation of the soil from PCPT, the pore pressure response during dissipation test is typically used. This method, however, requires the intermittent stopping of the advancement of the piezocone penetrometer for the dissipation test. Also, this method does not fully take into account the pore pressure interaction between near and far fields as pointed out by previous researchers (Kurup and Tumay, 1997).

Thus a new rational approach is investigated here. The proposed method utilizes the pore water pressure during the penetration of the piezocone penetrometer. By its nature, the pore pressure response around the cone tip is neither a fully drained nor a fully undrained condition, it is in between. Since this is a partially drained condition, the excess pore pressure during the piezocone penetration is the function of the hydraulic conductivity of the soil as well as the function of stress strain parameters. Inversely, the hydraulic conductivity of the soil can be predicted from the measured pore pressure response during piezocone penetration test.

In this study, an anisotropic modified Cam Clay model with micro-mechanical consideration is derived and incorporated with coupled theory of mixtures for large strains. The derived model is used to predict the hydraulic conductivity of the soil from the excess pore pressure generated during the piezocone penetration test. Updated Lagrangian reference frame is used for a more rational modeling of large strain behavior. Formulation of the equations is based on the theory of mixtures for inelastic porous media proposed by Prevost (1980) and in an updated Lagrangian reference frame by Voyiadjis and Abu-Farsakh (1997).

Model evaluation was conducted by comparing the results with the isotropic model. Comparisons were also made with the field data. The calibration chamber test results, existing field data, and the theoretically predicted results showed acceptable agreement with each other, and shed the promising light on the new method of determination of the hydraulic conductivity of soils from the continuous intrusion piezocone penetration test.

CHAPTER 1. INTRODUCTION

The piezocone penetrometer is becoming an important in situ soil investigation tool of choice for real time characterization and assessment of in situ states and soil properties. The piezocone penetration test (PCPT) provides continuous soil profiles, that are reliable, fast and economical and may be used in conjunction, supplementing conventional laboratory tests in order to obtain the engineering soil parameters. In recent years, it is being widely used for site exploration; construction control and assessment of ground improvement effectiveness; assessment of contaminant transport in geomaterials; and for direct correlation in the design of shallow and deep foundations.

Measurements of pore water pressures generated while advancing a probe into the ground, and their subsequent dissipation were first made in the early 1970's. No simultaneous measurements of cone resistance and sleeve friction were feasible at that time. In 1969-73, the Norwegian Institute of Technology used a piezometric probe that could measure only the pore pressures; it was necessary to carry out separate cone penetration tests (CPT) in order to combine the measurements of pore pressure and cone resistance. Subsequent developments in transducer technology during the early 1970's involved the incorporation of piezometric elements to the standard electric cone penetrometers which made it possible the simultaneous measurements of pore pressures, cone resistance, and sleeve friction (Tumay et al., 1981). The determination of coefficient of consolidation and hydraulic conductivity from PCPT utilizes the pore

pressure dissipation test data which were obtained during the stopping period of the Piezocone (Acar et el., 1982; Tumay and Acar, 1985.

However, this method has two major explicit drawbacks such that the required time for dissipation test is substantially long and the continuous hydraulic conductivity profile is impossible.

Typically, it takes several hours (including idling time) for one dissipation test. Without the dissipation test, the whole procedure for one piezocone penetration test takes 1.5 to 2 hours for a 30 m penetration. Thus, in fact, the dissipation test largely decreases the efficiency of the piezocone penetration test.

Also, because of the prolonged required time for the dissipation test, only a limited number of dissipation tests can be carried out. Thus, continuous hydraulic conductivity profiles cannot be obtained, even though other profiles (cone resistance, friction resistance, etc.) are practically continuous.

This research presents the new method of determining the hydraulic conductivity of soils utilizing the coupled theory of soil-water mixtures; which does not require the dissipation test; hence, does not require additional test time but provides a continuous hydraulic conductivity profile.

It is argued that the piezocone obtained hydraulic conductivity is for the disturbed condition, and not for the intact condition (Lunne et al., 1998). Thus, it is believed that the change of the soil structure may affect the hydraulic conductivity. The previous researches (Baligh and Levadoux, 1986; Robertson et al.; 1992), however, showed reasonable agreement between the laboratory test results and the

piezocone dissipation test results. Attempts such as freezing or solidifying the soils around the penetrating piezocone are considered but are not practical so far.

1.1 Historical Review

Crude types of penetrometers were introduced as early as the Roman era; at that time, the number of slaves required to push the rod into the ground was counted and used to quantify the strength of the ground. With the advent of modern science, this method was diversified and several kinds of penetrometers were developed, such as the cone penetrometer, the standard penetrometer, the Swedish penetrometer, etc. Among these penetrometers, the cone penetrometer was acknowledged as the most widely used penetrometer due to its superior capability (repeatability, convenience, economics and etc.).

A modern type of cone penetrometer was first introduced in the early 20^{th} century in European countries and it is called the mechanical cone penetrometer. Mechanical cone penetrometer pushed the cone into the ground by a mechanical driving system (chain + gear system), and measured the end resistance by the probing rings. Later a cone penetrometer that could measure both end bearing and friction simultaneously appeared, and it was called mantle cone penetrometer. Holland contributed a lot to the development of the modern cone penetrometer. It is probably, the country that used the cone penetrometer most widely in the earlier days. The name of the "Dutch Cone" is almost an international standard of the mechanical cone penetrometer. The mechanical cone penetrometer was not equipped with the modern sensors and automatic driving systems, but presented more consistent and more reliable results with less cost compared to its strong cousin SPT (Standard Penetration

Test): thus, it continued the evolution. Traditional mechanical cone penetrometers use the double rod system – inner rods and outer rods. The measurement was carried out by pushing the inner rods for resistance measurements, and subsequently by pushing the outer rods for the advancement of the whole system. Thus, the test procedure was not continuous, it was stop and go process.

With the aid of the modern sensors and electric technology, the electric cone penetrometer was introduced in 1970's (Torstensson, 1975), which resulted in the greatly increased productivity and overall performance. The electric cone penetrometer utilized the load cells and motorized driving system instead of the probing rings and manual driving system; thus, the reading could be done electronically without stopping the penetration process. The penetration speed could be also controlled more accurately.

The piezocone is a type of electric cone penetrometer, which has pore pressure monitoring capability to enhance the assessment of engineering parameters, especially the hydraulic properties of the soils. Measurement of the pore water pressure generated while advancing a cone tip into the ground, and its subsequent dissipation when the penetration is stopped was first made in Sweden in the early 1970's (Wissa et al., 1975; Torstensson, 1975). Early type of piezocone penetrometer did not have the capability of simultaneous measurement of cone resistance (end bearing and/or friction) and pore pressure. Subsequent developments in transducer technology during the early 1980's involved the incorporation of piezometric elements into the standard electric cone penetrometers. This made it possible to measure the pore pressures, cone resistance and skin friction simultaneously. Tumay et al.(1981) is known as the first

group who utilized the simultaneous measurement of cone resistance and pore pressure (Zuidberg et al., 1982). Later, many researchers contributed the valuable application of the simultaneous measurement of cone resistance and pore pressure (Baligh et al., 1981; Campenalla and Robertson, 1981; Muromachi, 1981; de Ruiter, 1981; Zuidberg et al., 1982; Smiths, 1982; Lunne et al., 1997), and opened the era for the fully equipped piezocone penetrometer.

Currently, many other sensors can be attatched to the cone probe at the same time in order to obtain the various soil properties. Accelerometers can be attatched to detect the seismic response of soils (Campanella, 1994). Electric resistivity sensors, thermal sensors or infrared sensors can be attatched to detect the ground contamination. A microphone may be also attatched to detect the sonic response of ground, while the radioactive sensors can be attatched to detect the radioactive materials in the ground (Muromachi, 1981; Lunne et al., 1997). Virtually any kind of sensors can be incorporated with the modern cone penetrometers. For geotechnical purposes, the most widely used combination is the two load cells for the end bearing and the side friction, one piezometer for pore pressure response, and one inclination sensor for the inclination check. All of these sensors are electronic sensors, and an industrial-computer based electronic readout is used, so most of the measured response is recorded and analyzed with real-time basis. In fact, many of the modern piezocone manufacturers also supply the real-time measuring readout and analysis software.

Recently, there are several efforts to increase the efficiency of the PCPT even further by mechanical improvement. Tumay et al. (1998) and Tumay and Kurup

(1999) developed the spiral rod for continuous advancing of the cone tip, which does not require the connection of the pushing rod. The Envi. Corp. (1996) developed the wireless piezocone penetrometer, which does not require the hassle of wiring during PCPT. Mayne (1996) developed the combination of pressure meter and cone penetrometer for the simultaneous tests of the pressure meter and cone penetrometer.

1.2 Determination of Hydraulic Conductivity or Coefficient of Consolidation

Along with the significant evolution of mechanics of PCPT, there were also, great achievements in the analysis method for the PCPT results. However, many of these works were concentrated on the interpretation of stress-strain properties of soils. From the view of utilization of the penetration pore pressure response, most of the efforts were focused on the correction of the end bearing and side friction, or soil classification purpose. Relatively fewer efforts were focused on the direct interpretation of penetration pore pressure response itself. In fact, even these efforts aimed at the analysis of the pore pressure dissipation data, and not at the analysis of the penetration pore pressure in order to obtain the hydraulic properties. Thus, in spite of the highly modernized and speedy features of the piezocone penetrometer, the determination of the hydraulic conductivity was not adequately modernized and was not speedy enough. This may be partly from the fact that most of the research was concentrated on the stress-strain behavior of the PCPT and(or) partly from the fact that the initial research on hydraulic conductivity started with a rather simpler method – the so called dissipation test or holding test method. Dissipation test method utilizes the pore pressure dissipation test results, which were obtained during the stopping (or

arresting) period of the piezocone. Even today, numerous research is conducted using this method. However, this method has two major explicit drawbacks as follows.

a. Required time for dissipation test is long: Typically, it takes more than 1 hour for the hydraulic conductivity test at one point. Without the dissipation test, the whole procedure for one piezocone penetration test takes 1.5 to 2 hours for a 30 m penetration. Thus the dissipation test largely decreases the efficiency of the piezocone penetration test.

b. Continuous hydraulic conductivity profile is impossible: Because of the prolonged required time for the dissipation test, only a limited number of dissipation tests can be carried out. Thus, continuous hydraulic conductivity profiles cannot be obtained, even though other profiles (cone resistance, friction resistance, etc.) are practically continuous.

The research presented in this work introduces a new method in order to determine the hydraulic conductivity of soils. It is based on the coupled equations of soil-water mixture (which does not require the dissipation test; hence, does not require additional test time) and provides a continuous hydraulic conductivity profile. The main idea of this research is using the back calculation method to determine the hydraulic conductivity of soils from the measured pore pressure data at the cone tip. In other words, the measured pore pressure will be used as an input data, and the hydraulic conductivity will be computed as an output.

The Chapters of this dissertation are organized as follows for easy understanding. Chapter one is the introduction of the proposed method. Chapter two is the literature review. Chapter three is the theoretical derivation of the anisotropic model with micro-mechanical considerations. Chapter four is the experimental procedure. Chapter five is the presentation of the theoretical and experimental results and discussions. Chapter six is the conclusions and the recommendations for future study.

CHAPTER 2. LITERATURE REVIEW

2.1 Overview

Along with the improvements of the hardware technology of PCPT, there were also considerable improvements in the analysis methods. Baligh et al. (1980), Lunne and Kleven (1981), Robertson et al.(1986), Lunne et al. (1985) developed the method to estimate the undrained shear strength from PCPT. Senneset and Janbu (1984), Jones and Rust (1982), Robertson et al. (1986) developed the soil classification systems. Vesic (1972), Battaglio et al. (1981), Randolph and Wroth (1979), Henkel and Wade (1966), Massarch and Broms (1981), Campanella et al. (1985) developed the relationship between the pore pressure (Δu) and the undrained shear strength based on the cavity expansion theory. Sandven et al (1988), Konrad and Law (1987), Sully et al (1988), and Mayne (1994) developed a method to obtain the pre-consolidation pressure from PCPT. Torstensson (1975, 1977), Randolph and Wroth (1979), Baligh and Levadoux (1980), Acar et al. (1982), Tumay and Acar (1985), Gupta and Davidson (1986) computed the coefficient of consolidation from the pore pressure dissipation data of PCPT. Zhang and Tumay (1999) developed the unique FUZZY approach for the soil classification.

Attempts have been made in recent years to develop analytical models for simulating the complex problem of the cone penetration process. Most solutions consider fully undrained or fully drained conditions, though the real conditions could be somewhere between the two extreme cases.

The consolidation of clayey soils around the advancing cone tip is essentially a large strain problem. Advanced one-dimensional consolidation theories incorporating

the finite strain, change of hydraulic conductivity and compressibility characteristics were developed by Gibson et al. (1967, 1981), and Schiffman (1980). Carter et al. (1977, 1979) and Prevost (1980, 1981) extended these theories to incorporate the elasto-plastic soil behavior and the finite strains in 3-D consolidation. Prevost (1980) developed a general theory for porous media based on the concepts of theory of mixtures. Voyiadjis and Abu-Farsakh (1997) and Abu-Farsakh et al. (1998) used the theory of mixtures and the effective stress concept in order to numerically simulate the cone penetrometer in clayey soils.

In the relatively earlier theories (Carter et al. and Prevost) the mathematical formulation has been formulated in the Eulerian coordinate frame using the Jauman stress rate. However, these theories limit the applicability of these methods to soils that do not exhibit kinematic hardening as was pointed out by Lee et al. (1983), Dafalias (1983), and Voyiadjis and Kattan (1989). Van der Berg (1993) suggested the use of ALE (Arbitrary Lagrangian Eulerian Coordinate) to improve this problem. Voyiadjis and Abu-Farsakh (1997) adopted the updated Lagrangian coordinate frame to avoid this problem and increase the accuracy.

In order to determine the hydraulic properties of soils from the PCPT by the traditional approach, the pore pressure dissipation method is used as follows.

2.2 Prediction of Initial Excess Pore Pressure and Subsequent Dissipation

The initial excess pore pressure distribution due to piezocone penetration in clay is an important factor affecting the interpretation of the coefficient of consolidation. Detailed parametric studies using different initial excess pore pressure distribution (constant, linear and logarithmic distribution) involving cylindrical and

spherical cavities have been performed by Levadous and Baligh (1980). Different methods have been also proposed based on cavity expansion theories, strain path method, finite element analysis, semi-empirical methods in order to predict the initial excess pore pressure distribution. The important features of these methods are given below.

2.2.1 Cavity Expansion Method

During the PCPT, some surface heave occurs at shallow depths of the penetration. At larger penetration depth, little surface heave is noticed and it has been argued that the soil moves predominantly outward. This has led to the modeling of the PCPT as a cylindrical cavity expansion process from zero radius to the radius of the cone penetrometer. The general form of soil movement at the penetrometer tip has been visualized as that due to the expansion of a spherical cavity from zero radius to an equivalent penetrometer radius 'r_o', (Torstensson, 1975, 1977). Theories for cylindrical and spherical cavity expansion in soils have been developed by Soderberg(1962), Ladanyi(1963), and Vesic (1972). These are one-dimensional models and do not take into account the two-dimensional nature of the penetration process. The method proposed by Torstensson assumes isotropic initial stress distribution, ideal elastic-perfectly plastic material, and undrained one-dimensional cavity expansion (cylindrical or spherical). It also neglects shear induced excess pore pressures and uses a linear, uncoupled finite difference scheme to analyze the pore pressure dissipation and consolidation.

The radius of the plastified zone (r_p) is given by:

Cylindrical cavity

$$r_p = r_o \sqrt{\frac{G}{s_u}} \qquad (2.2.1)$$

Spherical cavity

$$r_p = r_o \sqrt[3]{\frac{G}{s_u}} \qquad (2.2.2)$$

In equations (2.2.12) and (2.2.2) r_o = equivalent penetrometer radius, and G/s_u = I_r = rigidity index. The initial excess pore pressure distribution at any radius 'r' in the plastic zone is given by:

Cylindrical cavity

$$\Delta u_i = s_u \left[\ln \frac{G}{s_u} - 2 \ln \frac{r}{r_o} \right] \qquad (2.2.3)$$

Spherical cavity

$$\Delta u_i = 4 s_u \left[\frac{1}{3} \ln \frac{G}{s_u} - 2 \ln \frac{r}{r_o} \right] \qquad (2.2.4)$$

The initial excess pore pressure in the elastic zone is assumed to be zero. The following expression was suggested for the interpretation of the radial coefficient of consolidation:

$$c_r = \frac{T_{50} r_o^{\,2}}{t_{50}} \qquad (2.2.5)$$

In equation (2.2.5) T_{50} = time factor at 50% dissipation (given for both cylindrical and spherical solution), t_{50} = time for 50% dissipation, and r_o = equivalent penetrometer radius. The cylindrical cavity expansion model was considered to be applicable for filter elements located along the cylindrical shaft some distance away from the cone base. The spherical solution was considered to be more appropriate for

the filter elements located on the conical tip. For filter elements located just above the cone base, the interpretation is more complex especially in stiff overconsolidated soils because of large pore pressure gradients (and possible soil separation). The interpretation curve proposed by Torstensson for the cylindrical and spherical solutions are shown in Figure 2.2.1.

Closed form solutions developed by Randolph and Wroth (1979) and cavity expansion studies using work hardening elastoplastic soil models (Randolph, et al., 1979; Banerjee and Yousif, 1986, Chopra and Dargush, 1992) to analyze pile installation and subsequent consolidation may also be used to interpret PCPT results.

2.2.2 Strain Path Method (SPM)

The strain path method (Baligh, 1975, 1985) may be used to determine the initial excess pore pressure distribution during piezocone penetration. A linear, uncoupled or a nonlinear, coupled dissipation analysis can be performed. The determination of the initial excess pore pressure distribution using SPM (Levadoux and Baligh, 1980) is done in the following manner:

1. Predict soil velocities and strain rates using potential theory (for ideal compressible fluid flow) and a suitable distribution of sources and sinks to simulate the geometry of the cone.
2. The strain rates are integrated along streamlines to determine the strain path of the elements as they move past the cone.
3. Deviatoric stresses and shear-induced pore pressures are computed using a total stress soil model.
4. Determination of the excess pore pressures considering the equilibrium in the radial direction.

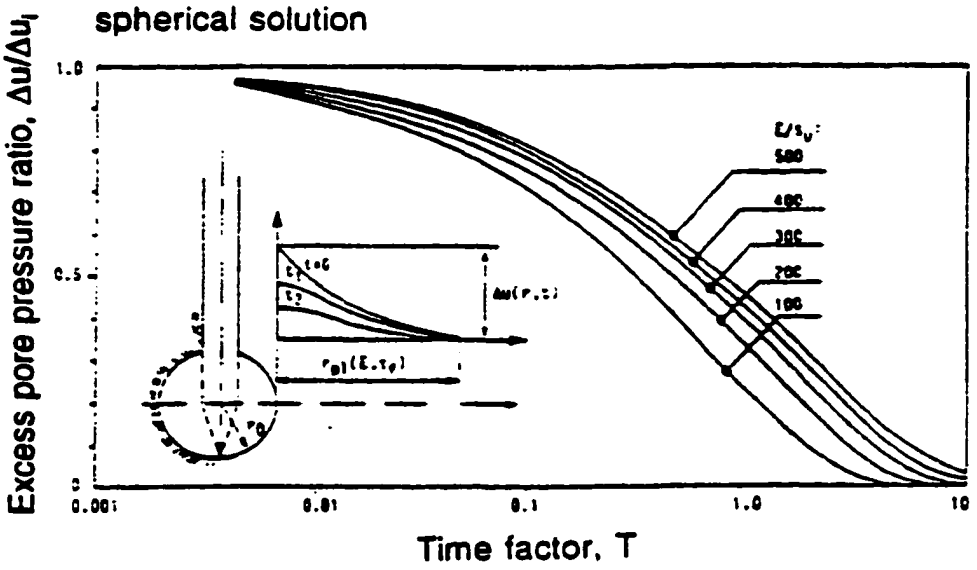

(a)

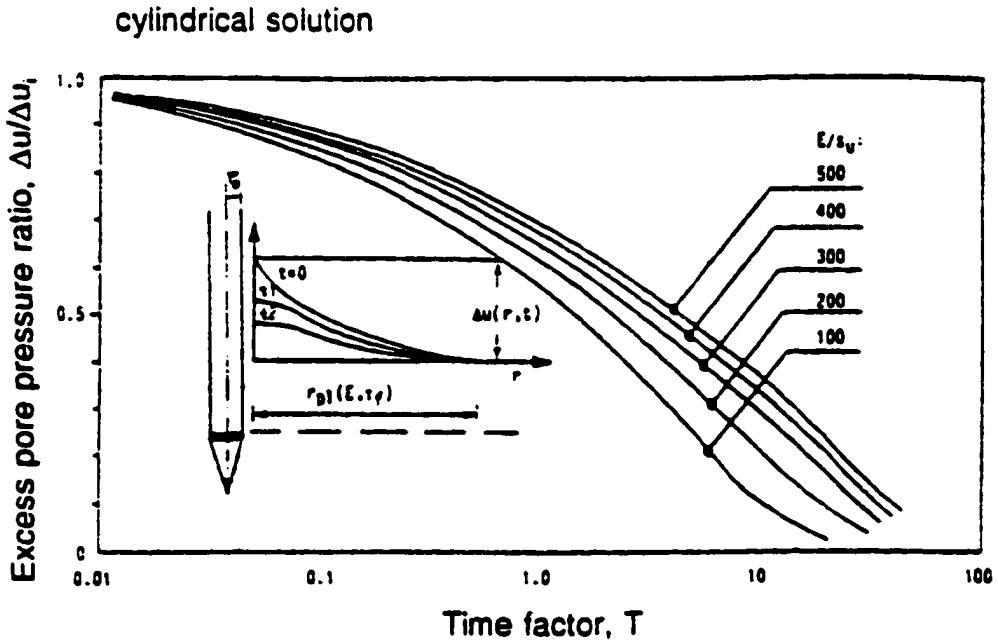

(b)

Figure 2.2.1, Time factors for Torstensson's model: (a) cylindrical solution; and (b) spherical solution

The SPM takes into account the two-dimensional aspect of the penetration phenomenon. Researchers studied the effects of stress-induced anisotropy, linear coupling, cone angle, filter element location and pore pressure measurement errors (Levadoux and Baligh, 1986). Excellent agreement was reported for the predicted normalized excess pore pressure distribution with the field measurements (Baligh and Levadoux, 1986). They also suggested that the initial normalized excess pore pressure distribution determined for Boston Blue Clay are reasonable applicable to other clays. The predicted values of time factor (Boston Blue Clay) for different cone angles, filter element location and degrees of consolidation is shown in Table 2.2.1.

The strain path method supplemented by a large strain finite element analysis was adopted by Houlsby and Teh (1988), Teh and Houlsby (1991) to analyze the PCPT in clays. Their method incorporated certain improvements over the previous methods suggested by Baligh and Levadoux (1986). Instead of attempting to reproduce and approximate penetrometer geometry by a combination of sources and sinks in a uniform field, the actual geometry of the penetrometer was included explicitly in the analysis.

An elastic-perfectly plastic material model of the von Mises type was used. The initial stress condition was obtained using the solution from the SPM. The inequilibrium of the initial stresses (reflecting the error in the assumed flow field) are corrected by applying incrementally equal and opposite forces: with the cone held stationary.

Table 2.2.1, Predicted values of time factor for Boston Blue clay
(after Levadoux and Baligh, 1986)

Cone Angle (°)	Location	Degree[b] of Consolidation (%)				
		20	40	50	60	80
60	Tip[c]	0.44	1.9	3.7	6.5	27
60	Cone Base	0.69	3.0	5.6	10	39
60	Shaft	7.3	22	33	47	114
18	Tip[d]	0.064	0.5	1.4	3.6	24
18	Midcone	0.52	2.6	4.7	8.2	34
18	Cone Base	1.8	6.2	10	17	53
18	Shaft	5.9	16	25	37	86

[a] Time factor, $T=c_r t/r_o^2$.
[b] Degree of consolidation = $(1 - \Delta u/\Delta u_i) \times 100$.
[c] Porous element location anywhere on the cone face.
[d] Apex of the cone

After the inequilibrium was eliminated, the cone was pushed further until a steady load was reached. A large strain finite element method was used.

The computed excess pore pressure was used as the initial condition in a dissipation analysis based on the Terzaghi-Rendulic uncoupled consolidation theory. The non-dimensional dissipation curves (for I_r = 100) for different filter element locations is shown in Figure 2.2.2. The dissipation curves depend on the initial pore pressure distribution (which is dependent on the value of I_r) and are hence not unique. In order to unify the results at different I_r values (Figure 2.2.3), they proposed a modified time factor T^* and the following expression was suggested to estimate c_r:

$$c_r = \frac{T_{50}^* r_o^2}{t_{50}} \sqrt{I_r} \qquad (2.2.6)$$

The values of T^* at various stages of dissipation and for different filter element locations are shown in Table 2.2.2.

2.2.3 Large Strain Finite Element Method

Large strain finite element technique have been used in the past to analyze the cone penetration problem (De Borst and Vermeer, 1984; Kiousis, et al., 1988). De Borst and Vermeer used an Eulerian approach, in which the soil is modeled as a von Mises matetial, flows through a fixed finite element mesh. Instead of adjusting the position of the nodes (as done in the updated Lagrangian method), the state of the material was adjusted by taking convection into account. The material flow through the fixed mesh was calculated by introducing prescribed material displacement of 1 mm at the bottom of the mesh. They used the above technique to avoid the numerical difficulties encountered in an updated Lagrangian finite element formulation.

Table 2.2.2, Modified time factors at different stages of dissipation (after Houlsby and Teh, 1988)

Degree of Consolidation (%)	Modified Time Factor T^*				
	Cone Tip	Cone Face	Cone Shoulder	5 radii above Cone Shoulder	10 radii above Cone Shoulder
20	0.001	0.014	0.038	0.294	0.378
30	0.006	0.032	0.078	0.503	0.662
40	0.027	0.063	0.142	0.756	0.995
50	0.069	0.118	0.245	1.11	1.46
60	0.154	0.226	0.439	1.65	2.14
70	0.345	0.463	0.804	2.43	3.24
80	0.829	1.04	1.600	4.10	5.24

$$T^* = \left[\frac{c_r t}{r_o^2}\right]\frac{1}{\sqrt{I_r}}$$

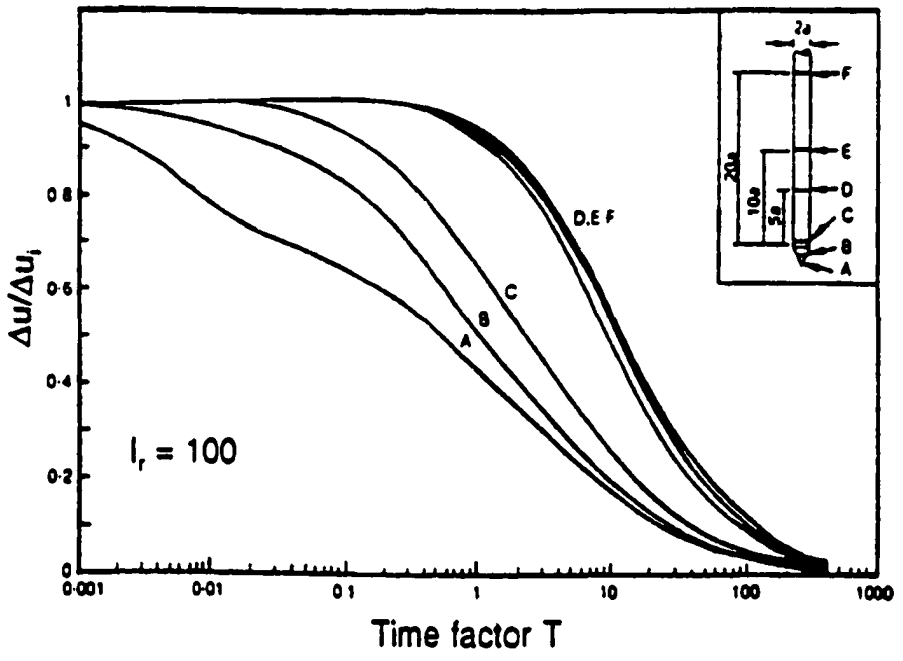

Figure 2.2.2, Time factors predicted by the strain path method for $I_r = 100$ (after Houlsby and Teh, 1988)

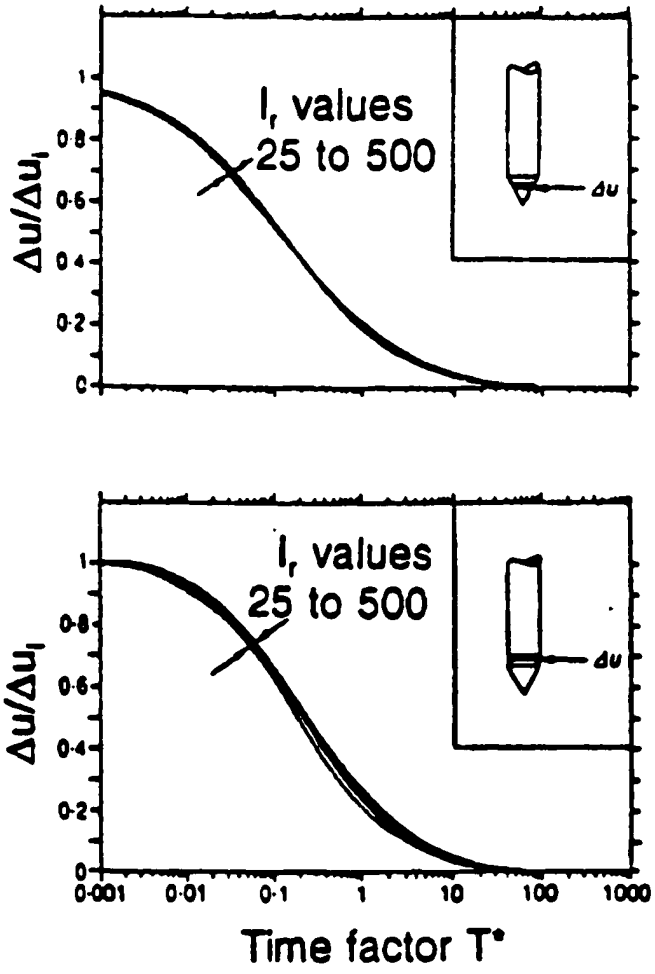

Figure 2.2.3, Modified time factor, T^*, by the strain path method (after Houlsby and Teh, 1988)

An FEM analysis of PCPT using an elasto-plastic large strain formulation was performed by Kiousis, et al. (1988). An elasto-plastic cap model (DiMaggio and Sandler, 1971) was used. The basic (non-rate) constitutive relation was developed in a spatial reference frame and were subsequently transformed in Lagrangian coordiantes. The rate equations were obtained through simple time differentiation. The method was implemented into a finite element program capable of dealing with moving boundary conditions to simulate the continuous process of cone penetration (Figure 2.2.4a). The analysis was based on the assumption of negligible interface between the soil and the penetrometer. Isotropic initial state of stress was assumed and penetration was started from a certain depth until complete failure was achieved. The excess pore water pressure distribution (Figure 2.2.4b) was obtained assuming undrained penetration and was calculated using the relation:

$$\dot{\phi} = K\dot{J} \qquad (2.2.7)$$

In equation (2.2.7) $\dot{\phi}$ = time derivative of the pore pressure, K = undrained bulk modulus of the soil-water system, and $\dot{J}$ = material time derivative of the Jacobian of deformation (expression of the volumetric strain rate).

A separation of the soil and cone shaft (for a length of 35 mm) just above the cone base and a pore pressure gradient around the cone tip was observed.

2.2.4 Semi-Empirical Methods

Chan (1982) used the normalized excess pore pressure distribution around the cone penetrometer obtained from field measurements as the initial pore pressure distribution.

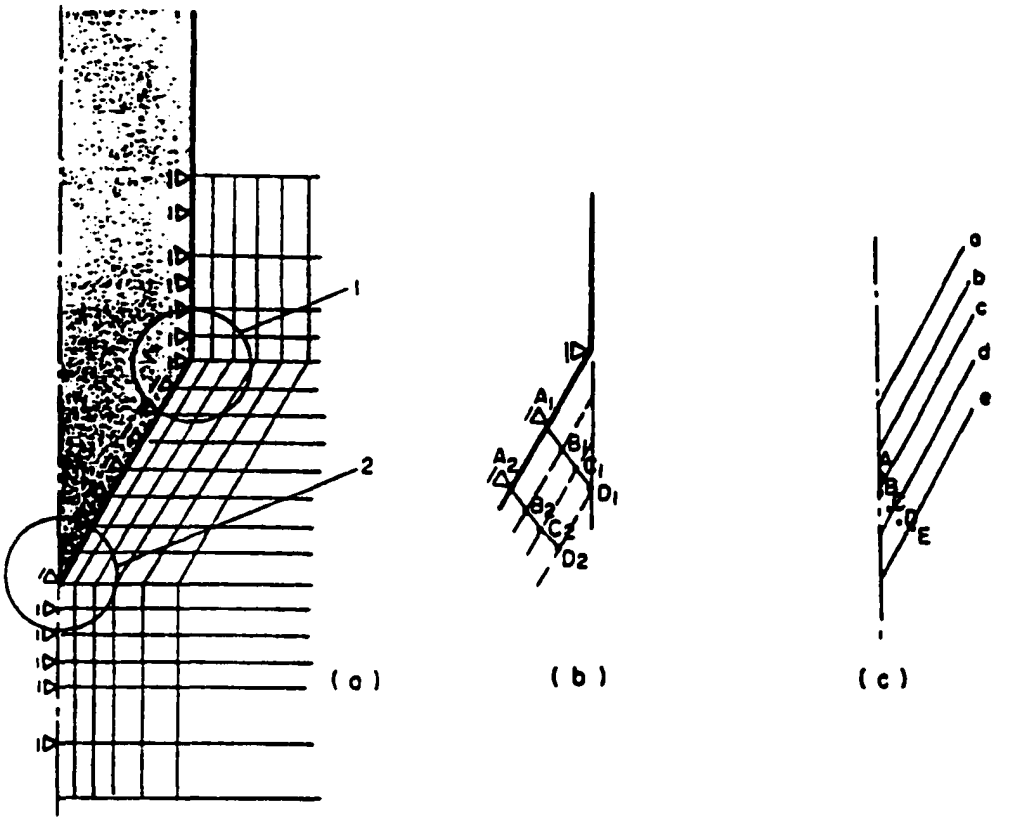

Figure 2.2.4a, Modeling piezocone penetration using large strain FEM
(after Kiousis, et al., 1988)

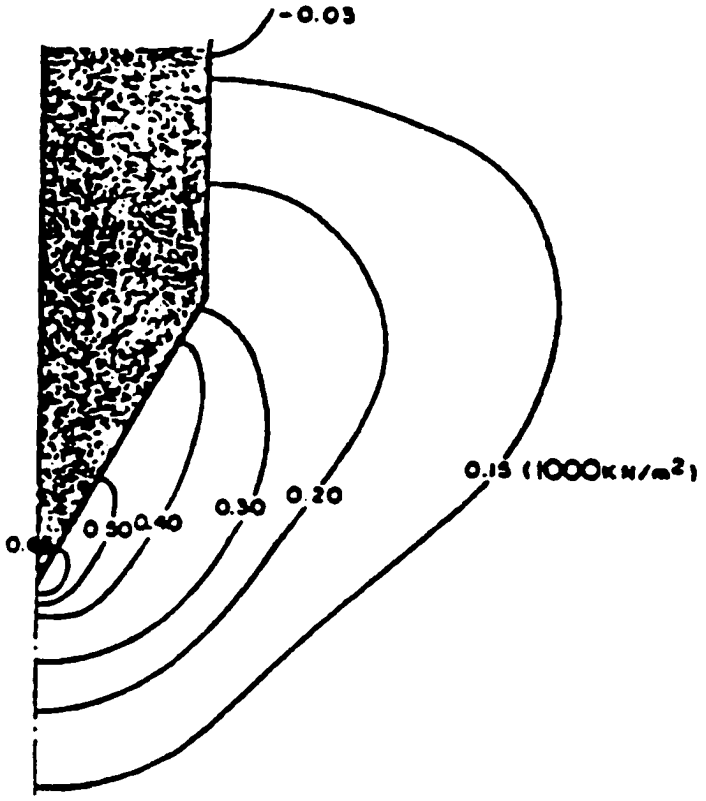

Figure 2.2.4b, Initial pore pressure distribution predicted by large strain FEM (after Kiousis et al., 1988)

A linear uncoupled dissipation analysis was performed to develop the interpretation time factors. This method assumes that the normalized initial excess pore pressure distribution is geometrically similar in all soils (NC).

The method suggested by Gupta and Davidson (1986) for determining the in situ coefficient of consolidation consists of matching the field piezometer probe dissipation curve with computer-generated dissipation plots. The computer plots were obtained by a two-dimensional uncoupled axisymmetric consolidation dissipation of an assumed initial excess pore pressure distribution. The method assumes that the advance of the cone produces in its immediate vicinity a series of successive spherical cavity expansions (Figure 2.2.5). The excess pore pressure distribution around the probe was related to the measured penetration pore pressure at that location by using Vesic's (1972) logarithmic distribution (spherical cavity expansion).

Computations are made in an incremental manner to permit pore pressure dissipation during the advance of the probe. Two-dimensional axisymmetric consolidation problem (for isotropic and anisotropic conditions) were solved with assumed values of in situ coefficient of consolidation until a good match between the field and computer generated dissipation curves were obtained.

2.3 Evaluation of Conventional Method of Determining Hydraulic Properties

Currently, most of the methods used for determination of the hydraulic conductivity of soils from the piezocone penetration test utilize the pore pressure dissipation test data (Torstensson, 1975, 1977; Baligh et al. 1980; Baligh, 1985; Baligh and Levadoux, 1980, 1986, Tumay et al. 1981; Jamiolkowski et al. 1985;

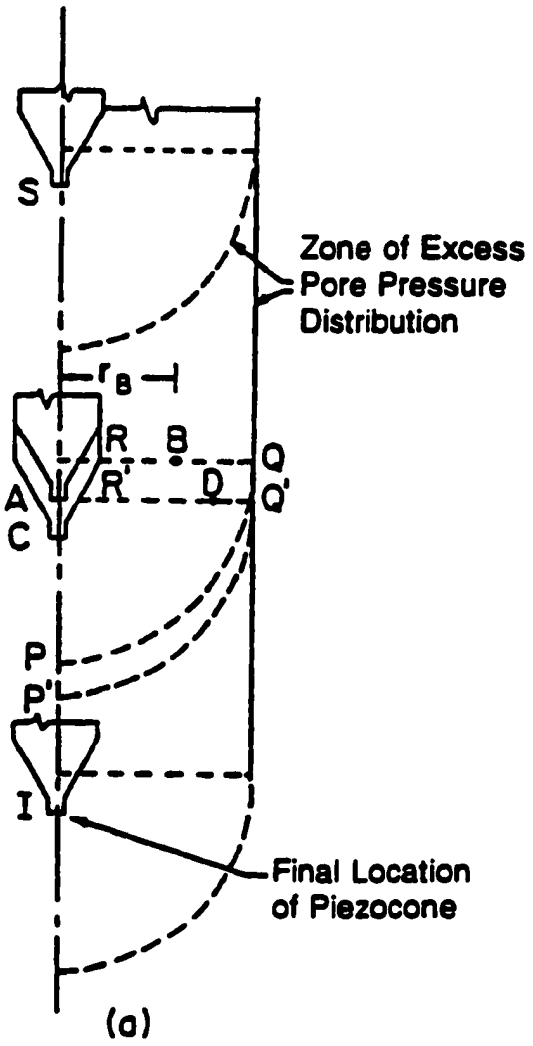

Figure 2.2.5, Modeling piezocone penetration as successive spherical cavity expansions (after Gupta and Davidson, 1986)

Campanella and Robertson, 1981; Campanella et al. 1985; Carter et al. 1977, 1979; Houlsby and Teh, 1988). This conventional method was first suggested by Torstensson (1975, 1977), and utilized the excess pore pressure (Δu) vs. time dissipation data and the proper boundary conditions around the cone tip. The advantage of this method is that it does not require the cumbersome coupled theory of mixtures and it is one of the most convenient methods. A typical procedure for determining the coefficient of consolidation from this method is shown in Table 2.3.1. This method is good for hand calculations though it has several implicit drawbacks which are discussed below.

The partial differential equations, boundary conditions and initial conditions for the method in Table 2.3.1 (for the consolidation of soils subjected to radial drainage) are shown below respectively:

Paitial Differential Equation:

$$\partial\sigma'/\partial t = (\partial\sigma/\partial t) - (\partial u/\partial t) = -c_h\,[(\partial^2 u/\partial r^2 + (1/R)\,(\partial u/\partial r)] + c_z\,[(\partial u^2/\partial z^2] \quad (2.3.1)$$

Boundary Conditions:

$u = 0$ at $r = \infty$, $z = \infty$, and $z = -\infty$

$u' = k$ at $r = R$, $z=0$

Initial Condition:

$F = g$ (stress strain functions such as those obtained from the cavity expansion theory)

In equation (2.3.1), σ' is the effective stress, σ is the total stress, u is the excess pore pressure, t is the elapsed time, c_h is the horizontal consolidation coefficient, c_z is the vertical consolidation coefficient, R is the radius of the cone, r is the radial axis and z is the vertical axis of the cylindrical coordinate system.

Table 2.3.1. Procedure for determining the coefficient of consolidation

Step	Activity	Remarks
1	Compare Δu vs. t curve with standard curves. If the Δu vs. t curve is similar to standard curves, then go to step 2. If not, this method is improper to calculate the coefficient of consolidation.	Δu: excess pore pressure t : elapsed time
2	From the curve obtain T_{50}, and t_{50}	T_{50} : time factor at 50% consolidation t_{50} : time for 50% consolidation
3	Compute $C_r=T_{50}\times R^2/t_{50}$	C_r : radial coefficient of consolidation R : radius of cone tip
4	$k= C_r \times \gamma_w/M$	k : hydraulic conductivity γ_w : unit weight of water M : constrained modulus

The solution of equation (2.3.1) is not straight forward. It can be solved using a special numerical technique such as the Crank - Nicholson technique. Torstensson (1975, 1977) assumed negligible vertical drainage (assumes the effect of c_z and related term is minor) and a constant total stress (assume $(\partial\sigma/\partial t) = 0$). Torstensson (1975, 1977) thus simplified equation (2.3.1) into equation (2.3.2):

Partial Differential Equation:

$$(\partial u/\partial t) = -c_h [(\partial^2 u/\partial r^2 + (1/R) (\partial u/\partial r)] \qquad (2.3.2)$$

Boundary Conditions:

$u = 0$ at $r = r_p$,
$u' = k$ at $r = R$

Initial Condition:

F = g(stress strain functions such as those obtained from the cavity expansion theory)

In equation (2.3.2), r_p is the plastic radius. Equation (2.3.2) is much simpler to solve than equation (2.3.1). Torstensson (1975, 1977) presented a convenient graphical solution which is similar to that of Terzaghi's (1943) one dimensional consolidation solution. Thus one can see that the above partial differential equations (2.3.1) and (2.3.2) can both be good simulations to the real phenomenon, if and only if the field conditions are close to the assumptions given by equation (2.3.1) or (2.3.2). However, inaccurate results can also result if the field conditions are not close to the assumptions given above. Gupta and Davidson (1986), used equation (2.3.1) instead of equation (2.3.2) with the assumed boundary conditions (since equation (2.3.1) cannot be solved with boundary conditions such as $u = 0$ at $r = \infty$.). Although Gupta and

Davidson (1986) obtained better results, however, the fundamental drawbacks of equation (2.3.1) or (2.3.2) are not removed.

Essentially, the pore pressure response from the piezocone penetration test should follow the curves shown in Figure 2.3.1. This figure shows a conceptual and a slightly exaggerated excess pore pressure response of the soil element which is located at the projected center line of the piezocone penetration route. Initially, the location of the piezocone tip is far above this soil element, and there is no excess pore pressure. This means that the soil element is very far from the cone tip and is not affected by the piezocone penetration. As the time progresses, the penetrating cone tip comes closer to the soil element, and the stress bulb of the penetrating cone tip gradually starts to distribute it to this soil element.

This will result in the gradual increase of the excess pore water pressure. This increase may or may not be linear. As the penetrating cone tip passes through this soil element, the maximum disturbance occurs and the maximum excess pore pressure takes place (for normally consolidated soils). When the penetrating cone tip stops at this soil element location, there will be an immediate drop of the excess pore pressure due to the reduced axial force. At the same time, the interaction of pore pressure between the near and far fields take place, and results in the small increase or small decrease of the pore pressure. As observed previously by Voyiadjis and Abu-Farsakh (1997), the pore pressure during penetration is maximum at the cone face (typically known as u_1 position). Thus, if one has the porous element at the cone tip location (typically known as $u_{1,tip}$) or u_2 position, a small increase of pore pressure will be expected because of the pore water inflow from the u_1 position.

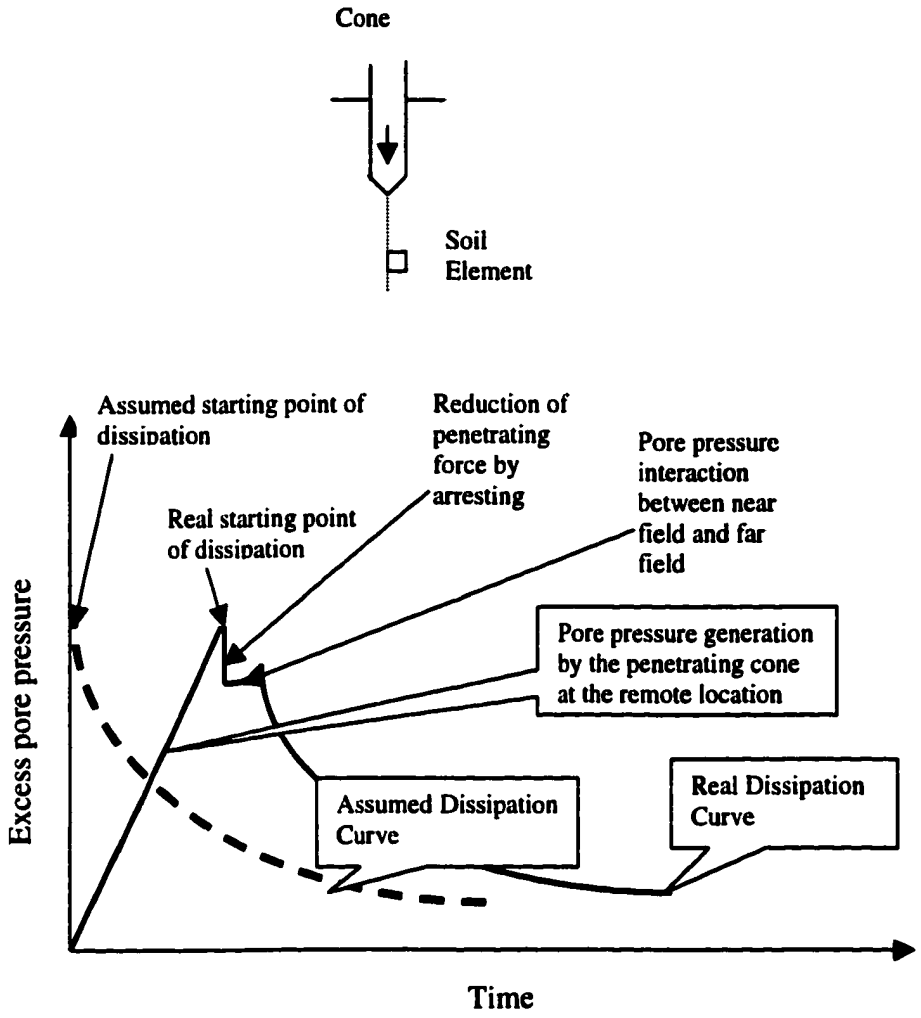

Figure 2.3.1, Conceptual shape of pore pressure response for a soil element during the penetration of piezocone penetration

If one has the porous element at the u_t element location, this change of pore pressure will be very small, and may not be distinguishable. This explanation is for the normally consolidated soils. For the over consolidated soils, similar behavior can be predicted if the dilation phenomenon is considered.

Considering the above discussed factors, one can accept that the dissipation test in the piezocone penetrometer is carried out in an unstable background pore pressure condition. But the assumed dissipation curve is based on the ideally stable background pore pressure condition. Thus the conventional method cannot avoid the disagreement in the boundary condition. Based on this discussion, the following drawbacks for the conventional method can be predicted.

The first drawback is that the time of the initial excess pore pressure (Δu_o) becomes difficult to determine and inaccurate. This is because the real starting time of the dissipation is somewhere between the assumed starting time and the real starting time of dissipation (see Figure 2.3.1.). Thus the resulting coefficient of consolidation is less reliable. Song et al. (1992) computed the coefficient of consolidation from the field measured pore pressure data, and pointed out the difficulties in determining the coefficient of consolidation for the case when the time of the initial pore pressure is unclear. Song et al. (1992) pointed out that the errors are especially large when the elapsed time is small. This is because the elapsed time is in the denominator of the equation for the coefficient of consolidation (see step 3 in Table 2.3.1). Thus, even a small change in the denominator(t_{50}) can result in a big change in the coefficient of consolidation when time is small.

The second drawback is described below. The penetration pore pressure is a combination of simultaneous generation and dissipation. From Figure 2.3.1 and Figure 2.3.2, it can be found that the pore pressure is generated well in advance of the piezometer location. Thus, the measured pore pressures at the piezometer location is the sum of the early generated and dissipated pore pressures and the newly generated pore pressures. This means that there is a doubt about the validity of the magnitude of the initial pore pressure.

Kurup and Tumay (1997) also pointed out the interference of pore pressure between near field and far fields (near field: location radially close to the cone tip; far field: location radially away from the cone tip). According to Kurup and Tumay (1997) and Kurup et el. (1994), the dissipation of pore pressure during piezocone penetration is unavoidable, and this phenomenon results in the interference of the spatial distribution of the pore pressure as shown in Figure 2.3.3.

In Figure 2.3.3, the measured pore pressure at the near field is already dissipated by a certain amount, and the measured pore pressure at the far field is already increased slightly due to the pore water inflow from the near field. This results in the more gentle dissipation slope than the theoretically predicted curve. The curvature represents the pore pressure dissipation rate; thus the computed hydraulic conductivity or coefficient of consolidation may not be correct. Senneset et al. (1988) pointed out the validity of Δu_o when $B_q<0.4$ (these soils correspond to clayey silts.). Conceptually B_q is the ratio between the pore pressure and the cone resistance. The small value of B_q implies a high hydraulic conductivity. Thus, the validity of Δu_o is questionable for the soils which have higher hydraulic conductivity than clayey silts.

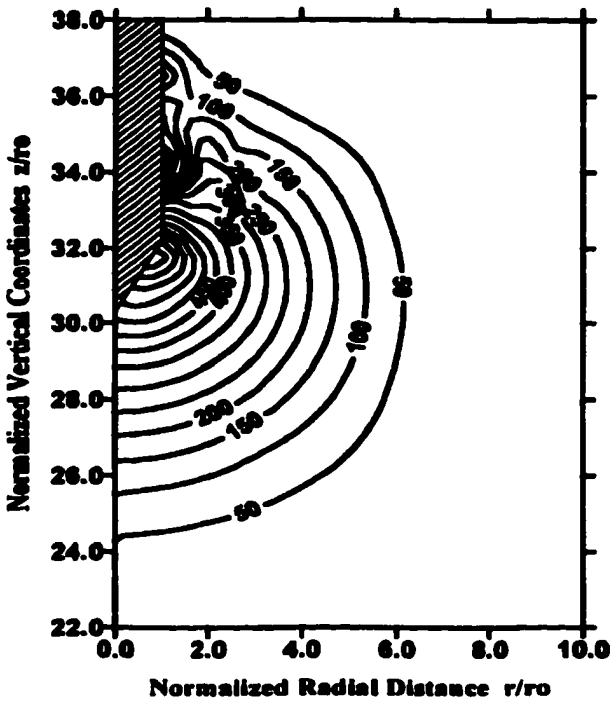

Figure 2.3.2, Generation of excess pore pressure around the cone tip
(after Voyiadjis and Abu-Farsakh, 1997)

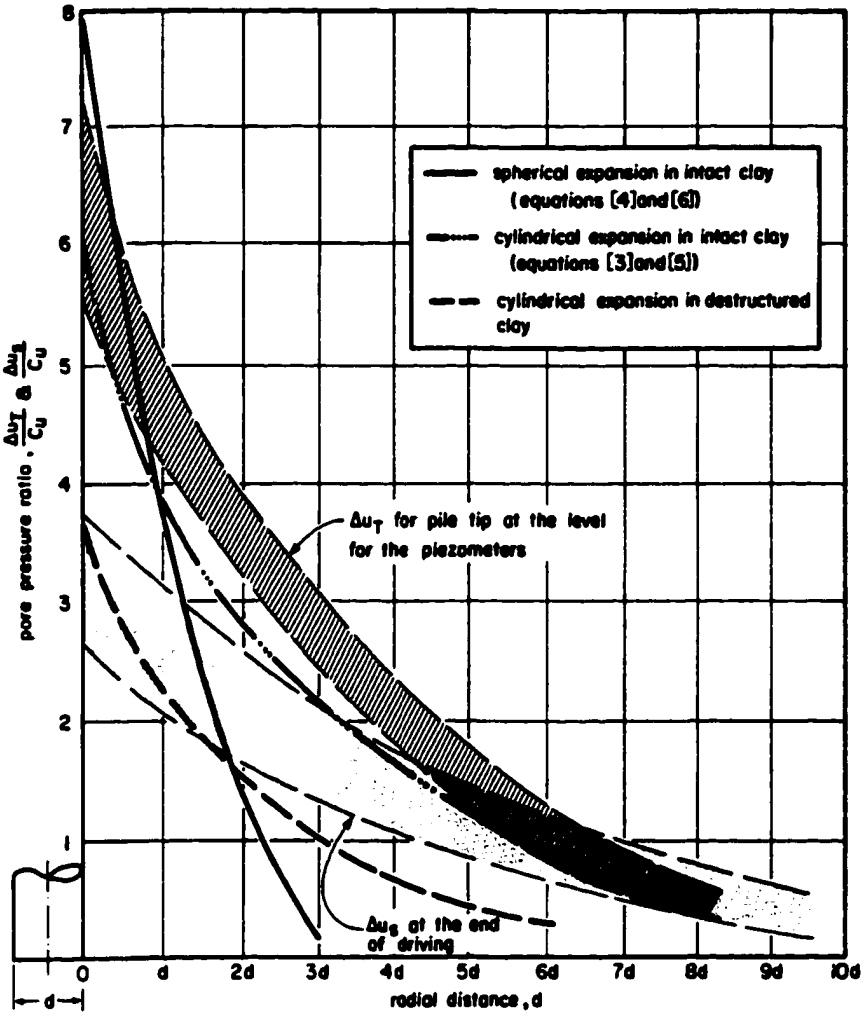

Figure 2.3.3, Spatial distribution of excess pore pressure around the protruding object (after Roy et al., 1981)

Senneset et al. (1988)'s statement is based on the empiricism, but it agrees well with what has already been discussed in this section. Elsworth (1993) showed that B_q can be a function of the hydraulic conductivity when $B_q<0.5$. Beyond that B_q is almost constant regardless of k (Figure 11 in Elsworth (1993)). This phenomenon shows that for permeable soils, the validity of Δu_o is questionable.

The effects of the boundary conditions were not discussed in detail. However, from the above discussion, it is clear that one cannot avoid several problems in determining the hydraulic conductivity of soils by using the current interpretation method of the piezocone penetration test. The error induced from the above difficulties may be negligible or may be significant depending on the soil condition. However, it is clear that a more rational approach for conducting the hydraulic conductivity test is needed.

Elsworth (1991, 1992, 1993) computed the hydraulic properties of soils with the linear elastic model using the dislocation method which is based on Cleary (1977)'s work. From the view point of computational cost, the evaluation of the hydraulic properties using the linear elastic model is quite efficient. Considering that the strain is high at the vicinity of the cone tip (or porous tip), the linear elastic solution is not a very desirable solution. Ultimately, one should go to the elasto-plastic large strain problem.

2.4 Determination of Hydraulic Conductivity or Coefficient of Consolidation Using Penetration Pore Pressure

In 1977, Cleary proposed equations for the formulations of pore pressure as the function of hydraulic conductivity on the basis of linear elasticity. Cleary's (1977)

solution, thus is valid for the small strain problems or for the incremental approach. Also, Clearly's solution was derived for the assumed loading condition; one point load, which disregards the shape of the loading condition. Thus, one can presume that Cleary's solution can analyze the response of the piezocone penetration test data approximately.

Elsworth (1991, 1993) computed the hydraulic conductivity of the soils from the penetration pore pressure based on Cleary's solution. Elsworth improved Cleary (1977)'s equation by considering the shape of the cone tip. The results of Elsworth (1993) showed agreement with test data in some aspects, but did not showed agreement in some other aspects. Particularly, the disagreement was substantial in the hydraulic conductivity by showing that the predicted hydraulic conductivity was much larger than the measured value. Elsworth (1993) also showed that the pore pressure dissipation test response with piezometric element at the side of the shaft is independent of the hydraulic conductivity or coefficient of consolidation. It seems that these limitations of Elsworth (1991, 1993) is because that the fundamental soil model is linear elastic material, while in reality, it is large strain elasto-plastic material.

Elsworth (1991, 1993) was the first one who tried to compute the hydraulic conductivity of soil from the piezocone penetration pore pressure, and not from the dissipation tests. However, it is clear that the large strain approach must be adopted for the rational modeling of the piezocone penetration problem.

Manasaro (1994) proposed the unique method to predict the hydraulic conductivity of slurry wall, however, it did not attract the popular concern.

CHAPTER 3. PROPOSED METHOD

3.1 Overview

Soil consists of an assemblage of particles with different sizes and shapes which form a skeleton whose voids are filled with water and air or gas. The word "soil", therefore, implies a mixture of assorted mineral grains with various fluids. Hence, soil in general must be looked at as a multiphase material whose state is to be described by the stresses and displacements (velocities) within each phase. The stresses carried by the soil skeleton are conventionally termed "effective stresses" in the soil mechanics literature (Terzaghi, 1943), and those by the water are called the "pore water pressures". When free drainage conditions prevail, the steady state pore-water pressure depends only on the hydraulic conditions and is independent of the soil skeleton response to external loads. Therefore, in that case, a single phase continuum description of soil behavior is certainly adequate. Similarly, a single phase description of soil behavior is also adequate when no drainage (i.e. no flow) conditions prevail. However, in intermediate cases in which some flow can take place, there is an interaction between the skeleton strains and the pore water flow. The solution of these problems requires that the soil behavior be analyzed by incorporating the effect of the transient flow of the pore-water through the voids and the stress-strain behavior of soils. Therefore, a multiphase continuum formulation is required for porous media.

Conversely, when the response of a soil is known, the hydraulic characteristics of the soil can be known from the hydro-mechanical analysis – the so called coupled theory of mixtures. Biot (1955, 1978) first developed such a theory for an elastic porous medium.

However, it is observed experimentally that the stress-strain-strength behavior of the soil skeleton is strongly non-linear, anisotropic, and elastoplatic. An extension of Biot's theory into the non-linear, anisotropic range is, therefore, necessary in order to analyze the transient response of soil deposits. This extension has acquired considerable importance in recent years due to the increased concern with the dynamic behavior of saturated soil deposits and associated liquefaction of saturated sand deposits under seismic loading conditions. Such an extension of Biot's formulation was proposed by Prevost (1980).

Prevost (1980)'s theory of mixture was coupled with Terzaghi (1943)'s effective stress theory for finite strain by Kiousis and Voyiadjis (1985), and Voyiadjis and Abu-Farsakh (1997), thus a complete coupled theory of mixture was obtained. In this study, the works of Voyiadjis and Abu-Farsakh (1997) is further extended for the anisotropic stress condition with the micro-mechanical consideration.

The main idea of this research is to determine the hydraulic conductivity of cohesive soils using the piezocone PCPT without relying on the pore pressure dissipation data. This method uses the hydro-mechanical analysis by the coupled theory of mixtures. Thus, the test time can be reduced significantly and the continuous hydraulic conductivity profile can be obtained. Also, this method utilizes the fundamental behavior of soils, thus it can avoid the problems (boundary condition problem, Mandel-Cryer effect, problems of determining initial pore pressure, interference of radial pore pressure etc.) in the conventional method of determining the hydraulic conductivity using the piezocone penetration test. To perform this, the formulation of the coupled field equations for soils using the theory of mixtures in an

updated Lagrangian frame based on the principle of virtual work and implemented in a finite element program will be used. An, axi-symmetric finite element program which is capable of describing the behavior of soils with the advance of piezocone tips will be coded. Finally, the validity of the proposed model will be examined by comparing it with well-documented test results from previous research.

3.2 Coupled Theory of Mixtures

As discussed previously, the drainage condition around the penetrating cone tip is somewhere between the fully drained and the fully undrained condition. This condition is called the partially drained condition or the transient flow condition. For the transient flow condition it can be presumed that the pore pressure is a function of the hydraulic conductivity and other parameters (stress-strain parameters). Full derivation of the coupled theory of mixtures can be referred to Prevost (1980). In this study, a relatively concise derivation is shown.

The general form of Darcy's law for the flow of water through the porous medium is given by:

$$(v^w - v^s) = -\frac{1}{\gamma_w} K^{WS} (grad(P_w) - \rho_w b) \qquad (3.2.1)$$

In equation (3.2.1), the superscripts w and s do not indicate tensors but the water and solid phases respectively. **b** is the body force vector, γ_w is the unit weight of water, and K^{WS} is the hydraulic conductivity tensor in (m/sec). Also from Prevost (1980), the following divergency equation is obtained:

$$div(v^s) - div(v^w) = \frac{1}{n^w}[div(v^s) + (v^w - v^s) grad(n^w)] \qquad (3.2.2)$$

Taking the divergence of both sides of equation (3.2.1) and substituting the results into equation (3.2.2) one obtains:

$$div(\boldsymbol{v}^s) - div[\frac{n^w}{\gamma_w} \boldsymbol{K}^{WS} (grad(P_w) - \rho_w \boldsymbol{b})] = 0 \tag{3.2.3}$$

Making use of the following relation:

$$div(\boldsymbol{v}^s) = d^s_{kk} = X^s_{k,A} X^s_{k,B} \dot{\varepsilon}_{AB} \tag{3.2.4}$$

then equation (3.2.3) can be re-written as follows:

$$d^s_{kk} - \frac{\partial}{\partial Z_a} [\boldsymbol{K}^{WS}_{ab} (grad(P_w) - \rho_w \boldsymbol{b}_b)] = 0 \tag{3.2.5}$$

Also making use of the following relationship for the coordinate transformation, one obtains equation (3.2.10):

$$K^{WS}_{ab} = X^s_{a,A} X^s_{b,B} K^{WS}_{AB} \tag{3.2.6}$$

$$b_b = X^s_{b,B} B_B \tag{3.2.7}$$

$$\frac{\partial P_w}{\partial Z_b} = X^s_{C,b} \frac{\partial P_w}{\partial X_C} \tag{3.2.8}$$

$$\frac{\partial}{\partial Z_a} = X^s_{D,a} \frac{\partial}{\partial X_D} \tag{3.2.9}$$

$$J^s C^{s^{-1}}_{ij} \dot{\varepsilon}_{ij} - J^s C^{s^{-1}}_{ij} C^{s^{-1}}_{ij} X^s_{D,a} \frac{\partial}{\partial X_D} [\frac{n^w}{\gamma_w} K^{WS}_{AB} X^s_{a,A} \{\frac{\partial P_w}{\partial X_B} - \rho_w B_B\}] = 0 \tag{3.2.10}$$

In equation (3.2.10) $C^s_{ij} = X^s_{k,i} X^s_{k,j}$. Equation (3.2.10) is the coupled equation in an updated Lagrangian reference frame.

3.3 Anisotropic Modified Cam Clay Model

The anisotropic modified Cam clay model is used in this study in order to describe the plastic behavior of soils. When a material is subjected to large deformation, substructure changes may take place. Thus the substructure changes need to be taken into account for a more reasonable analysis of the material behavior. This substructure change is minimal for the small strain problems such as linear elastic problems. However, it becomes more pronounced and vital when the strain becomes finite. The substructure change is caused by the external work energy, thus it should be taken into account for the correct equilibrium of energy.

For geo-materials, this behavior is more prominent because the bonding force between the particle is relatively weak compared to other materials such as steel. Also, the strain range for some of the geotechnical problems such as after failure problems, cone penetration tests, etc, are several tens to several hundreds percent. Thus, severe substructure changes can take place.

Another main characteristic of geo-material is the anisotropy. By nature of deposition of the granular materials, inherent anisotropy exists in geo-materials. During the deformation, the material undergoes a new anisotropy because of the substructure change of the material. This means that geo-materials have initial anisotropy and this anisotropy evolves with the strain. Thus for an accurate consideration of the anisotropy of geo-materials, one should incorporate the substructure change. Consideration of the substructure change is discussed in the next section.

3.4 Micro-mechanical (Substructure) Consideration

Large deformation formulation of inelasticity often requires the use of stress rates in the constitutive equations. For small deformation theories, the problem of choosing a proper stress rate is not a critical one as for the strictly linear behavior, all stress rates are approximately the same. For large deformations, however, the problem becomes important as different stress rates lead to dramatically different results. Indeed, it was first noted by Truesdell (1955) that an oscillatory stress solution is obtained when a standard linearly hypoelastic material is subject to large deformation as shown in Figure 3.4.1. He attributed the phenomenon to plastic effects, calling it simply hypoelastic yield, without discussing further its physical relevance. It seems that this behavior did not appeal to Prager (1961) who produced a non-oscillatory solution to the simple shear problem by retaining the Jaumann stress rate but incorporating extra terms into the standard constitutive equation of linear hypoelasticity. Again, however, he provided neither a motivation for the extra terms nor an explicit discussion on the appropriateness of oscillatory stresses.

It appears that the first to question the physical relevance of oscillatory solutions in connection with standard linear hypoelasticity theory was Dienes (1979) who attributed the effect to the use of the Jaumann rate into the constitutive equation. He obtained non-oscillatory response by using, instead, a different objective rate and retaining the same constitutive equation. In fact, this rate was based on a spin earlier introduced by Green and Naghdi (1965) and used by Green and McInnis (1967) on the basis of an intermediate unrotated configuration uniquely defined in terms of the rotation $\mathbf{R}$ obtained from the polar decomposition of the deformation gradient $\mathbf{F}$.

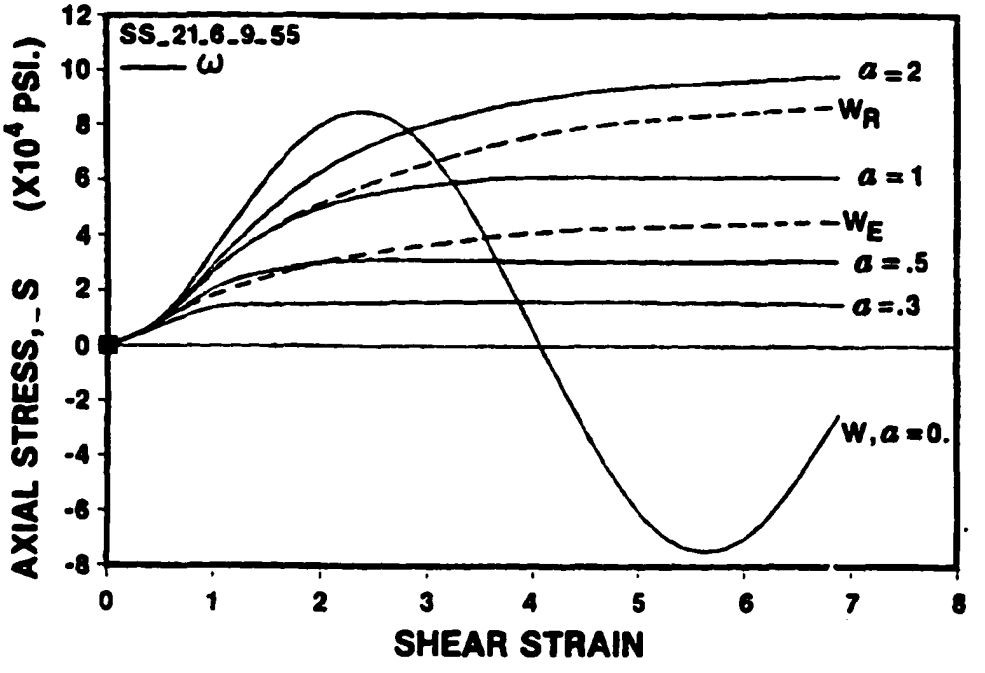

Figure 3.4.1, Oscillatory behavior for large strains (after Zbib and Aifantis, 1988)

The work on corotational stress rates and the related issue of oscillatory response seems to have passed rather unnoticed until a workshop in Stanford, where Nagtegaal and de Jong (1982) presented numerical solutions of the simple shear problem by employing a von Mises material and a Prager-Ziegler kinematic hardening rule together with the use of Jaumann rates for the stress and the back stress. Again, an oscillating stress results in response to a monotonically increasing strain and the effectt was attributed to the inadequacy of the Prager-Ziegler hardening rule. Immediately thereafter Lee et al. (1983) suggested that the problem lies in the use of the Jaumann rate rather than the constitutive equation, and they proposed yet another corotational rate defined by the angular velocity or spin of a unit vector attached to the material and instantaneosuluy oriented along a principal direction of the back stress. They illustrated that oscillatory effects are removed this way. Subsquently, Johnson and Bammann (1984) and Dafalias (1983) solved independently the above kinematic hardening problem by employing the same corotational rate that Dienes (1979) used earlier for hypoelasticity. Both of these works presented analytic solutions illustrating the removal of oscillations even in the case of linear kinematic hardening. In the same paper, Dafalias (1983) suggested the possibility of using a new corotational rate for the evolution of the back stress α which is attached to the material substructure, and must rotate with a spin given by the difference between the overall spin of the continuum (vorticity or total spin W) and the spin induced by the substructure (plastic spin $\mathbf{W}^{\mathbf{P}}$). This suggestion was directly motivated by the earlier works of Mandel (1971) and Kratochvil (1971) who, essentially, pointed out the need of constitutive equations for the plastic spin but did not pursue the matter further. Dafalias (1983,

1985) and independently Loret (1983) and Onat(1984) were the first to assume a simple relation for the plastic spin $\mathbf{W}^P$ and show, among other things, that oscillations do not occur in the solution of simple shear problem with kinematic hardening when the rate of back stress is taken corotationally with respect to the difference between the total and the plastic spins. The particular expression used for the plastic spin is $\mathbf{W}^P = \zeta(\alpha\mathbf{D}^P - \mathbf{D}^P\,\alpha)$ with ζ being a constant, α the back stress, and $\mathbf{D}^P$ the symmetric part of the plastic velocity gradient. Dafalias and Aifantis (1984) rigorously derived it using a microscopic basis.

A seemingly different approach to the aforementioned problem of oscillatory stress was proposed by Atluri (1984). He insisted on the use of the Jaumann rate but suggested to generalize the constitutive equations of linear hypoelasticity for the rate of stress and Prager-Ziegler kinematic hardening rule for the rate of back stress. This approach, being reminiscent to the practice suggested by Prager (1961) and the opinion expressed by Nagtegaal and de Jong (1982), does suppress the oscillations in simple shear problems but does not provide any insight or systematic way on how to meaningfully generalize the constitutive equation.

Zbib and Aifantis (1988) (Figure 3.4.1) proposed a method for selecting the appropriate stress rate to be used in the constitutive equations. It rests upon utilizing the concept of non-coaxiality between stress and strain rate. The suggestion is based on the fact that if such non-coaxiality is not properly accounted for it may lead to undesirable predictions; for example, oscillatory stresses.

More details of the methodologies are discussed at the next section.

3.4.1 Relative Spin

The relative spin concept was proposed by Zbib and Aifantis (1988b). The fundamental ideas are as following:

The corotational rate that one chooses to express the constitutive equation is computed with respect to the spin $\mathbf{W}_s$ corresponding to the material frame whose angular velocity coincides with that of stress. In lieu of a prior knowledge of this spin, one expresses it as the difference between the overall spin of the continuum W and the relative spin $\mathbf{W}_{D/S}$ signifying the angular velocity of the principal directions of strain rate relative to that of the principal directions of stress. Then it is natural to assume that $\mathbf{W}_{D/S}$ is a function of **D** and **S** which in view of invariance considerations of frame indifference has a definite polynomial-like representation with the first term being of the form ζ(**SD-DS**). This is reminiscent of the expression for the plastic spin $\mathbf{W}^P$ earlier adopted by Dafalias (1983), Loret(1983) and Onat (1984) but is more general in concept as it does not require the notion of plasticity or an underlying substructure. Indeed, it can be shown that a relatively simple structural model for the continuum leads to a rigorous derivation of the expression $\mathbf{W}_{D/S} = \zeta$(**SD-DS**) without invoking the notion of plasticity or slip. If an appeal is made to constitutive theory, then higher-order terms appear in the representation of $\mathbf{W}_{D/S}$ and this, in effect, may be used to illustrate the formal equivalence between the approach of ad hoc generalizations of constitutive equations with Jaumann rates and the approach of replacing the Jaumann rate by suitable corotational rates via the use of the relative spin $\mathbf{W}_{D/S}$ and appropriate constitutive representations for it. In some other references (Dafalias, 1998), the relative spin is termed material spin.

3.4.2 Plastic Spin

The plastic spin approach is similar to the relative spin in considering the micro-mechanical behavior of soil through the plastic spin. However, it is different from relative spin by not making use of the co-axial (of stress and strain rate) concept, but to modify the plastic spin itself. The following equations show the similarity and difference of plastic spin and relative spin.

If **F** (det **F**>0) denotes the deformation gradient, the polar decomposition theorem reads:

$$\mathbf{F} = \mathbf{VR} = \mathbf{RU} \tag{3.4.1}$$

In equation (3.4.1), **V** and **U** are the left and right stretch tensors respectively, and **R** is the rotation. When assuming that the common eignevalues of **V** and **U** are real, we can write:

$$\mathbf{V} = \mathbf{R}_E \Lambda \mathbf{R}_E^T \tag{3.4.2}$$

$$\mathbf{U} = \mathbf{R}_L \Lambda \mathbf{R}_L^T \tag{3.4.3}$$

In equations (3.4.2) and (3.4.3), $\Lambda$is the diagonal matrix of the eigenvalues (λ_i, i = 1, 2, 3) while the proper orthogonal tensors $\mathbf{R}_E$ and $\mathbf{R}_L$ are commonly known as the Eulerian and Lagrangian rotations respectively.

On the basis of **R**, $\mathbf{R}_E$, $\mathbf{R}_L$ we can define corresponding spins by the relations as follows (Zbib and Aifantis, 1987):

$$\mathbf{W}_R = \dot{\mathbf{R}}\mathbf{R}^T \tag{3.4.4}$$

$$\mathbf{W}_E = \dot{\mathbf{R}}_E \mathbf{R}_E^T \tag{3.4.5}$$

$$\mathbf{W}_L = \dot{\mathbf{R}}_L \mathbf{R}_L^T \tag{3.4.6}$$

These equations are less familiar than the vorticity or spin of the continuum defined as usual by:

$$\mathbf{W} = \frac{1}{2}(\mathbf{L} - \mathbf{L}^T) \tag{3.4.7}$$

Equation (3.4.7) represents the antisymmetric part of the velocity gradient **L** whose symmetric part **D** is the stretching tensor, i.e.

$$\mathbf{L} = grad\ \mathbf{v} \tag{3.4.8}$$

$$\mathbf{D} = \frac{1}{2}(\mathbf{L} + \mathbf{L}^T) \tag{3.4.9}$$

$$\mathbf{L} = \mathbf{D} + \mathbf{W} \tag{3.4.10}$$

When we consider a unit vector v attached to the material:

$$\dot{v} = \mathbf{W}_v\, v \tag{3.4.11}$$

$$\mathbf{W}_v = \mathbf{W} - [(v \otimes v)\mathbf{D} - \mathbf{D}(v \otimes v)] \tag{3.4.12}$$

The concept of relative spin by Zbib and Aifantis (1987) is expressed as follows:

$$\mathbf{W}^r = \mathbf{W} - \omega \tag{3.4.13}$$

Literally, **W** is the spin of the "geometric structureless continuum" and ω is the "underlying structural material" (Zbib and Aifantis, 1988a). Quoting Dafalias (1998), the same term ω takes into account the sub-structural change. Quoting Lee (1993), ω takes into account the correction of embedded stress which causes the sub-structure change. By choosing $\mathbf{W}_v$ in equation (3.4.12) to represent the material spin **W** such that v coincides with an eigenvector of the back stress, and substituting it into equation (3.4.13) one obtains:

$$\mathbf{W}^r = (v \otimes v)\mathbf{D} - \mathbf{D}(v \otimes v) \tag{3.4.14}$$

For the background for the subsequent analysis, some fundamental kinematic relationships for large deformation elasto-plasticity are listed on the basis of multiplicative decomposition as follows:

$$\mathbf{F} = \mathbf{R}^m \mathbf{U}^e \mathbf{F}^p \tag{3.4.15}$$

In equation (3.4.15) $\mathbf{R}^m$ denotes the material rotation (as opposed to the rotation of the continuum), $\mathbf{U}^e$ is the elastic stretch, and $\mathbf{F}^p$ represents the purely plastic part of the deformation gradient. The velocity gradient $\mathbf{L}$ can now be computed by equation (3.4.15) as follows:

$$\mathbf{L} = \dot{\mathbf{F}}\mathbf{F}^{-1} = \mathbf{R}^m \mathbf{R}^{m^T} + \mathbf{R}^m \dot{\mathbf{U}}^e \mathbf{U}^{e^{-1}} \mathbf{R}^{m^T} + \mathbf{R}^m \mathbf{U}^e \dot{\mathbf{F}}^p \mathbf{F}^{p^{-1}} \mathbf{U}^{e^{-1}} \mathbf{R}^{m^T} \tag{3.4.16}$$

Noting that the symmetric and anti-symmetric part of equation (3.4.16) by subscripts "s" and "a" respectively one obtains:

$$\mathbf{D} = \mathbf{D}^e + \mathbf{D}^p \tag{3.4.17a}$$

$$\mathbf{W} = \omega + \mathbf{W}^e + \mathbf{W}^p \tag{3.4.17b}$$

In equation (3.4.17) the terms are defined as follows:

$$\omega = \dot{\mathbf{R}}^m \mathbf{R}^{m^T} \tag{3.4.18a}$$

$$\mathbf{D}^e = (\mathbf{R}^m \dot{\mathbf{U}}^e \mathbf{U}^{e^{-1}} \mathbf{R}^{m^T})_S \tag{3.4.18b}$$

$$\mathbf{W}^e = (\mathbf{R}^m \dot{\mathbf{U}}^e \mathbf{U}^{e^{-1}} \mathbf{R}^{m^T})_a \tag{3.4.18c}$$

$$\mathbf{D}^p = (\mathbf{R}^m \mathbf{U}^e \dot{\mathbf{F}}^p \mathbf{F}^{p^{-1}} \mathbf{U}^{e^{-1}} \mathbf{R}^{m^T})_S \tag{3.4.18d}$$

$$\mathbf{W}^p = (\mathbf{R}^m \mathbf{U}^e \dot{\mathbf{F}}^p \mathbf{F}^{p^{-1}} \mathbf{U}^{e^{-1}} \mathbf{R}^{m^T})_a \tag{3.4.18e}$$

Equation (3.4.18) shows that for pure plastic deformaion ($\mathbf{U}^e$=1), the elastic stretching and spin vanish ($\mathbf{D}^e = \mathbf{W}^e = 0$), but the material spin w is clearly different

than zero and adds up with the plastic spin $\mathbf{W}^p$ to give the total spin of the continuum or vorticity W. The physical relevance of $\mathbf{W}^e$ and $\mathbf{W}^p$ and their relation to $\mathbf{W}^r$ is understood by comparing equations (3.4.18) and (3.4.14) from which we obtain:

$$\mathbf{W}^r = \mathbf{W}^e + \mathbf{W}^p \tag{3.4.19}$$

Equation (3.4.19) shows that the summation of elastic spin and plastic spin is the relative spin. To proceed further one can assume that the internal orientation of the body is described by a unit vector v which is attached to the material and denotes the direction of anisotropy. From equations (3.4.11) and (3.4.12), and using equation (3.4.18) one obtains the following:

$$\mathbf{W}^e = (v \otimes v)\mathbf{D}^e - \mathbf{D}^e(v \otimes v) \tag{3.4.20a}$$

$$\mathbf{W}^p = (v \otimes v)\mathbf{D}^p - \mathbf{D}^p(v \otimes v) \tag{3.4.20b}$$

Assuming small elastic deformations so that elastic spin is essentially zero, one obtains the following expression:

$$\omega = \mathbf{W} - \mathbf{W}^p \tag{3.4.21}$$

Equation (3.4.21) suggests that the plastic spin and relative spin are identical for this case and they are both determined by the direction of anisotropy (v) and the rate of plastic deformation ($\mathbf{D}^p$). In equation (3.4.21), W is also called the constitutive spin (Dafalias, 1998).

Dafalias (1998) also showed that the factors for plastic spin are not only the texture change or crystal re-orientation but can be any kind of sub-structure change. These additional sub-structure changes can be incorporated as the extra term in equation (3.4.21) as follows:

$$\omega = \mathbf{W} - (\mathbf{W}^{p_1} + \mathbf{W}^{p_2} + \mathbf{W}^{p_3} + \ldots + \mathbf{W}^{p_n}), \text{ where } n = 1, 2, 3, \ldots \tag{3.4.22}$$

3.4.3 Microplane Model

The microplane model was proposed by Zienkiewicz and Pande(1977), Bazant (1984), Bazant and Kim (1986), and Prat and Bazant (1989). This model is quite different from the relative spin or plastic spin model. While the relative spin or plastic spin model is plasticity based model, microplane model is the microscopic material characteristics based model which is a kind of the classical slip theory of plasticity.

The original idea of microplane method is due to Taylor (1938), who proposed that the stress-strain relation be specified independently on planes of various orientations in the material. He also assumed that either the stresses on that plane (now called the microplane) are the resolved components of the macroscopic stress tensor (static constraint), or the strains on the plane are the resolved components of the macroscopic strain tensor (kinematic constraint). The response on the planes of various orientations are then related to the macroscopic response simply by super position or, as has been done in recent works (Bazant, 1984; Carol et al. 1990), by means of the principle of virtual work. In the initial application to metals, beginning with Batdorf and Budiansky (1949), only the static constraint was considered. So it was the early applications to soils (Zienkiewicz and Pande, 1977; Pande and Sharma, 1980, 1983; Pande and Xiong, 1982) which successfully described some basic aspects of soil behavior, other than strain softening. It appeared, however, that the microplane system under a static constraint becomes unstable when strain softening takes place (Bazant and Oh, 1983, 1985; Bazant and Gambarova, 1984). To cope with these problems, Prat and Bazant (1989) improved the microplane model for dynamic constraint.

In application for clays, the microplanes may be imagined to represent the slip on the contact planes between clay platelets or the planes normal to the platelets on which slip is manifested by normal strain as shown in Figure 3.4.2. Although the correlation to the microstructural mechanism of inelastic deformations is largely intuitive, the microplane model has the advantage that it can distinguish among the intensities of inelastic strains at various orientations and describe how they are mutually constrained. Therefore, the microplane strains ε_N and ε_T in Figure 3.4.3 may be imagined to represent the sum of the inelastic relative displacements on all the weak planes contained within a unit volume of the material, plus the associated elastic deformations of all the particles. The equilibrium equation for constitutive law was set up by equating the macro level strain energy is equal to the summation of the micro level strain energy caused by ε_N and ε_T as follows.

$$\Delta V_o \sigma_{ij} \delta\varepsilon_{ij} = \int_\Omega \Delta V_o (\sigma'_N \delta\varepsilon_N + \sigma'_T \delta\varepsilon_T) \Psi_N d\Omega \qquad (3.4.23)$$

In equation (3.4.23), ΔV_o = unit volume, σ_{ij} = macroscopic stress tensor, $\delta\varepsilon_{ij}$ = increment of macroscopic strain tensor, σ'_N = normal stress in microplane, σ'_T = tangential stress in microplane $\Psi_N = \alpha_N \nu_N$, and $d\Omega = \sin\theta \, d\theta \, d\phi$, with θ and ϕ = angular spherical coordinates.

The prior advantage of microplane model is that the constitutive law is written in terms of the current stresses and strains (not in terms of their increments), which allows the model to be explicit with all the numerical advantages shown by Carol et al. (1990).

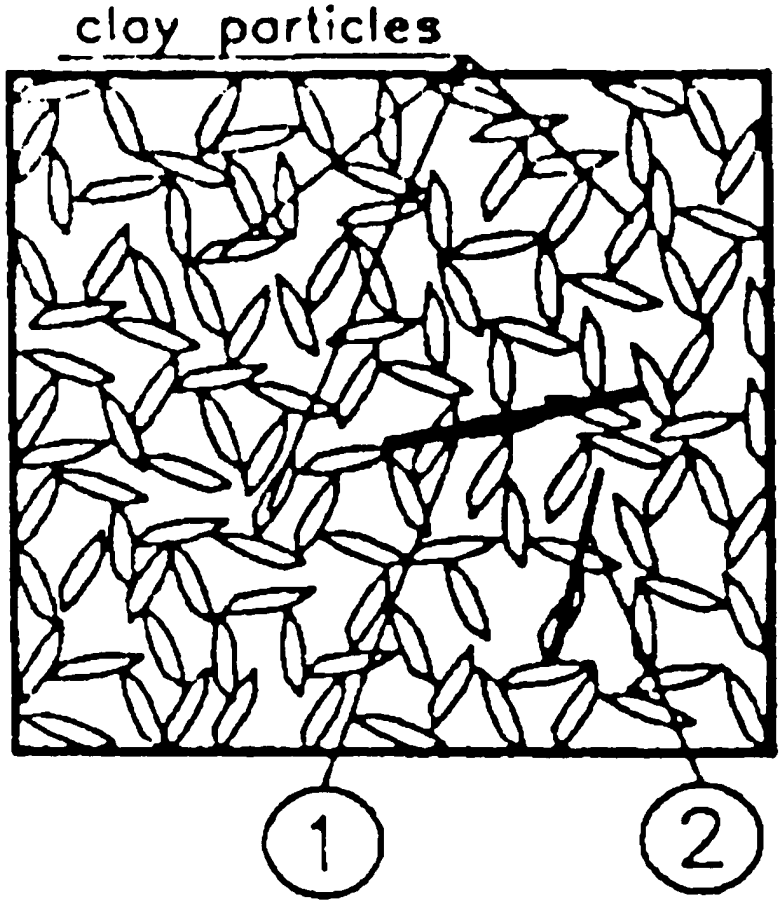

Figure 3.4.2, Microplane in Cohesive Soil: 1 = Microplane as Slip Plane between Clay Platelets; 2 = Microplane as Normal Plane to Clay Platelets (after Prat and Bazant, 1990)

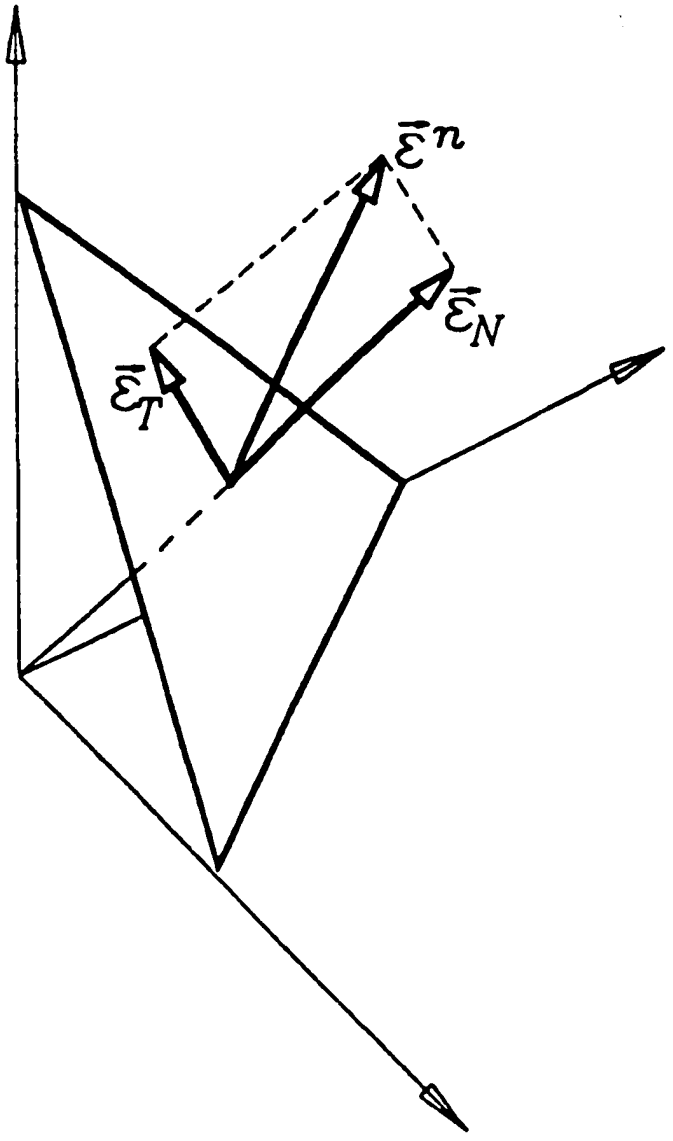

Figure 3.4.3, Strain Components on Microplane
(after Prat and Bazant, 1990)

However, it is also pointed out by Prat and Bazant (1989) that it is impossible for the effective microplane stresses σ'_N and σ'_T to equilibrate the effective macrostress σ'_{ij} exactly since the microplanes are constrained kinematically.

3.4.4 Particulate Mechanics

This approach may be said to be the advanced method since it deals with each particle of soils. This method, by its nature needs extended computation time. At the current stage, its application is limited only to sandy soils. It assumes that the behavior of sand aggregate is very similar to that of polycrystals since the individual grain packing within the sand could be considered in first approximation to behave like randomly oriented crystals (Voyiadjis et al., 1995, 1992). However, the main difference is that the properties of these grain packing are pressure dependent and the amount of slip in each of these packing, in contrast to the polycrystalline aggregate, depends on the mean stress. For example, a simple cubic array of equal spheres is a pressure dependent monocrystal with three sliding planes, and with each plane containing two sliding directions (Voyiadjis and Foroozesh, 1990). Moreover, sand may experience dilation under shear that does not occur in polycrystalline aggregates. Finally, unlike metals, soils exhibit nonlinear inelastic stress strain behavior even at very small strains.

The definition of "yielding" in granular media is critical since yielding in soils is likely to be a controversial statement. This is a result of the nonlinear force-deformation behavior (Mindlin and Deresiewicz, 1953) at the interparticle contacts that causes granular media to exhibit nonlinear inelastic stress-strain behavior at very

small strain levels. Therefore, strictly speaking, cohesionless aggregates, unlike metals, do not have a clear "linear elastic region" defined by an initial yield surface.

There are two distinct deformation mechanisms which take place during loading of a granular medium. At very small strains ($\gamma<10^{-2}$ %) there are no particles sliding and all macroscopic nonlinearity is the result of nonlinearlites at the inter-granular contacts and of the redistribution of contact forces (one aspect of the material fabric) during loading. The normal component of the deformation at the contact is nonlinear elastic, while the tangential component is nonlinear inelastic as a result of the slip at the edges of the contact annulus between two spheres (Mindlin and Deresiewicz, 1953). In soils, hysteric behavior is observed during low level shear strain cycling in the resonant column device, but no permanent volumetric changes or pore pressure buildup accumulates.

At larger strains ($\gamma>10^{-2}$ %), there is sliding between particles which move and rearrange themselves. Therefore, the geometric aspects of the fabric changes as well. This change of geometric fabric manifests itself by irreversible volumetric changes if the loading takes place under drained conditions. The strain level at which this occurs has been experimentally determined (Dobry, 1985) to be on the order of 10^{-2} % for the level of mean stress used in soil testing (40 - 270 kPa) and it is called the threshold strain, r_t. This sliding of particles is directly analogous to the "slip" in metals. The macroscopic strain caused by grain slipping at the contact annulus is an order of magnitude smaller than the macroscopic strain caused by grain sliding, and can be considered to be a second order effect. Therefore, one possible definition of yielding,

in a manner directly analogous to yielding in metals, is the point in stress space at which the geometric fabric of the material changes irreversibly; that is when the first grain slides. Since the sliding of the first particle is very difficult to monitor in the laboratory, yielding could be defined as the locus of all points in stress space at which the value of the octahedral shear strain is equal to, or less than 10^{-2} %.

Following the above logic, the yield will be defined as the locus of all points in stress space $[\tau_{z\theta}, (\sigma_{zz} - \sigma_{rr})/2]$ that has the same value of total (elastic plus plastic) octahedral shear strain, $\gamma^{t}_{oct} = \gamma^{e}_{oct} + \gamma^{p}_{oct}$. The value of γ^{e}_{oct} should be as close to the threshold value as possible, given the restrictions posed by the experimental device, so that γ^{p}_{oct} will be close to zero. While a criterion of an octahedral shear strain of 10^{-2} % does not necessarily imply that only one sphere has slipped, it is assumed that a small percentage of particles have slipped and that the yield loci obtained using this approach are homothetic to the true yield surface. Numerical simulations (Petrakis et. al. 1991b) support this last hypothesis. In the experiments performed by Petrakis and Dobry (Petrakis et al., 1991a; Dobry et al., 1991) at Rensselaer Polytechnic Institute, due to restrictions imposed by the accuracy of the measuring devices, the "yield" criterion was set to $3x10^{-2}$%. This value caused plastic strains to accumulate during the probing portion of the tests. The strain for yield is typically set at $1x10^{-2}$ % or less.

With the proper constitutive model, this method is expected to include most of the micro-mechanical behavior and hardening characteristics of the yield surfaces of a granular medium under various levels of pre-strain, and the observed normality and flow rules.

As mentioned previously this model is one of the advanced one. However, the major difficulty is the computation cost, and its application to clayey soils is not yet feasible.

3.4.5 Selection of Micro-Mechanical Consideration

As discussed previously, there are many approaches in order to incorporate the micro-mechanical considerations. In this study, the plastic spin is selected due to its convenience and simplicity in its formulation. There are other more rigorous methods, which may be probably better. However, the required effort to evaluate the material parameters, and incorporate them into the soil model makes them not feasible at this stage.

3.5 Formulation of the Anisotropic, Elasto-Plastic Large Strain Constitutive Relation with Micro-mechanical Considerations

3.5.1 Original Modified Cam Clay Model (isotropic)

From the equilibrium of work done and dissipated energy, equation (3.5.1) is obtained (Burland: 1965; Schoefield and Wroth: 1968) as follows:

$$p d\varepsilon_v^p + q d\varepsilon_s^p = p\{(d\varepsilon_v^p)^2 + M^2 (d\varepsilon_s^p)^2)^{1/2} \qquad (3.5.1)$$

In equation (3.5.1), the variables are defined as follows:

p = mean principal stress = $(\sigma_1 + \sigma_2 + \sigma_3) / 3 = (\sigma_1 + 2\sigma_3) / 3$

q = deviatoric stress = $(\sigma_1 - \sigma_2) / 2$

ε_v^p = plastic-volumetric strain

ε_s^p = plastic-shear strain

M = slope of critical state line in p vs. q space

From equation (3.5.1), one can derive the well known yield criterion as follows:

$$f = p^2 + p_o p + (1/M^2)q^2 = 0 \qquad (3.5.2)$$

In equation (3.5.2), p_o is the p at the hydrostatic condition (q = 0). Equation (3.5.2) is the equation of an ellipse which passes through the origin and the (p_o, 0) is as shown in Figure 3.5.1.

3.5.2 Anisotropic Modified Cam Clay Model

Equation (3.5.2) shows the evolution of the yield locus with an isotropic hardening behavior. p_o in equation (3.5.2) is the isotropic hardening parameter. However, the real soil is subjected to the anisotropic stress condition, and therefore the Anisotropic Modified Cam Clay Model (hereafter called AMCCM) is developed here following the work of Dafalias (1987). The shape of AMCCM in the principal stress space is oval shaped as shown in Figure 3.5.2. The cross section of the oval shape can be a circle, hexagon, or similar shape (not specifically known). However, one can guess that shape will be somewhere between the anisotropic von-Mises and Tresca type. When the yield locus in the principal stress space undergoes kinematic hardening, the yield locus will move around the π-plane. This behavior will appear as the rotation of the oval shape yield locus in the principal stress space. In the p vs. q plane p is the space diagonal and q is the deviatoric stress, thus the shape of the yield locus is the inclined cut of the three dimensional yield locus that appears in Figure 3.5.3. Therefore the yield locus of MCCM is of an elliptical shape. Thus the kinematic hardening will result in the rotation of the elliptical yield locus in the p vs. q space for which the origin does not change.

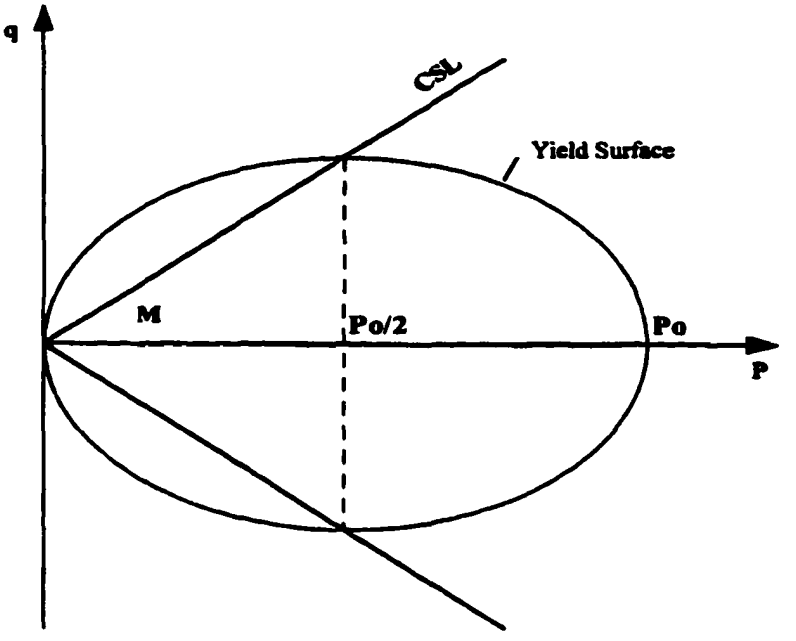

Figure 3.5.1, Yield Locus of Isotropic Cam Clay Model

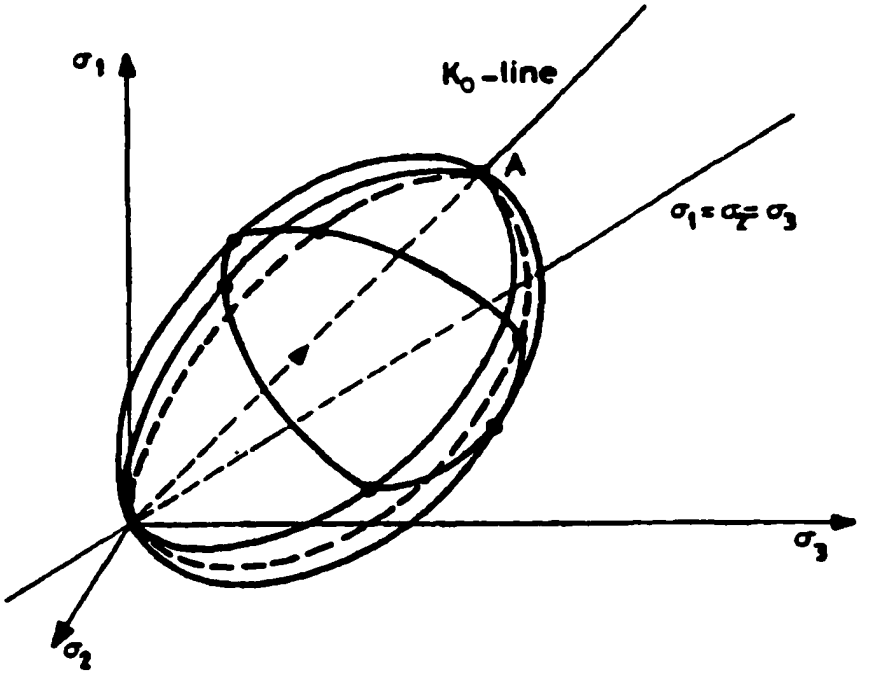

Figure 3.5.2, Anisotropic MCCM in the principal stress space
(after Banerjee and Yousif, 1986)

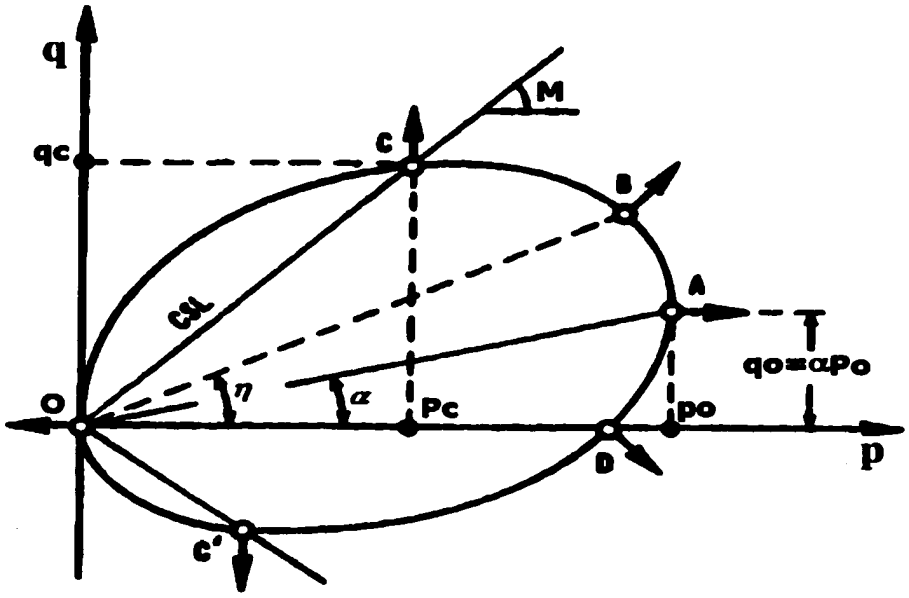

Figure 3.5.3, Kinematic hardening of AMCCM in p vs. q space (p is the mean principal stress, q is the deviatoric stress) (after Dafalias, 1987)

Consequently, the shape of the yield locus will be the distorted ellipse when subjected to the anisotropic hardening.

The anisotropic modified cam clay model for general stress state is obtained as follows (Dafalias, 1987),:

$$f = p^2 - pp_o + \frac{3}{2M^2}\{(s_{ij} - p\alpha_{ij})(s_{ij} - p\alpha_{ij}) + (p_o - p)p\alpha_{ij}\alpha_{ij}\} = 0 \quad (3.5.3)$$

$$\dot{\alpha}_{ij} = <\lambda>\{\frac{1+e_o}{\lambda-\kappa} | tr\frac{\partial f}{\partial \sigma_{mn}} | \frac{c}{p_o}(s_{ij} - xp\alpha_{ij})\} \quad (3.5.4)$$

In equation (3.5.3), <> is the Macauley bracket, <λ> is the loading index, λ is the compression index in e vs. ln p curve, κ is the recompression index in *e* vs. ln p curve, e_o is the initial void ratio, c and x are constants.

3.5.3 Elasto-Plastic Constitutive Relation

Also, from the normality rule (flow rule), equation (3.5.5) is obtained:

$$d\varepsilon_{ij}^p = \lambda\frac{\partial f}{\partial \sigma_{ij}} = \lambda B_{ij} \quad (3.5.5)$$

For the case of small elastic strains one makes use of the additive decomposition of the incremental strain,

$$d\varepsilon_{ij}^e = d\varepsilon_{ij} - d\varepsilon_{ij}^p \quad (3.5.6)$$

In order to obtain the constitutive relation one uses the following relations:

$$d\sigma_{ij} = C_{ijkl}(d\varepsilon_{kl} - d\varepsilon_{kl}^p) \quad (3.5.7a)$$

$$= C_{ijkl}d\varepsilon_{kl} - C_{ijkl}d\varepsilon_{kl}^p \quad (3.5.7b)$$

$$= C_{ijkl}d\varepsilon_{kl} - C_{ijkl}\lambda B_{kl} \quad (3.5.7c)$$

In equation (3.5.7), ε_{ij}^{e} is the elastic strain, ε_{ij} is the total strain, ε_{ij}^{p} is the plastic strain, and C_{ijkl} is the elastic stiffness matrix.

Using equations (3.5.4) and (3.5.5), the incremental stress strain relation is given as follows

$$d\sigma_{ij} = (C_{ijkl} - \frac{C_{ijkl}B_{mn}B^{T}{}_{rs}C_{mnrs} + C_{ijpq}\frac{\partial f}{\partial \alpha_{mn}}d\alpha_{mn}B_{pq}\frac{1}{3}d\varepsilon_{kl}^{-1}}{B_{ab}C_{abcd}B_{cd} - \frac{\partial f}{\partial \varepsilon_{v}^{p}}B_{aa}})d\varepsilon_{kl} \quad (3.5.8)$$

Equation (3.5.8) is the well known elasto-plastic stiffness equation in the form, $[D^{ep}] = [D^{e}] - [D^{p}]$ (where, $[D^{ep}]$ represents the elasto-plastic stiffness, $[D^{e}]$ represents the elastic stiffness, and $[D^{p}]$ represents the plastic reduction). The explanation of the variables is presented in the next section. From equation (3.5.8), one can find that the back stress α_{ij} directly affects the plastic stiffness.

3.5.4 Correlation of the Elasto-Plastic Constitutive Relation with the Material Properties

From Dafalias (1987) $\dot{\alpha}_{ij}$ is defined by equation (3.5.5). Integrating equation (3.5.5) with respect to time t, and expressing it in the incremental form, one obtains:

$$d\alpha_{ij} = 3\frac{1+e_{o}}{\lambda-\kappa}\,|\,d\varepsilon_{v}^{p}\,|\,\frac{c}{p_{a}}(ds_{ij} - xdp\alpha_{ij}) \quad (3.5.9)$$

3.5.5 Micro-Mechanical Consideration (Plastic Spin)

Comprehensive understanding of this substructure change and anisotropy is not well known yet. Theoretical and experimental studies were performed by many researchers (Anandarajah, 1994). The model presented here considers the substructure change and anisotropy, and used the anisotropic modified Cam Clay model with plastic spin.

To deal with this substructure change and related anisotropy, one should go down to the substructure level (micro-mechanical behavior of the geo-materials) essentially. As discussed earlier there are several approaches for incorporating the micro-mechanical behavior of soils into the macro-mechanical modeling of soils such as the micorplane approach (Bazant and Kim,1986), modified spin tensor (Dafalias, 1998; Lee, 1993), micro-mechanical models (Dobry et al., 1991) etc. Even though the atomic or molecular level approach will be the ultimate goal for implementing the micro-behavior of the material, however, the above mentioned methods are computationally feasible at this time (computation time, numerical error accumulation). The plastic spin tensor method modifies the spin tensor in the constitutive equation due to the substructure change. Substructure change may be illustrated by the rotation or realignment of soil grains. Rotation or realignment of the soil grains is the result of residual stresses which are embedded in the soil grains or other substructures. The embedded residual stress energy is part of the applied energy, thus the constitutive equation must consider these terms for the correct equilibrium conditions. The beauty of the plastic spin approach is that it is physically correct and can be incorporated easily into the macro-mechanical modeling.

The embedded stress is the definition of back stress. Thus by incorporating the back stress in the modified Cam Clay model, the plastic spin and the theory of mixtures, a fully anisotropic, finite strain soil constitutive equation is obtained

With the anisotropic Modified Cam Clay model, the combined isotropic and kinematic hardening behavior is simulated. In equation (3.5.8), the elasto-plastic

modulus is expressed in terms of the back stress $p\alpha_{ij}$. Using the back stress $p\alpha_{ij}$, the plastic spin is computed as will be indicated in this section. From now on $p\alpha_{ij}$ is expressed as α_{ij}, for convenience.

Equation of equilibrium of the external and internal forces in an updated Lagrangian reference frame

A schematic diagram of the updated Lagrangian reference frame is shown in Figure 3.5.4. As shown in Figure 3.5.4, the incremental scheme is used and the configuration is updated at every calculation step. From Bathe (1996), the principle of virtual work in an updated Lagrangian reference frame is obtained by equation (3.5.10):

$$ {}^{n+1}R = \int_{{}^{n}V} {}^{n+1}_{n}S_{AB}\,\delta({}^{n+1}_{n}\varepsilon_{AB})\,d^{n}V \qquad (3.5.10) $$

In equation (3.5.10), ${}^{n}V$ is the volume of the element at the n^{th} configuration, ${}^{n+1}_{n}S_{AB}$ is the second Piola – Kirchoff stress from n^{th} to $(n+1)^{th}$ configuration, $\delta\,{}^{n+1}_{n}\varepsilon_{AB}$ is the increment of Green – Lagrangian strain from n^{th} to $(n+1)^{th}$ configuration and ${}^{n+1}R$ is the external force at the $(n+1)^{th}$ configuration.

Equation (3.5.10) can be now expressed as follows:

$$ {}^{n+1}R = \int_{{}^{n}V} ({}^{n}\sigma_{AB} + \Delta_{n}S_{AB})\,\delta({}^{n}e_{AB} + {}^{n}\eta_{AB})\,d^{n}V $$

$$ = \int_{{}^{n}V} ({}^{n}\sigma_{AB}\;\delta({}^{n}e_{AB} + {}^{n}\eta_{AB})\,d^{n}V + \int_{{}^{n}V} \Delta_{n}S_{AB}\,\delta({}^{n}e_{AB} + {}^{n}\eta_{AB})\,d^{n}V \qquad (3.5.11) $$

In equation (3.5.11), $\Delta_{n}S_{AB}$ is the increment of the second Piola – Kirchoff stress at the n^{th} configuration. ${}^{n}e_{AB}$ is the linear strain at the n^{th} configuration, and ${}^{n}\eta_{AB}$ is the non-linear strain at the n^{th} configuration.

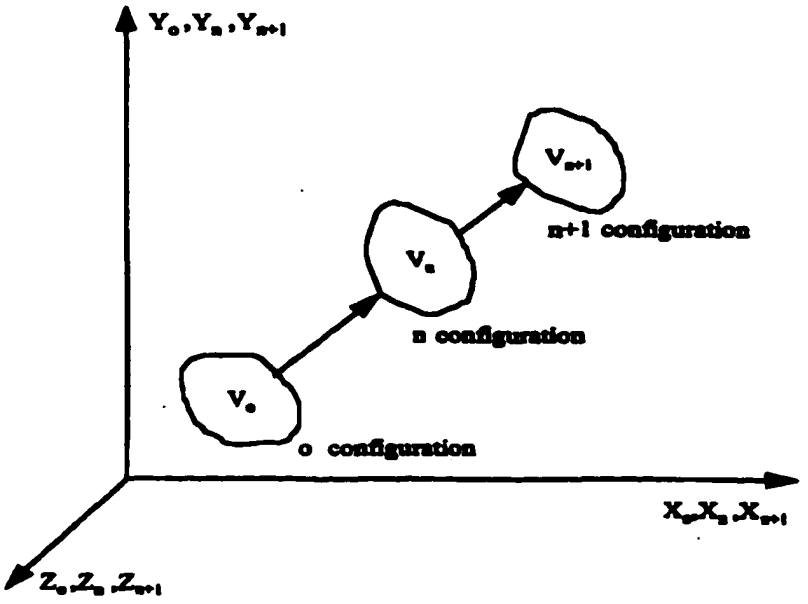

Figure 3.5.4, Updated Lagrangian reference frame

In equation (3.5.11), $\Delta_n S_{AB}$ can be expressed as:

$$\Delta_n S_{AB} = \int_t^{t+\Delta t} \dot{S}_{AB} dt \tag{3.5.12}$$

In equation (3.5.12) $\dot{S}_{AB}$ is the time rate of second Piola-Kirchoff stress. From Voyiadjis and Abu-Farsakh (1997), Voyiadjis (1988), and Voyiadjis and Kattan (1989), $\dot{S}_{AB}$ can be expressed as follows considering the effective stress and the pore water pressure, but assuming the plastic spin to be zero:

$$\dot{S}_{AB} = D^{*}_{ABCD}\dot{\varepsilon}_{CD} + J^{s} X^{s}_{A,a} X^{s}_{B,b} \dot{P}_w \delta_{ab} \tag{3.5.13}$$

The superscript "s" is used to distinguish the stress and strains of soils from those of water. In equation (3.5.13), D^{*}_{ABCD} is expressed as follows:

$$\begin{aligned} D^{*}_{ABCD} = [&D_{abcd} - \sigma'^{s}_{cb}\delta_{ad} - \sigma'^{s}_{ac}\delta_{bd} + \sigma'^{s}_{ab}\delta_{cd} + P_w\delta_{ab}\delta_{bd} \\ &- 2P_w\delta_{ac}\delta_{bd}]J^{s} X^{s}_{A,a} X^{s}_{B,b} X^{s}_{C,c} X^{s}_{D,d} \end{aligned} \tag{3.5.14}$$

The symbol "' " is used to describe the effective stress. In equations (3.5.13) through (3.5.14), D^{*}_{ABCD} is the modified elasto plastic modulus, $X^{s}_{A,a} = \partial^{n+1} X^{s}_{A} / \partial^{n} X^{s}_{a}$, $\dot{\varepsilon}_{CD}$ is the strain rate, P_w is the pore water pressure, $\dot{P}_w$ is the pore pressure rate, D_{abcd} is the elasto-plastic modulus, and J is the Jacobian.

However, the plastic spin may not be neglibible in reality though it is agreed that the plastic spin is not considered in the general (isotropic) MCCM. In this paper, kinematic hardening is coupled with AMCCM, and the plastic spin is incorporated.

Plastic Spin

By incorporating the plastic spin, equation (3.5.13) is modified such that:

$$\dot{S}_{AB} = [D_{abcd} - \sigma'^{s}_{cb}\delta_{ad} - \sigma'^{s}_{ac}\delta_{bd} + \sigma'^{s}_{ab}\delta_{cd} - P_w\delta_{ab}\delta_{bd}$$

$$+2P_w\delta_{ac}\delta_{bd}]J^s X^s_{A,a}X^s_{B,b}X^s_{C,c}X^s_{D,d}\dot{\varepsilon}_{CD}$$
$$+[\sigma'^s_{mb}W^{s''}_{ma}+\sigma'^s_{aj}W^{s''}_{jb}]J^s X^s_{A,a}X^s_{B,b}+J^s X^s_{A,a}X^s_{B,b}\dot{P}_w\delta_{ab} \qquad (3.5.15)$$

Equation (3.5.15) is expressed into a simpler form such that:

$$S'_{AB}=D^{*}_{ABCD}\dot{\varepsilon}_{CD}+D^{**}_{ABCD}\dot{\varepsilon}_{CD}-J^s X^s_{A,a}X^s_{B,b}\dot{P}_w\delta_{ab} \qquad (3.5.16)$$

In equation (3.5.16), D^{*}_{ABCD} is the one defined by equation (3.5.14).

D^{**}_{ABCD} is explained as follows. The relation between the plastic spin tensor and the backstress tensor is given by Dafalias (1983, 1985), Lee et al. (1983), Paulin and Pecherski (1985), and Voyiadjis and Kattan (1989, 1990, 1991) as shown below:

$$W^{s''}=\dot{\eta}(\alpha d^{s''}-d^{s''}\alpha) \qquad (3.5.17)$$

In equation (3.5.17), $\dot{\eta}$ is a scalar function. The strain rate d^s represents the strain rate of solid grains, and can be decomposed as shown below:

$$d^s_{mn}=d^{s'}_{mn}+d^{s''}_{mn} \qquad (3.5.18)$$

In equation (3.5.18), d^s_{mn} is the total strain rate, $d^{s'}_{mn}$ is the elastic strain rate, and $d^{s''}_{mn}$ is the plastic strain rate. d^s_{mn} is the same as $\dot{\varepsilon}_{mn}$, however, it is denoted as d^s_{mn} for consistency with most notations implying strain rates for finite deformations.

The plastic component of the strain rate can be expressed as follows:

$$d^{s''}_{ij}=\frac{<L>}{H}n_{ij} \qquad (3.5.19)$$

In equation (3.5.19), L is $\overset{\circ}{\sigma}{}^{ss}_{ij}\,n_{ij}$, H is the hardening modulus, and n_{ij} is the normal to the yield surface. For the elastic behavior one obtains:

$$\overset{\circ}{\sigma}{}^{ss}_{kl}=E'^s_{klmn}d'^s_{mn} \qquad (3.5.20)$$

In equation (3.5.20) $E^{'s}_{klmn}$ is the modulus of elasticity corresponding to the solid grains, and is expressed as follows:

$$E^{'s}_{klmn} = \lambda^s \delta_{kl}\delta_{mn} + G^s(\delta_{km}\delta_{ln} + \delta_{kn}\delta_{lm}) \tag{3.5.21}$$

In equation (3.5.21), λ^s and G^s are Lame's constants. Using equations (3.5.18), (3.5.19), and (3.5.20), equation (3.5.22) is obtained.

$$\overset{\circ}{\sigma}{}^{'s}_{kl} = E^{'s}_{klmn}\left(d^{'s}_{mn} - \frac{<L>}{H} n_{mn}\right) \tag{3.5.22}$$

Taking the inner product of the corotational stress tensor with the normal to the yield surface $\overset{\circ}{\sigma}{}^{'s}_{kl}\, n_{kl}$, one obtains:

$$\overset{\circ}{\sigma}{}^{'s}_{kl}\, n_{kl} = E^{'s}_{klmn} d^{s}_{mn} n_{kl} - \frac{E^{'s}_{klmn} L\, n_{kl} n_{mn}}{H} \tag{3.5.23}$$

But $\overset{\circ}{\sigma}{}^{'s}_{kl}\, n_{kl}$ = L, thus equation (3.5.23) is rewritten into the following form:

$$L(H + E^{'s}_{klmn} n_{kl} n_{mn}) = H E^{'s}_{klmn} d^{s}_{mn} n_{kl} \tag{3.5.24}$$

One can now solve for L:

$$L = \frac{H E^{'s}_{klmn} d^{s}_{mn} n_{kl}}{H + E^{'s}_{abcd} n_{ab} n_{cd}} \tag{3.5.25-a}$$

$$= cH E^{'s}_{klmn} d^{s}_{mn} n_{kl} \tag{3.5.25-b}$$

In equation (3.5.25-b), c is given as follows:

$$c = \frac{H}{H + D^{'s}_{abcd} n_{ab} n_{cd}} \tag{3.5.26}$$

Substituting equation (3.5.25-b) into equation (3.5.19), one obtains:

$$d^{s''}_{ij} = \frac{c E^{'s}_{klmn} d^{s}_{mn} n_{kl}}{H} n_{ij} \tag{3.5.27}$$

Equation (3.5.27) may be rewritten in a simpler form:

$$d_{ij}^{s^*} = M_{ijmn} d_{mn}^{s} \tag{3.5.28}$$

In equation (3.5.28), $\mathbf{M} = c\ C'^{ss}_{klmn} n_{kl} n_{ij} / H$.

Substituting equation (3.5.28) into equation (3.5.17) gives:

$$W^{s^*} = \dot{\eta}(\alpha_{am} d_{mb}^{s^*} - d_{an}^{s^*} \alpha_{nb}) \tag{3.5.29}$$

$$= \dot{\eta} N_{abcd} d_{cd}^{s} \tag{3.5.30}$$

In equation (3.5.30), N_{abcd} is defined as ($\alpha_{am} M_{mbcd} - M_{ancd} \alpha_{nb}$).

Constitutive Relation Including Plastic Spin

The expression $[\sigma'^{s}_{mb} W_{ma}^{s^*} + \sigma'^{s}_{aj} W_{jb}^{s^*}]$ in equation (3.5.15) is obtained as follows:

$$[\sigma'^{s}_{mb} W_{ma}^{s^*} + \sigma'^{s}_{aj} W_{jb}^{s^*}] = [\sigma'^{s}_{mb} \dot{\eta} N_{macd} d_{cd}^{s} + \sigma'^{s}_{aj} \dot{\eta} N_{jbcd} d_{cd}^{s}] \tag{3.5.31-a}$$

$$= \dot{\eta}[\sigma'^{s}_{mb} N_{macd} + \sigma'^{s}_{aj} N_{jbcd}] d_{cd}^{s} \tag{3.5.31-b}$$

By making use of the relation $d_{cd}^{s} = X_{C,c} X_{D,d} \dot{\varepsilon}_{CD}$, and multiplying $J\ X_{A,a} X_{B,b}$ to both sides equation (3.5.31-b) is rewritten in the following form:

$$[\sigma'^{s}_{mb} W_{ma}^{s^*} + \sigma'^{s}_{aj} W_{jb}^{s^*}] J\ X_{A,a} X_{B,b}$$

$$= \dot{\eta}[\sigma'^{s}_{mb} N_{macd} + \sigma'^{s}_{aj} N_{jbcd}](J X_{A,a} X_{B,b} X_{C,c} X_{D,d}) \dot{\varepsilon}_{CD} \tag{3.5.32-a}$$

$$= D^{**}_{ABCD} \dot{\varepsilon}_{CD} \tag{3.5.32-b}$$

In equation (3.5.32-b) D^{**}_{ABCD} is defined as:

$$D^{**}_{ABCD} = \dot{\eta}[\sigma'^{s}_{mb} N_{macd} + \sigma'^{s}_{aj} N_{jbcd}](J X_{A,a} X_{B,b} X_{C,c} X_{D,d}) \tag{3.5.33}$$

From equation (3.5.33) and (3.5.16), equation (3.5.34) is obtained:

$$\dot{S}_{AB} = D^{*}_{ABCD} \dot{\varepsilon}_{AB} + D^{**}_{ABCD} \dot{\varepsilon}_{AB} - J^{s} X^{s}_{A,a} X^{s}_{B,b} \dot{P}_{w} \delta_{ab} \tag{3.5.16}$$

$$\dot{S}_{AB} = D^{***}_{ABCD}\dot{\varepsilon}_{AB} - J^s X^s_{A,a} X^s_{B,b} \dot{P}_w \delta_{ab} \tag{3.5.34}$$

In equation (3.5.34), D^{***}_{ABCD} is defined as $D^{*}_{ABCD} + D^{**}_{ABCD}$. Substituting equation (3.5.34) into equation (3.5.13) one obtains the new expression for the second Piola-Kirchhoff stress:

$$\Delta_n S_{AB} = \int_t^{t+\Delta t} \dot{S}_{AB} dt \tag{3.5.13}$$

$$= D^{***}_{ABCD}\Delta\varepsilon_{CD} + J^s X^s_{A,a} X^s_{B,b} \Delta P_w \delta_{ab} \tag{3.5.35}$$

Substituting equation (3.5.35-b) into equation (3.5.12) and neglecting $\Delta\eta\cdot\eta$ term (infinitesimal in incremental scheme), equation (3.5.36) is obtained:

$$\begin{aligned}
{}^{n+1}R = & \int_{{}^nV} ({}^n\sigma'^s_{AB} + {}^nP_w\delta_{AB})\delta^n e_{AB} d^nV \\
& + \int_{{}^nV} ({}^n\sigma'^s_{AB} + {}^nP_w\delta_{AB})\delta^n \eta_{AB} d^nV \\
& + \int_{{}^nV} D^{***}_{ABCD}(\Delta_n e_{AB} + \Delta^n\eta_{AB})\delta^n e_{AB} d^nV \\
& + \int_{{}^nV} D^{***}_{ABCD}(\Delta_n e_{AB})\delta^n \eta_{AB} d^nV \\
& + \int_{{}^nV} J^s X^s_{A,a} X^s_{B,b_w} \delta_{ab} \Delta P_w ({}^n e_{AB} + {}^n\eta_{AB}) d^nV
\end{aligned} \tag{3.5.36}$$

Equation (3.5.36) is the equation of equilibrium of the external and internal forces in an updated Lagrangian reference frame expressed in terms of the effective stress and pore water pressure.

So far, the relationship between the pore water pressure and the hydraulic conductivity is not shown. This relationship can be derived from Prevost (1980) such that:

$$-div\,[(n^w/\rho^w)\,\boldsymbol{K}^{ws}(grad\,P_w - \rho_w\boldsymbol{b} + \rho_w\boldsymbol{a}^w)] + div\,\boldsymbol{v}^s = 0 \qquad (3.5.37)$$

In equation (3.5.37), ρ^s is the mass density of the soil, ρ^w is the mass density of the water, $\mathbf{a}^w$ is the acceleration of water, $\mathbf{K}^{ws}$ is the hydraulic conductivity tensor, ρ_w is the density of water, $\mathbf{v}^s$ is the solid velocity, P_w is the pore water pressure, and $\mathbf{b}$ is the body force vector. In the case when the acceleration is negligible, equation (3.5.37) reduces to;

$$-div\,[(n^w/\rho^w)\,\boldsymbol{K}^{ws}(grad\,P_w - \rho_w\boldsymbol{b})] + div\,\boldsymbol{v}^s = 0 \qquad (3.5.38)$$

For an upgraded Lagrangian reference frame, equation (3.5.38) can be expressed as follows:

$$J^s C^s_{ij}\dot{\varepsilon}_{ij} - JC^{s-1}_{ij}C^{s-1}_{ij}X^s_{D,a}\frac{\partial}{\partial X_p}\times[\frac{n_w}{\rho_w}K^{ws}_{AB}X^s_{a,A}(\frac{\partial P_w}{\partial X_B} - \rho_w B_B)] = 0 \qquad (3.5.39)$$

In equation (3.5.39), $C^s_{ij} = X^s_{K,I}X^s_{K,I}$, $\dot{\varepsilon}_{ij}$ is the strain rate tensor, $X^s_{a,A} = \partial^{n+1}X_a/\partial^n X_A$, $B_b = b_b/X^s_{b,B}$, and J is the Jacobian. Using equations (3.5.37) and (3.5.39), the coupling of the stress, deformation, pore water pressure, and hydraulic conductivity is obtained. In matrix form, the coupling of equations (3.5.36) and (3.5.39) is expressed as shown below:

$$\begin{bmatrix} {}_nK & -{}_n\Omega \\ -{}_n\Omega^t & {}_n\Psi\delta t \end{bmatrix}\begin{bmatrix}\Delta U \\ \Delta W\end{bmatrix} = \begin{bmatrix} {}_n\Phi \\ {}_n\Pi\end{bmatrix} \qquad (3.5.40)$$

In equations (3.5.40), ${}_nK$ is the stiffness matrix, ${}_n\Omega$ is the coupling matrix, ${}_n\Psi$ is the flow matrix, ΔU is the incremental nodal displacement, ΔW is the incremental pore water pressure, and t is the incremental time. More details of equations (3.5.40) are given below:

$$ {}_nK = {}_nK_L + {}_nK_{nL} + {}_n K^T_{nL} + {}_nK^s \tag{3.5.41} $$

$$ {}_nK_L = \int_{{}^nV} {}_nB^T_L D^{***}\, {}_nB_L d^nV \tag{3.5.42} $$

$$ {}_nK_{nL} = \int_{{}^nV} B^T_L D^{***}\, {}_nB_{NL} d^nV \tag{3.5.43} $$

$$ {}_nK^s = \int_{{}^nV} {}_nB^{*T}_{NL}\, {}^n\sigma_b B^*_{NL} d^nV \tag{3.5.44} $$

B^*_{NL} is the geometric nonlinear strain displacement matrix

ΔU = incremental nodal displacement

$$ {}_n\Omega = \int_{{}^nV} J^s X^s_{A,a} X^s_{B,b} ({}_nB^T_L + {}_nB^T_{nl}) \bar{N}_{ab} d^nV \tag{3.5.45} $$

$$ \bar{N} = mN, m^T = \{1,1,0\} \tag{3.5.46} $$

ΔW = incremental nodal pore water pressure

$$ {}_n\Phi = {}^{n+1}R - \int_{{}^nV} {}_nB^T_L\, {}^n\sigma \; d^nV \tag{3.5.47} $$

$$ {}_n\Psi = \int_{{}^nV} J^s (n^w / \rho_w) C^{s-1}_{ij} C^{s-1}_{ij}\, {}_nK^{ws}_{AB} N_{,A} N_{,B} d^nV \tag{3.5.48} $$

$$ {}_n\Pi = \delta G - \delta\Psi W^n + \int_{{}^nS} q_n \bar{P}_w d^nV \tag{3.5.49} $$

$$ G = -\int_{{}^nV} J^s n^w C^{s-1}_{ij} C^{s-1}_{ij}\, {}_nK^{ws}_{AB} N_{,A} N_{,B} d^nV \tag{3.5.50} $$

Thus, by solving equation (3.5.40), one can predict the behavior of the soil with AMCCM which is coupled with the large strain elasto-plastic constitutive equations in an updated Lagrangian reference frame which is again coupled with the theory of mixtures.

The previously discussed AMCCM and plastic spin theory were coded in a FORTRAN finite element program with the incremental scheme and analyses were carried out for the piezocone penetration test.

3.6 Numerical Formulation

The finite element discretization is used here for the displacement **u** and the pore water pressure P_w as follows:

$$\mathbf{u} = \mathbf{h} \cdot \mathbf{U} \tag{3.5.51}$$

$$P_w = \mathbf{N} \cdot W \tag{3.5.52}$$

In equation (3.5.52), **h** is the displacement shape function, **N** is the pore water pressure shape functions, **U** is the nodal displacement, and W is the nodal pore water pressure. The linear and nonlinear strains can be expressed as follows:

$$\mathbf{e} = \mathbf{B}_L \cdot \mathbf{U} \tag{3.5.53a}$$

$$\boldsymbol{\eta} = \frac{1}{2}\mathbf{B}_{NL} \cdot \mathbf{U} \tag{3.5.53b}$$

The variation of the linear and nonlinear strains are given as follows:

$$\delta\mathbf{e} = \mathbf{B}_L \cdot \delta\mathbf{U} \tag{3.5.54a}$$

$$\delta\boldsymbol{\eta} = \frac{1}{2}\mathbf{B}_{NL} \cdot \delta\mathbf{U} \tag{3.5.54b}$$

The pore water pressure gradient is given such that:

$$\frac{\partial P_w}{\partial X_B} = \mathbf{N}_{,\mathbf{B}} W \tag{3.5.54c}$$

In equation (3.5.54) $\mathbf{B}_L$ and $\mathbf{B}_{NL}$ are the linear and nonlinear strain-displacement matrices. Substitution of equations (3.5.52) and (3.5.54) into equation (3.5.36), one obtains:

$$\delta \mathbf{U}^T ({}_n\mathbf{K}_L + {}_n\mathbf{K}_{NL} + {}_n\mathbf{K}_{NL}^T + {}_n\mathbf{K}^s)\Delta\mathbf{U} - \delta\mathbf{U}^T \, {}_n\boldsymbol{\Omega}\Delta\mathbf{W} = \delta\mathbf{U}^T {}_n\boldsymbol{\Phi} \quad (3.5.55)$$

The equation is valid for any $\delta\mathbf{U}^T$ and therefore one obtains:

$$({}_n\mathbf{K}_L + {}_n\mathbf{K}_{NL} + {}_n\mathbf{K}_{NL}^T + {}_n\mathbf{K}^s)\Delta\mathbf{U} - {}_n\boldsymbol{\Omega}\Delta\mathbf{W} = {}_n\boldsymbol{\Phi} \quad (3.5.56)$$

Making use of the following expression:

$${}_n\mathbf{K} = ({}_n\mathbf{K}_L + {}_n\mathbf{K}_{NL} + {}_n\mathbf{K}_{NL}^T + {}_n\mathbf{K}^s)$$

the above equation is expressed as follows:

$${}_n\mathbf{K}\Delta\mathbf{U} - {}_n\boldsymbol{\Omega}\Delta\mathbf{W} = {}_n\boldsymbol{\Phi} \quad (3.5.57)$$

The components of ${}_n\mathbf{K}$ are expressed as follows:

$${}_n\mathbf{K}_L = \int_{n_V} {}_n\mathbf{B}_L^T D^{***} {}_n\mathbf{B}_L \, d^nV \qquad \text{(linear stiffness matrix)} \quad (3.5.58)$$

$${}_n\mathbf{K}_{NL} = \int_{n_V} {}_n\mathbf{B}_L^T D^{***} {}_n\mathbf{B}_{NL} \, d^nV \qquad \text{(non-linear stiffness matrix)} \quad (3.5.59)$$

$${}_n\mathbf{K}^s = \int_{n_V} {}_n\mathbf{C}_{NL} \, d^nV \quad \text{(non-linear geometric stiffness matrix)} \quad (3.5.60\text{-a})$$

where, $\mathbf{C}_{NL}$ is

$${}_n\mathbf{C}_{NL} = {}_n\mathbf{B}^{*T}_{NL} \, {}^n\boldsymbol{\sigma} \, {}_n\mathbf{B}_{NL} \quad (3.5.60\text{-b})$$

${}_n\boldsymbol{\Omega}$ in equation (3.5.85) is expressed as follows:

$${}_n\boldsymbol{\Omega} = \int_{n_V} J^s X^s_{A,a} X^s_{B,b} ({}_nB_L^T + {}_nB_{NL}^T)\overline{N}_{ab} \, d^nV \qquad \text{(coupling matrix)} \quad (3.5.61)$$

where

$$\overline{\mathbf{N}} = \mathbf{m}\mathbf{N} \quad (3.5.62)$$

In equation (3.5.62), $\mathbf{m}^T = \{1\ 1\ 0\}$ for two dimensions and $\mathbf{m}^T = \{1\ 1\ 1\ 0\ 0\ 0\}$ for three dimensions such that:

$$\sigma = \sigma' + \mathbf{m}P_w \quad (3.5.63)$$

${}_n\Phi$ in equation (3.5.58) is expressed as follows:

$${}_n\Phi = {}^{n+1}\mathbf{R} - \int_{n_V} {}_n\mathbf{B}_L^T {}^n\sigma \, d^nV \tag{3.5.64}$$

The condition that the continuity equation (3.5.39) applies throughout the continuum and using Galerkin's weighted residual method requires that:

$$\int_{n_V} [J^s C_{ij}^{s^{-1}} \dot{\varepsilon}_{ij} - J^s C_{ij}^{s^{-1}} C_{ij}^{s^{-1}} \frac{\partial}{\partial X_A} \{\frac{n^w}{\gamma_w} K_{AB}^{WS} (\frac{\partial P_w}{\partial X_B} - \rho_w B_B)\}] \overline{P}_w d^nV = 0 \tag{3.5.65}$$

The weak form of above equation is obtained by applying Green's theory (Zienkiewicz, 1977) as follows:

$$\int_{n_V} J^s C_{ij}^{s^{-1}} \dot{\varepsilon}_{ij} \overline{P}_w d^nV - \int_{n_V} \frac{n^w}{\gamma_w} J^s C_{RS}^{s\ -1} C_{RS}^{s\ -1} K_{AB}^{WS} (\frac{\partial P_w}{\partial X_B} - \rho_w B_B)\}] \frac{\partial \overline{P}_w}{\partial X_A} d^nV$$

$$- \int_{n_S} q_n \overline{P}_w d^nA = 0 \tag{3.5.66}$$

where,

$$\overline{P}_w = \mathbf{N}\overline{w} \tag{3.5.67}$$

is the weighted residual (virtual pore pressure). The pressure gradient is given as follows:

$$\frac{\partial \overline{P}_w}{\partial X_A} = \mathbf{N}_{,A} \ \overline{w} \tag{3.5.68}$$

q_n is the seepage velocity normal to the boundary surface. Substituting equation (3.5.54) and (3.5.68) into equation (3.5.66), one obtains:

$$-{}_n\Omega^T \dot{\mathbf{u}} + {}_n\Psi W = \mathbf{G} - \int_{n_S} q_n \overline{P}_w d^nA \tag{3.5.69}$$

$${}_n\Psi = \int_{n_V} \frac{n^w}{\gamma_w} J^s C_{RS}^{s\ -1} C_{RS}^{s\ -1} K_{AB}^{WS} N_{,A} N_{,B} B_B d^nV \tag{3.5.70}$$

Equation (3.5.69) can be solved by various processes of time stepping as follows:

$$\mathbf{u}^{n+1} = \mathbf{u}^{n} + \delta \mathbf{t}_{n}\, \dot{\mathbf{u}}^{n+\beta} \tag{3.5.71}$$

where

$$\mathbf{u}^{n+\beta} = (1-\beta)\dot{\mathbf{u}}^{n} + \beta \dot{\mathbf{u}}^{n+1} \tag{3.5.72}$$

such that a particular value of β corresponds to a particular integration rule. For example, β=0 corresponds to a forward difference integration, β = 1/2 corresponds to a linear variation and the trapezoidal integration, and β = 1 corresponds to a backward difference integration. Considering the stability of the numerical time integration scheme, it is found that for stability $\beta \geq \frac{1}{2}$ is required (Prevost, 1981). Here the backward difference scheme is adapted with β = 1. Therefore equation (3.5.71) becomes:

$$\mathbf{u}^{n+1} = \mathbf{u}^{n} + \delta \mathbf{t}_{n} \dot{\mathbf{u}}^{n+1} \tag{3.5.73}$$

Equation (3.5.69) maybe expressed as follows:

$$-_{n}\, \Omega^{T} \delta \mathbf{t}\ \dot{\mathbf{u}}^{n+1} +_{n} \Psi \delta \mathbf{t}_{n}\, W^{n+1} = \delta \mathbf{t}_{n} \mathbf{G} - \delta \mathbf{t} \int_{n_S} q_{n} \overline{P}_{w} d^{n} A \tag{3.5.74}$$

Utilizing the following relationships:

$$\Delta \mathbf{U} = \delta \mathbf{t}_{n} \dot{\mathbf{u}}^{n+1} \tag{3.5.75}$$

$$\mathbf{W}^{n+1} = \mathbf{W}^{n} + \Delta \mathbf{W} \tag{3.5.76}$$

equation (3.5.74) can be rewitten as follows:

$$-_{n}\, \Omega^{T}\, \Delta \mathbf{U} +_{n} \Psi \delta \mathbf{t} \Delta \mathbf{W} =_{n} \Pi \tag{3.5.77}$$

where, $_{n}\Pi$ is defined as follows:

$$ {}_n\Pi = \delta \mathbf{t}_n \mathbf{G} - \delta \mathbf{t}_n \, \Psi W^n - \int_{n_S} q_n \overline{P}_w d^n A \tag{3.5.78} $$

Upon assembly of equations (3.5.58) and (3.5.77), one obtains the following coupled equations for the two-phase media:

$$ \begin{bmatrix} {}_nK & -{}_n\Omega \\ -{}_n\Omega^t & \delta t_n \Psi \end{bmatrix} \begin{bmatrix} \Delta U \\ \Delta W \end{bmatrix} = \begin{bmatrix} {}_n\Phi \\ {}_n\Pi \end{bmatrix} \tag{3.5.79} $$

3.7 Finite Element Implementation

The proposed coupled system of equations derived earlier are implemented into the finite element program CS-Soil developed by the author under the supervision of Dr. Voyiadjis. This program is used for the solution of the time-dependent deformation of the soil problem. In order to illustrate the process, element matrices are derived for 8-noded isoparametric plane strain element Q8P4. The use of the isotroparametric elements has an advantage due to their capability in describing the curved boundaries in the deformed configuraions. The shape functions N for the 8-noded isoparametric element is given as follows:

$$ \mathbf{h} = \begin{bmatrix} h_1 & 0 & h_2 & 0 & h_3 & 0 & h_4 & 0 & h_5 & 0 & h_6 & 0 & h_7 & 0 & h_8 & 0 \\ 0 & h_1 & 0 & h_2 & 0 & h_3 & 0 & h_4 & 0 & h_5 & 0 & h_6 & 0 & h_7 & 0 & h_8 \end{bmatrix} \tag{3.5.80} $$

The element displacements are related to the nodal displacement using the shape functions **h** as follows:

$$ u_i = \sum_{k=1}^{8} h_k u_i^{(k)} \tag{3.5.81} $$

The linear and nonlinear incremental strains are related to the displacement derivatives as follows:

$$ {}_n e_{AB} = \frac{1}{2}({}_n u_{A,B} + {}_n u_{B,A}) \tag{3.5.82} $$

$$ {}_n \eta_{AB} = \frac{1}{2}({}_n u_{K,A} \cdot {}_n u_{K,B}) \tag{3.5.83} $$

Since the shape functions h are expressed in terms of the local coordinates r and s, the chain rule is applied in order to refer the displacement derivatives in terms of the global coordinates. The chain rule implies the following:

$$ \begin{Bmatrix} \frac{\partial h}{\partial r} \\ \frac{\partial h}{\partial s} \end{Bmatrix} = [J] \begin{Bmatrix} \frac{\partial h}{\partial {}^n X_1} \\ \frac{\partial h}{\partial {}^n X_2} \end{Bmatrix} \tag{3.5.84} $$

where

$$ [J] = \begin{bmatrix} J_{11} & J_{12} \\ J_{21} & J_{22} \end{bmatrix} = \begin{bmatrix} \frac{\partial {}^n X_1}{\partial r} & \frac{\partial {}^n X_2}{\partial r} \\ \frac{\partial {}^n X_1}{\partial s} & \frac{\partial {}^n X_2}{\partial s} \end{bmatrix} \tag{3.5.85} $$

The inverse of equation (3.5.84) gives the following relations:

$$ \begin{Bmatrix} \frac{\partial h}{\partial {}^n X_1} \\ \frac{\partial h}{\partial {}^n X_2} \end{Bmatrix} = [J]^{-1} \begin{Bmatrix} \frac{\partial h}{\partial r} \\ \frac{\partial h}{\partial s} \end{Bmatrix} \tag{3.5.86} $$

The displacement derivatives with respect to the global coordinates are given as follows:

$$ \frac{\partial u_i}{\partial {}^n X_j} = \sum_{k=1}^{8} \frac{\partial h_k}{\partial {}^n X_j} U^{(k)} \qquad (i = 1, 2 ; j = 1, 2) \tag{3.5.87} $$

where

$$\frac{\partial h_k}{\partial {}^nX_j} = J_{j1}^{-1}\frac{\partial h_k}{\partial r} + J_{j2}^{-1}\frac{\partial h_k}{\partial s} \tag{3.5.88}$$

By using the previous expressions and the nodal displacements, the deformation gradient matrix **F** for the increment displacement can be obtained as follows:

$$\mathbf{F} = \left\{\frac{\partial \mathbf{u}_i}{\partial {}^nX_j}\right\} = \begin{Bmatrix} \frac{\partial \mathbf{u}_1}{\partial {}^nX_1} & \frac{\partial \mathbf{u}_1}{\partial {}^nX_2} \\ \frac{\partial \mathbf{u}_2}{\partial {}^nX_1} & \frac{\partial \mathbf{u}_2}{\partial {}^nX_2} \end{Bmatrix} \tag{3.5.89}$$

Once the deformation gradient matrix is obtained, the linear and nonlinear incremental strains can be computed. Using the definition of equation (3 5.82), the linear strain displacement matrix $\mathbf{B_L}$ is expressed as follows:

$$[\mathbf{B}_L] = \begin{bmatrix} {}^nh_{1,1} & 0 & {}^nh_{2,1} & 0 & {}^nh_{3,1} & \cdots & {}^nh_{7,1} & 0 & {}^nh_{8,1} & 0 \\ 0 & {}^nh_{1,2} & 0 & {}^nh_{2,2} & 0 & \cdots & 0 & {}^nh_{7,2} & 0 & {}^nh_{82} \\ {}^nh_{1,2} & {}^nh_{1,1} & {}^nh_{2,2} & {}^nh_{2,1} & {}^nh_{3,2} & \cdots & {}^nh_{7,2} & {}^nh_{7,1} & {}^nh_{82} & {}^nh_{8,1} \end{bmatrix} \tag{3.5.90}$$

From equation (3.5.90), the nonlinear strain-displacement matrix $\mathbf{B_{NL}}$ can be expressed as follows:

$$\mathbf{B}_{\mathrm{NL}} = \mathbf{G}\cdot\mathbf{Q}\cdot\mathbf{H} \tag{3.5.91}$$

where

$$[\mathbf{G}] = \begin{bmatrix} {}^nh_{1,1} & 0 & {}^nh_{1,1} & 0 & {}^nh_{2,1} & 0 & \cdots & {}^nh_{8,1} & 0 & {}^nh_{8,1} & 0 \\ 0 & {}^nh_{1,2} & 0 & {}^nh_{1,2} & 0 & {}^nh_{2,2} & \cdots & 0 & {}^nh_{8,2} & 0 & {}^nh_{82} \\ {}^nh_{1,2} & {}^nh_{1,1} & {}^nh_{1,2} & {}^nh_{1,1} & {}^nh_{2,2} & {}^nh_{2,1} & \cdots & {}^nh_{8,2} & {}^nh_{8,1} & {}^nh_{82} & {}^nh_{8,1} \end{bmatrix} \tag{3.5.92}$$

$$[\mathbf{Q}]^T = \begin{bmatrix} {}^n u_1^1 & 0 & 0 & 0 & {}^n u_1^2 & 0 & 0 & 0 & \dots & {}^n u_1^8 & 0 & 0 & 0 \\ 0 & {}^n u_1^1 & 0 & 0 & 0 & {}^n u_1^2 & 0 & 0 & 0 & \dots & {}^n u_1^8 & 0 & 0 \\ 0 & 0 & {}^n u_2^1 & 0 & 0 & 0 & {}^n u_2^2 & 0 & 0 & 0 & \dots & {}^n u_2^8 & 0 \\ 0 & 0 & 0 & {}^n u_2^1 & 0 & 0 & 0 & {}^n u_2^2 & 0 & 0 & 0 & \dots & {}^n u_2^8 \end{bmatrix} \quad (3.5.93)$$

$$[\mathbf{H}] = \begin{bmatrix} {}^n h_{1,1} & 0 & {}^n h_{2,1} & 0 & \dots & {}^n h_{7,1} & 0 & {}^n h_{8,1} & 0 \\ {}^n h_{1,2} & 0 & {}^n h_{2,2} & 0 & \dots & {}^n h_{7,2} & 0 & {}^n h_{82} & 0 \\ 0 & {}^n h_{1,1} & 0 & {}^n h_{2,1} & \dots & 0 & {}^n h_{7,1} & 0 & {}^n h_{8,1} \\ 0 & {}^n h_{1,2} & 0 & {}^n h_{2,2} & \dots & 0 & {}^n h_{7,2} & 0 & {}^n h_{8,2} \end{bmatrix} \quad (3.5.94)$$

The nonlinear matrix ${}_n\mathbf{C}_{NL}$ is given as follows:

$$[{}_n\mathbf{C}_{NL}] = [{}_n\mathbf{B}^*_{NL}]^T [{}_n\boldsymbol{\sigma}][{}_n\mathbf{B}^*_{NL}] \quad (3.5.95)$$

The geometric nonlinear strain displacement matrix $[\mathbf{B}^*_{NL}]$ can be arranged in the following form:

$$[B^*_{NL}] = \begin{bmatrix} {}^n h_{1,1} & 0 & {}^n h_{2,1} & 0 & \dots & {}^n h_{7,1} & 0 & {}^n h_{8,1} & 0 \\ {}^n h_{1,2} & 0 & {}^n h_{2,2} & 0 & \dots & {}^n h_{7,2} & 0 & {}^n h_{82} & 0 \\ 0 & {}^n h_{1,1} & 0 & {}^n h_{2,1} & \dots & 0 & {}^n h_{7,1} & 0 & {}^n h_{8,1} \\ 0 & {}^n h_{1,2} & 0 & {}^n h_{2,2} & \dots & 0 & {}^n h_{7,2} & 0 & {}^n h_{8,2} \end{bmatrix} \quad (3.5.96)$$

and the stress $[{}_n\boldsymbol{\sigma}]$ is given by:

$$[{}^n\boldsymbol{\sigma}] = \begin{bmatrix} {}^n\sigma_{11} & {}^n\sigma_{21} & 0 & 0 \\ {}^n\sigma_{21} & {}^n\sigma_{22} & 0 & 0 \\ 0 & 0 & {}^n\sigma_{11} & {}^n\sigma_{21} \\ 0 & 0 & {}^n\sigma_{21} & {}^n\sigma_{22} \end{bmatrix} \quad (3.5.97)$$

3.8 Program Algorithm

In order to solve the system of nonlinear equations that arise from the mathematical formulation of the coupled equations, the penetration process is applied incrementally and iterations are performed within each incremental penetration. The full Newton-Raphson iterative method is used in order to obtain the convergency. An abridged algorithm procedure is shown as follows. Full details of the algorithm procedure can be referred to Abu-Farsakh (1997) and Kiousis (1985).

Incremental Loop:

The total penetration length is divided into smaller increments. At the beginning of each penetration increment, the incremental displacement ΔU_{appl} is computed by the total penetration length divided by the number of increments. The Newton-Raphson iterative procedure is carried out within each increment in order to solve for the incremental load R_{inc} and excess pore pressures ΔP_w.

Iterative Loop:

The applied iterative incremental load, R_{iter} for the first iteration is given by:

$$R_{iter}=R_{inc}$$

The Newton-Rapson iteration loop is then carried out as described by the following steps:

1) Convert the iterative applied loads, R_{iter} to account for the skew boundaries, such that the degrees of freedom at the skew boundary nodes are normal and tangential to the skew boundary.

2) Loop over the whole elements

3) Assemble the global stiffness matrix

4) Use a linear solver to solve the nonlinear equations for the iterative incremental scheme

5) Rotate back the iterative incremental displacements and loads at the skew boundaries to the original coordinate system.

6) Add the iterative incremental displacement to the previously computed ones.

7) Compute the Lagrangian iterative incremental strains $\Delta\varepsilon^i$ with respect to the previous configuration from the iterative incremental displacements ΔU^i.

8) Compute the iterative incremental stresses $\Delta\sigma^i$ using the sub-incrementation technique and applying certain corrections due to the crossing the yield surface and the return to the yield surface (see Abu-Farsakh (1997) and Kiousis (1985) for details).

9) Update the constitutive matrix D and calculate the equilibrating forces for the element stresses (R_{equil}).

10) Calculate the out of balance (the corrected) load vector from the accumulated applied load vector, R_{appl} and the equilibrium load vector, R_{eqt} as follows:

$$R_{cor}=R_{appl}-R_{equil}$$

11) Check the convergence of the solution using a particular convergence criterion. In this work, the displacement criterion is adapted, where the criterion is satisfied when:

$$\sqrt{\sum u_{iter} u_{iter}} \leq tol \sqrt{\sum u_{inc} u_{inc}}$$

where the tolerance, *tol* is taken as 5% in this work.

If covergence does not meet, repeat the iterative steps 1 through 11.

If convergence meets the criteria, then proceed to the next step.

12) Update the nodal coordinates, by adding the incremental nodal displacements.

13) Move to the next load increment until the total load is applied.

3.9 Application to PCPT to determine Hydraulic Conductivity

Equations (3.5.106) can be applied to PCPT in two ways. The direct application of the above theory to the magnitude of the measured pore pressure is one method. For this case one needs only one value of the pore pressure (thus called one point method, OPM). Typically the pore pressure at the u_1 position is known to be the most stable one, thus this value shall be used for the OPM.

Equations (3.5.106) can also be used for evaluation of the consolidation of soils (zero displacement but extended time). For this case one needs two pore pressure data at the same location but for different time (thus called the two points method, TPM). Typically the pore pressures at u_2 and u_3 positions are suitable for this purpose, and consequently these values shall be used for the TPM.

3.9.1 One Point Method (OPM)

In equation (3.5.106), one can solve it for ΔW by inputting the hydraulic conductivity matrix and stress-strain parameters. Also, computing the hydraulic conductivity matrix is possible if the ΔW matrix is known. However, the ΔW matrix

represents the distribution of the incremental excess pore pressures around the cone tip, which is not known. The accumulated excess pore pressure at the piezo-element location is the only known (measured). Thus, a straightforward procedure is not possible.

The possible procedure is using the trial and error method by assuming the hydraulic conductivity matrix. With the assumed hydraulic conductivity matrix, the excess pore pressure at the piezo-element location can be computed. This computed value can be compared to the measured value. If both of these two values are close, the assumed hydraulic conductivity matrix is the representative hydraulic conductivity matrix of the soil. These procedures are shown in Figure 3.9.1.

3.9.2 Two Points Method (TPM)

This proposed method utilizes the difference of pore water pressure at u_2 and u_3 locations (See Figure 3.9.2 for u_2 and u_3 locations). This method is valid only when there is a substantial difference between the pore pressure difference at u_2 and u_3 locations and the hydraulic properties. The test data and analytical results show that there is a clear difference between u_2 and u_3 locations. Whittle and Aubeny [1991] showed analytically that there is a clear difference in pore pressure at u_2 and u_3 locations (See Figure 3.9.3. Robertson et al. [1986] and Juran and Tumay [1989] showed experimentally this behavior. Also, the typical data showed the clear difference in pore pressures at u_2 and u_3 locations (See Figure 3.9.4). Thus, undoubtedly one can see that there is a clear difference between the pore pressures at u_2 and u_3 locations. However, one can predict that the difference is very small for the fully undrained condition or the fully drained condition.

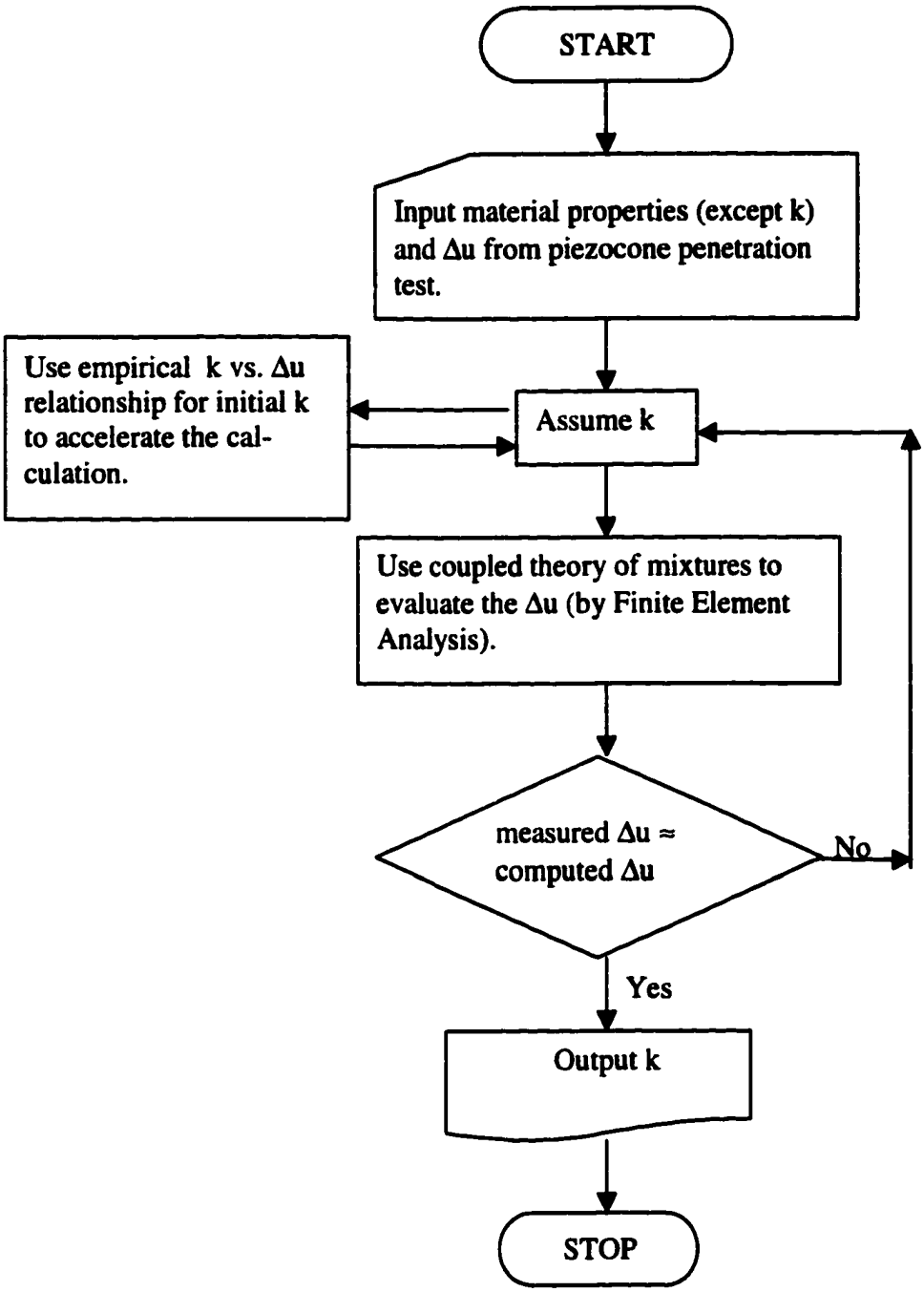

Figure 3.9.1 Flow chart for the computation of the hydraulic conductivity using the coupled theory of mixtures (Isotropic hydraulic conductivity was assumed for convenience)

From Figure 3.9.5, one can expect that two values of the hydraulic conductivity are obtained from the one value of the pore pressure difference between the u_2 and u_3 locations. Thus, the direct relationship between the amount of pore pressure difference at u_2 and u_3 locations and the hydraulic conductivity may not be a reasonable way for the quantification.

A second method is utilizing the ratio of the pressure difference to the excess pore pressure at u_2 or u_3 locations by modeling the full length of penetration which is equal to the distance between u_2 and u_3. For real soils, this ratio will be small for low hydraulic conductivity and high for high hydraulic conductivity. This can be a better way for the quantification. However, this method requires the modeling of PCPT for 15 cm (approximate distance between u_2 and u_3 locations) penetration approximately. Modeling PCPT for 15 cm penetration for large strain incremental loading requires exhaustive computational effort, and is not feasible.

A third method is the consolidation approach. The pore pressure at u_2 and u_3 locations is different because of consolidation as well as the stress conditions. One can see the possibility that the pore pressure at the u_3 location is the dissipated pore pressure of the u_2 location. At the steady state penetration one can reasonably assume that the shearing stress at u_2 and u_3 locations is identical. Then the pore pressure difference between u_2 and u_3 locations is due to the normal stress difference and pore pressure dissipation. Thus, if one can separate the shear stress induced pore pressure and normal stress induced pore pressure, one can compute the amount of the pore pressure dissipation between the u_2 and u_3 locations.

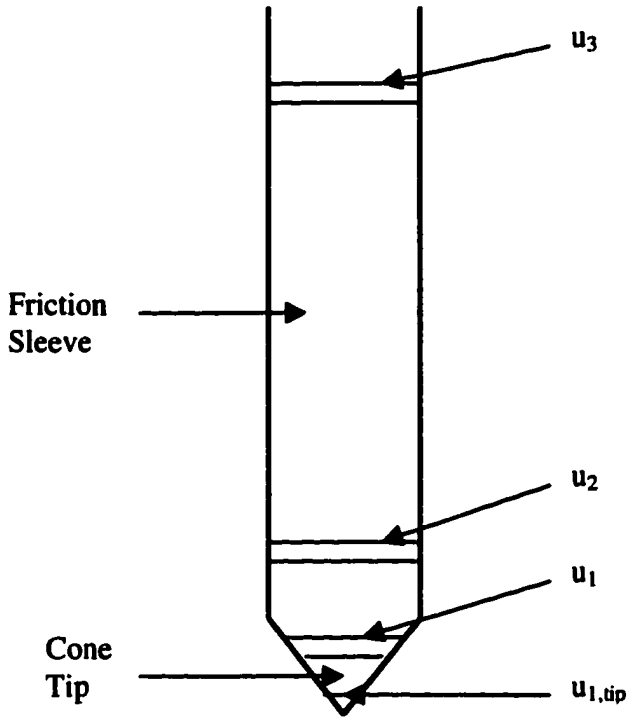

Figure 3.9.2, Typical locations of piezo-elements for piezocone penetrometer

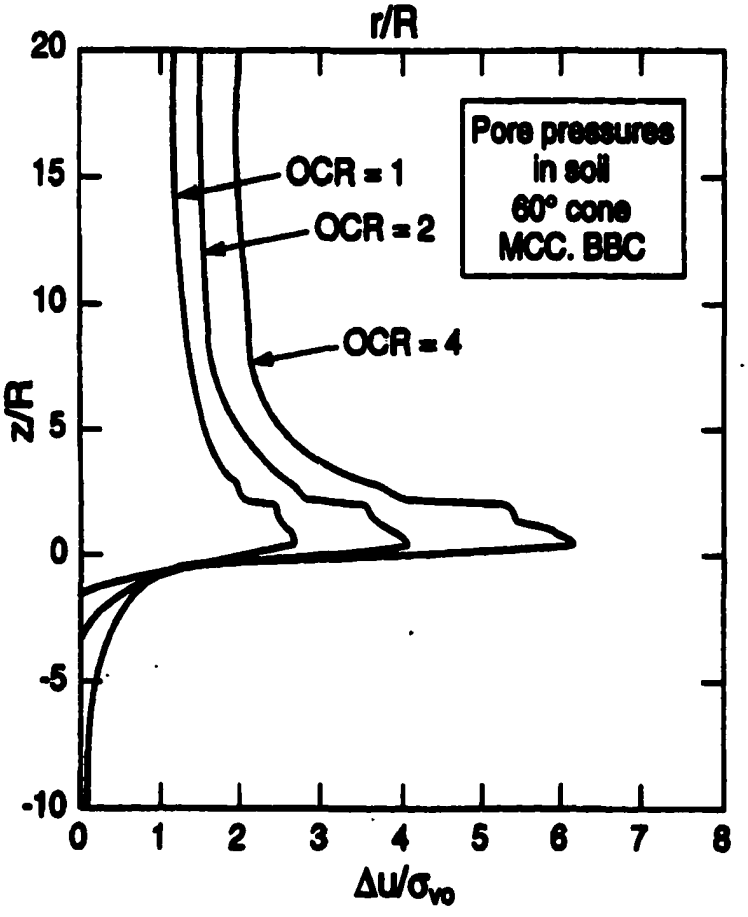

Figure 3.9.3, Excess pore pressure distribution around the cone tip
(after Whittle and Aubeny, 1991)

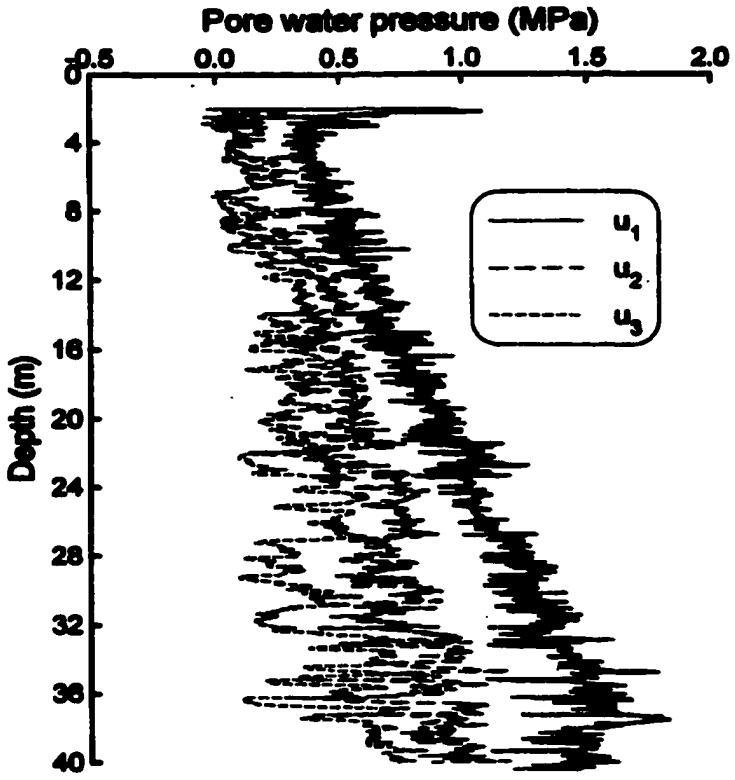

Figure 3.9.4, Field measured pore pressure from PCPT at Pentre, U.K.
(after Powell and Quarterman, 1997)

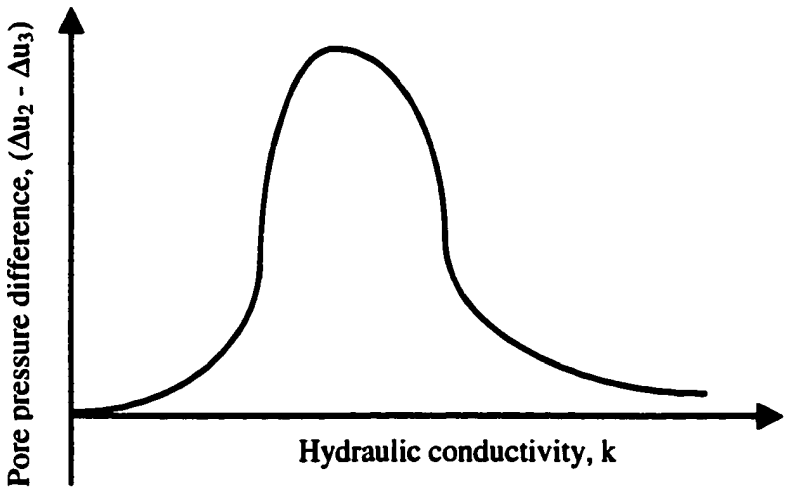

Figure 3.9.5, Conceptual relation between pore pressure difference and hydraulic conductivity

This would lead to the hydraulic conductivity of the soil from the u_2 and u_3 that is directly measured during the PCPT. This concept is similar to the second method but it has great computational advantage.

Conclusively, the basic idea is that the pore pressure distribution at u_2 and u_3 represents the dissipation curve of the normal stress induced excess pore pressure. Thus, starting the virtual consolidation at u_2 location for the normal stress induced pore pressure with the assumed hydraulic conductivity; one can obtain the pore pressure at u_3 location. For the consolidation, u_2 is not taken as the initial pore pressure. The simultaneous generation and dissipation for the pore water is taken into account from the beginning of the PCPT throughout the virtual consolidation. Thus, the implicit drawbacks of the conventional method are inherently removed as well as the explicit drawbacks.

CHAPTER 4. EXPERIMENTS

Both conventional laboratory experiments and calibration chamber penetration tests were carried out in this study. Laboratory tests were aimed to obtain the fundamental material properties for analytical work. Calibration chamber tests were aimed to obtain the penetration pore pressure response at the highly controlled condition.

4.1 Laboratory Experiments

Triaxial tests (CU, UU) and hydraulic conductivity tests are carried out for test specimen (K-33 specimen) according to the referencing ASTM procedure. Details of test results are presented in Table 4.1.1 and Table 4.1.2.

4.2 Calibration Chamber Tests

The Louisiana State University Calibration Chamber System (LSU/CALCHAS) (Figure 4.2.1) is designed by de Lima (1990), de Lima and Tumay (1991, 1992), and Tumay and de Lima (1992). It consists of a calibration chamber, a control panel, data acquisition system, a hydraulics and chucking system, a penetration depth measurement system and cone penetrometers.

4.2.1 Double Wall Flexible Chamber

The LSU/CALCHAS is a double walled flexible chamber (Figure 4.2.2) that can house specimen 525 mm in diameter and 815 mm in height. The two cylindrical shells made of stainless steel 304 plates are 6.35 mm thick. The internal diameter of the inner and outer shells are 560 mm and 580 mm, respectively, and 910 mm high. The shells are designed to withstand a maximum pressure of 1440 kN/m^2. The sample top plate is 525 mm in diameter and 38.1 mm thick, and made of 6061 T-6 aluminum.

Table 4.1.1, Summary of laboratory test results (K-33)

Test Name	Results		Remarks
UU Tri-axial Compression Test	s_u (t/m^2)	80 – 85 kPa	Average of 3 tests
	Hydraulic conductivity, k (m/sec)	2.1×10^{-8}	
Hydraulic conductivity Test (Constant Head)	Compression Index, Cc	0.075	Conducted for triaxial specimen without filter paper around the specimen body
Consolidation Test	Coefficient of Consoli-dation, Cv (m^2/sec)	28.3×10^{-3} cm^2/sec	Kurup (1993), Lim (1999) K-33 specimen
Index Test	Atterberg Limit (%)	See Table 4.2	Kurup (1993), Kim (1999)
	Natural Water Content (%)	18.5	Kurup (1993), Lim (1999)

Table 4.1.2, Fundamental Properties of the soil mixtures

Soil	Liquid Limit (%)	Plastic Limit (%)	Plasticity Index (%)	Specific Gravity (G_s)
Kaolinite	54	28	26	2.66
Edgar Sand	.	.	.	2.67
K-33	20	14	6	

The bottom plate is the base plate of the slurry consolidometer and is similar to the top plate. The sample bottom plate rests on a 525 mm diameter piston. The rubber membrane around the specimen is sealed (watertight) around the top and bottom plates using four "O" rings. The top plate transfers the vertical thrust of the piston on the specimen into the chamber top lid. The top lid made of 6061 T-6 aluminum is 635 mm in diameter and 38.1 mm high. The top lid and top plate have provisions for tests to be conducted at six locations (for the cone to be inserted) in the specimen (Figure 4.2.2). These holes are sealed by adapters during specimen reconsolidation against back pressure. The adapters are specially designed to permit PCPT under back pressure. The top lid is connected to the piston cell ring using twelve stainless steel 304 rods (12.7 mm in diameter). This acts as a self-reacting frame when the specimen is stressed and also provides reaction for the push jack during cone penetration. The inner cell (annular space between the specimen and the inner shell) and outer cell (space between the inner and outer shells) is filled with de-aired water by water lines connected to the top lid.

More details of the calibration chamber equipment can be obtained from de Lima (1990), Lim (1999)

4.2.2 Specimen Boundary Conditions

The LSU/CALCHAS was initially designed for Ko consolidation and to test soils for the following conditions.

BC1: Constant vertical stress and constant lateral stress

BC2: Zero vertical strain and zero lateral strain

BC3: Constant vertical stress and zero lateral strain

BC4: Zero vertical strain and constant lateral stress

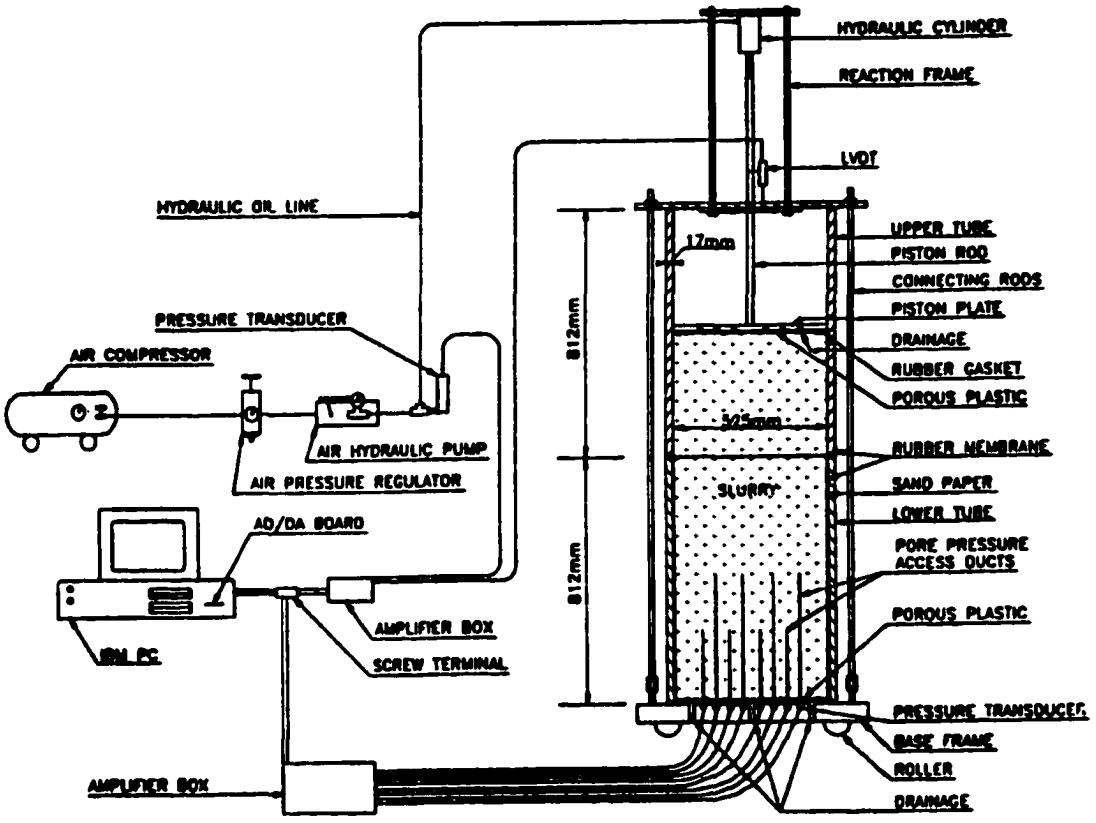

Figure 4.2.1, Louisiana State University Calibration Chamber System (LSU/CALCHAS) (after Tumay and de Lima, 1992)

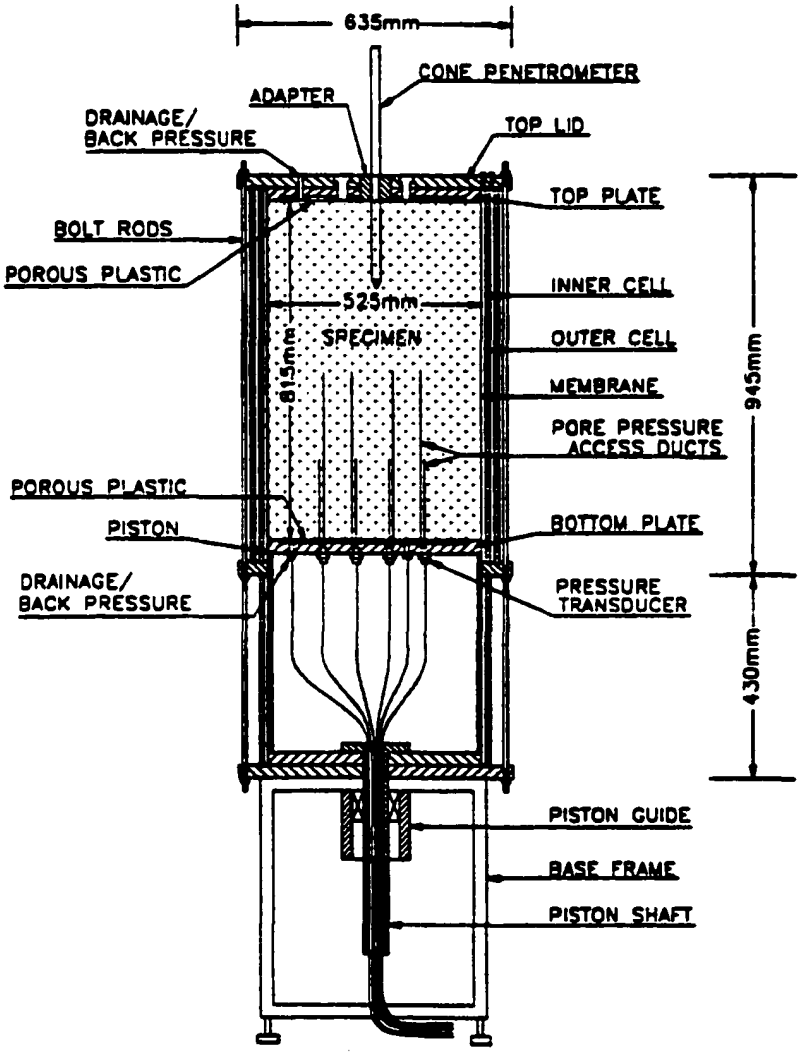

Figure 4.2.2, Schematics of the flexible double wall calibration chamber (after Kurup, 1993)

Also, a back pressure system was included to ensure saturation of the specimens. In this test, boundary conditions were controlled to achieve the Ko condition.

4.3 The Three-Piezo-element Miniature Penetrometer

4.3.1 Equipment

The three piezo-element miniature penetrometer used for the tests was conceptualized at LSU and fabricated at SAGE Engineers, Houston, Texas specially for this study. A schematic view of the penetrometer is shown in Figure 4.3.1. It has a projected cone area of 2 cm^2 and a cone apex angle of 60°. The maximum pore pressure capacity is 100 psi (700 kPa). The penetrometer has two set-ups for the combination of the filter location. The available set-ups are for the u_1, u_3, u_4 configuration and u_2, u_3, u_4 configuration (see Figure 4.3.1). The pore pressure transducers are Precision Measurement Miniature Pressure Transducer Model 150F full bridged electric resistor strain gauge type sensors. For u_1 or u_2 location, the conventional leader hole is used to transmit the water pressure to the sensor (See Figure 4.3.1). During the saturation process, a hypodermic needle is used to inject water in the leader hole. However, for u_3 and u_4 locations, the leader hole is not adapted by placing the sensing membrane directly on the next to the porous protective cover (see Figure 4.3.1). With this method, saturation process for u_3 and u_4 piezometers is substantially simplified and the volume displacement during the pore pressure measurement is minimized.

There is no friction sleeve or end resistance measuring transducers. Only three pore pressure transducers are used because of the limited space in the penetrometer body. For the cone resistance and friction data, the separate cone penetration tests are

carried out with another miniature cone penetromenter conducted by Lim (1999).

4.3.2 Experimental Procedure

Sample Preparation

The clay specimens are prepared in two stages: (1) slurry consolidation in a consolidometer from a high water content soil slurry, and (2) reconsolidation in a calibration chamber to higher stresses which is free from the rigid boundary effects of a slurry consolidometer. This technique is known to produce high quality cohesive soil (Krizek and Sheeran, 1970; Huang, et al., 1988).

Slurry Consolidation

Soil slurry is prepared by mixing kaolin and fine sand (D_{60}/D_{10} = 1.4) with de-ionized water at the water content of twice the liquid limit. This initial water content is found to be appropriate to minimize air entrapment in the slurry during mixing and placement in the consolidometer. A higher slurry water content is observed to lead to segregation of the soil grains and also requires higher consolidation times. The grain size distribution of the kaolin and fine sand is shown in Figure 4.3.2. Mixing is done in two large 40 gallon polyethylene tanks using a specially designed hand held heavy duty agitator. A mixture of 33% kaolin and 67% Edgar fine sand by weight is used to prepare the K-33 specimens. The Atterberg limits of the soil mixture are shown in Table 4.1.2. Slurry is placed very carefully inside the consolidometer by placing it with a large spoon. A vertical consolidation stress (vertical) of 138 kPa is applied to the slurry. The vertical stress is selected so as to obtain an initial soil specimen of just sufficient strength to withstand its own weight. Higher stresses would require greater time to consolidate the specimens.

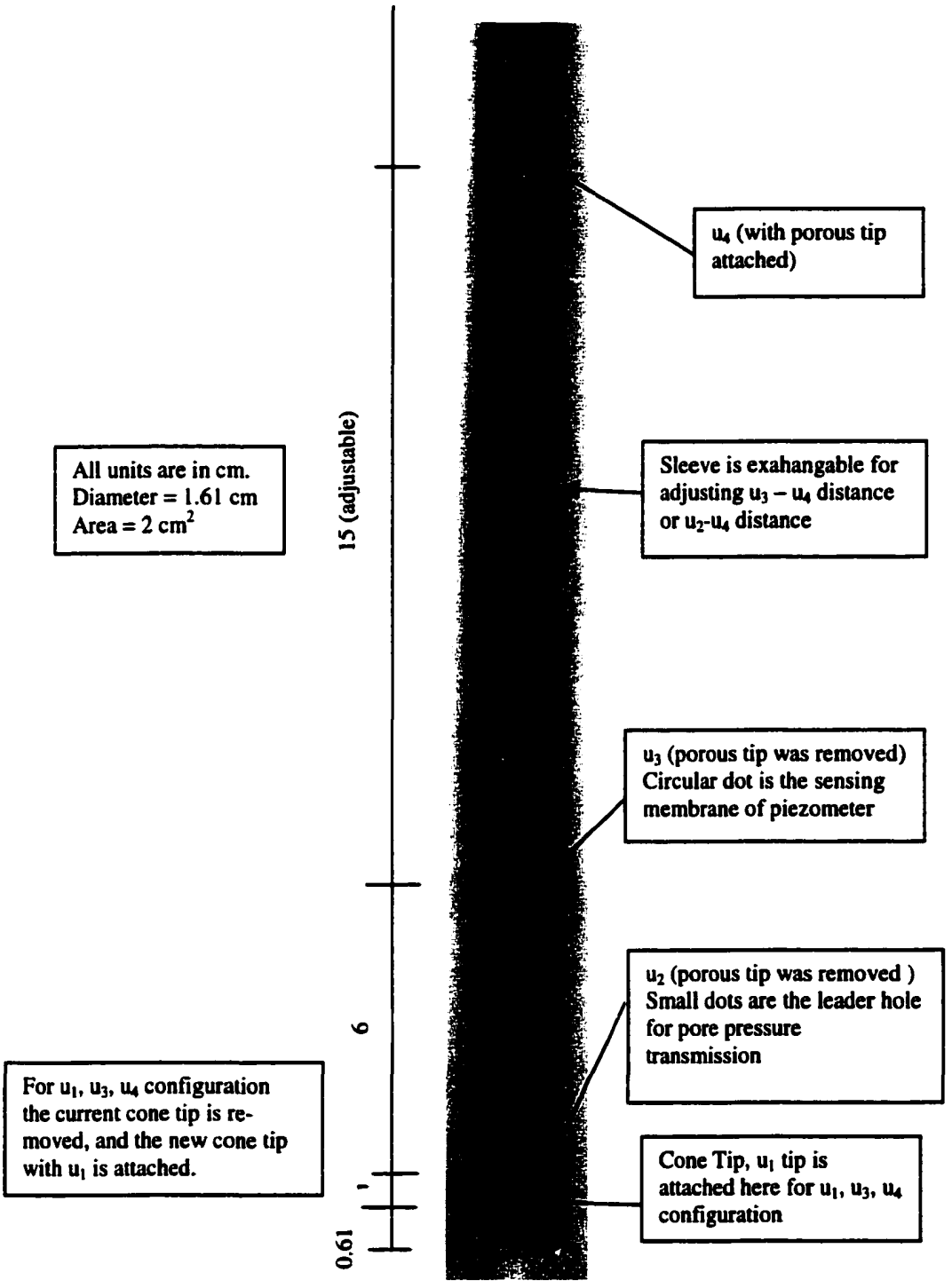

Figure 4.3.1, Schematics of the miniature penetrometer (showing u_2, u_3, u_4 configuration)

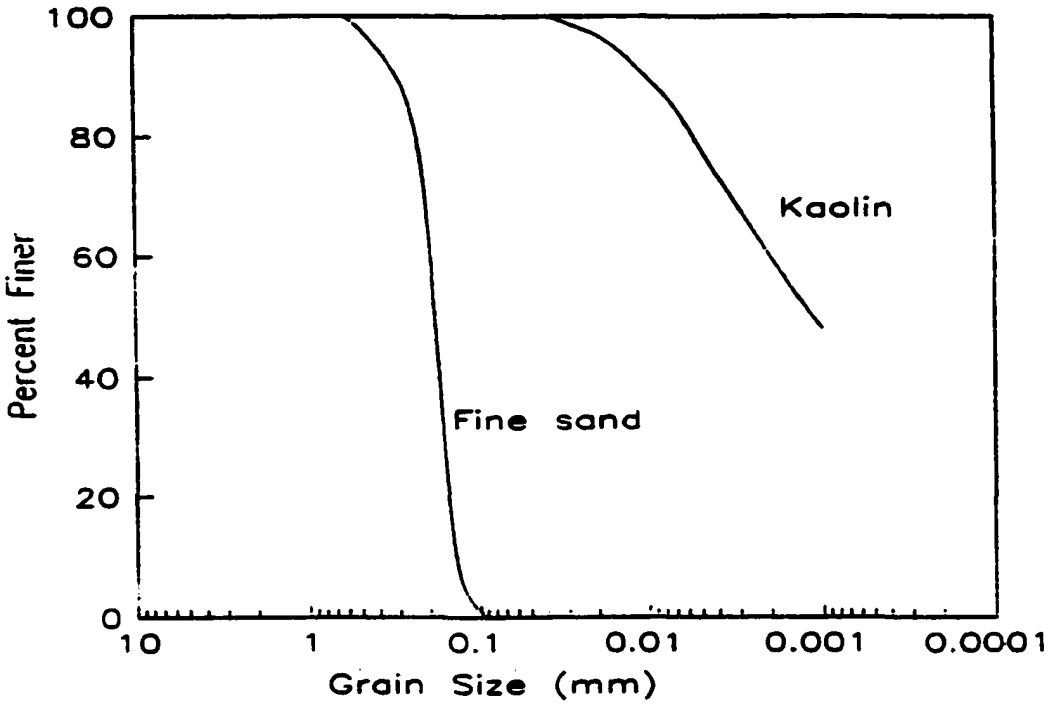

Figure 4.3.2, Particle size distribution curves (after Kurup, 1993)

Pore pressures are monitored at two different elevations and at various radial distances.

Re-consolidation in a Calibration Chamber

At the end of the first stage of slurry consolidation, the specimen enclosed in the membrane is transferred to the calibration chamber where it is subjected to a second stage of consolidation to the higher stresses. The chamber consolidation is performed with the initial back pressure (u_o) of 138 kPa to ensure saturation. After checking the B parameter for saturation, the confining pressure is adjusted for the desired pressure condition. In this research, the pressure is adjusted to $\sigma_v' = 182$ kPa, $\sigma_h' = 75$ kPa for Ko (=0.42) condition (OCR=1.5). Vertical stress is applied through the vertical loading jack. Horizontal stress is applied through the cell pressure. The properties of the specimen are shown in Table 4.1.1.

Test Procedure Using Three-Piezo-Element Miniature Penetrometer

Saturation of Piezometer

De-airing or saturation of the porous elements and the transducer cavity is an important step in piezocone penetration testing. A badly saturated transducer assembly will result in a slow and sluggish pore pressure response during the penetration and dissipation phase of a piezocone penetration test. Example of inaccurate pore pressure response due to the poor saturation have been given by Campanella and Robertson (1981) and Lacasse and Lunne (1982). In this research the following multi-stage de-airing technique is used.

(1) The filter elements are first boiled in water and then saturated by applying a vacuum in the Nold De-Aerator with the filter elements submerged in water. The

Nold DeAerator (Juran and Tumay, 1989) consists of a vacuum tight cell, an electric motor, a magnetic clutch, impeller, and a vacuum pump. Cavitation forms at ultra-high vacuum around the rotating impeller that violently agitiates and beasks the fluid (water) into a fine mist (nucleation). The dissolved gases are hurled up by centrifugal force into the partially evacuated space above the water and removed through the vacuum tube. This phenomena of nucleation and cavitation is a more efficient method of removing dissolved gases, then the conventional boiling and vacuum methods.

(2) The transducer cavity (for u_1 or u_2 position) is flushed with de-aired water using a syringe inserted in each of the three ports connecting to the transducer cavity. This procedure is carried out with the piezocone inverted and submerged in a funnel of de-aired water. Water acts as a magnifying lens and the presence of any minute air bubble can be visually seen. However, it is designed that u_3 and u_4 positions do not have a transducer cavity. Therefore, this process using the syringe is omitted for the u_3 and u_4 positions.

(3) The saturated filter element and the cone tip are assembled while submerged in the funnel of de-aired water.

(4) In the final state, the assembled piezocone is once again subjected to a vacuum in the Nold DeAerator

(5) The final saturated piezocone assembly is kept enclosed in a thin rubber membrane filled with de-aired water, while connecting to the hydraulic push jack and preparing for the penetration test. The prepared piezocone is pre-inserted into the soil specimen and the pore pressure response is checked in two ways. First, the

pore pressure response from the piezometers installed in the specimen is monitored. Second, the pore pressure response from the piezocone is monitored. Typically, the pore pressure response from the piezocone is a little slower initially. However, at the increased back pressure, the response is almost the same. Then it is assumed that the specimen is ready for the penetration test.

Penetration Test

Three penetration tests are carried in the soil specimens. Dissipation tests are performed at the end of the piezocone penetration tests. The hydraulic system used for the cone penetration consists of dual pistons, double acting hydraulic jacks on collapsible frame. It is mounted on top of the top lid of the chamber and allows for penetrating the sample in a single stroke of 640 mm or less. Such a single stroke continuous penetration is desirable especially in saturated cohesive specimens where stress relaxation and pore pressure dissipation can occur during a pause in between strokes. The penetration depth is measured using an electronic analog to digital converter depth decoding system. All tests are conducted at the standard penetration rate of 2 cm/sec. A total of three penetration tests are performed. Tests 1 and 2 are performed for the two different piezo-element configurations, u_1, u_3, u_4 configuration and u_2, u_3, u_4 configuration, respectively. Test 3 has the same configuration as Test 2, and the main purpose is for the repeatability check.

Data acquisition is carried both manually and automatically. The pore pressure response is recorded with the digital multimeter (Radio Shack DMM 22-168A, Hewlett Packard DMM 3000) which are hooked up to the computer's data acquisition system. Also, the readings of digital voltmeters are recorded by a video camera in case

of an emergency. Data are taken every one second. During the dissipation test, the sampling frequency is reduced due to the prolonged measuring time. The testing equipment set up is shown in Figure 4.3.3.

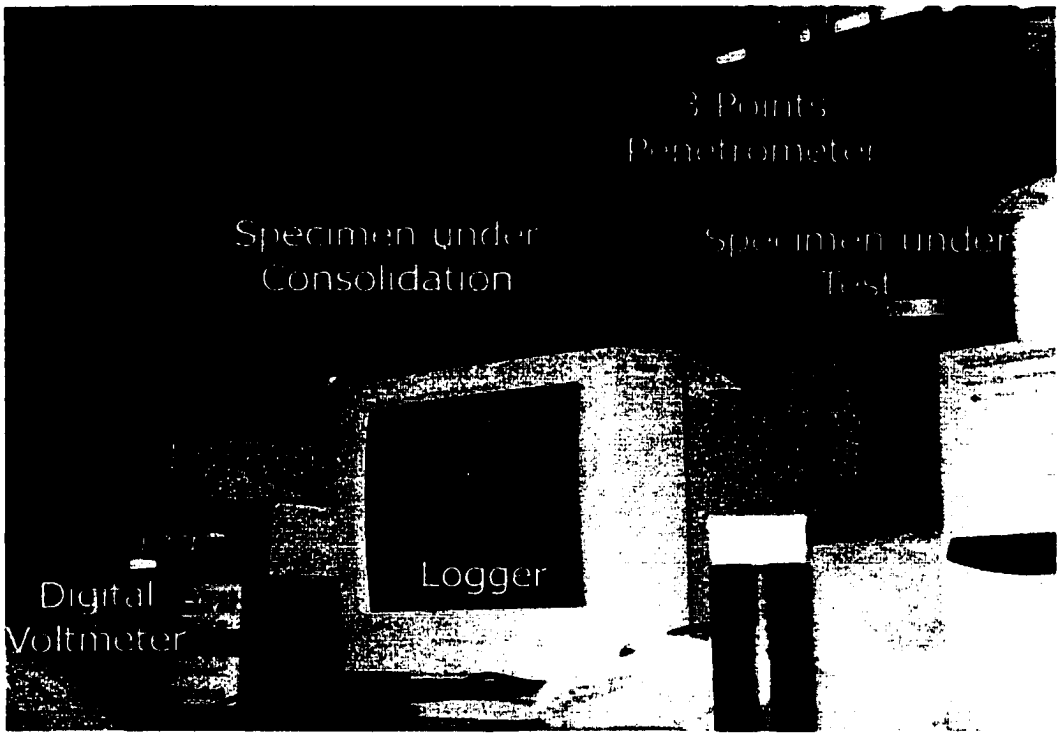

Figure 4.3.3, Test Set Up

CHAPTER 5. RESULTS AND DISCUSSION

5.1 Preliminary Evaluation of the Proposed Method

5.1.1 One Point Method (OPM)

This proposed method is valid only when there is a distinct relationship between the hydraulic conductivity and the piezocone induced excess pore pressure. To evaluate these relationships, the preliminary analyses are carried out by using the FEM program CS-S (Coupled Systems – Soil) for various hydraulic conductivities and strength parameters. Figure 5.1.1 is the results for the condition as Table 5.1.1. From Figure 5.1.1, one can see the response is sensitive both to the hydraulic conductivity and the stress strain parameters. However for the some range of hydraulic conductivity, Figure 5.1.1 shows that there are clear and predominant relationships between the hydraulic conductivity and the piezocone induced excess pore pressures. This is for the hydraulic conductivity range of 10^{-9} m/sec to 10^{-6} m/sec. Typically, the soils for this range of hydraulic conductivity are clayey silt to fine sand. Thus it seems that using the coupled theory of mixtures has a strong potential to provide an excellent prediction of hydraulic conductivity for these soils. Beyond or below this range, it seems that the drainage conditions are close to the fully drained or fully undrained conditions. Typically, the soils for this range of hydraulic conductivity are sands or very plastic clays.

5.1.2 Two Point Method (TPM)

This method is valid only when there is a distinct relationship between the hydraulic conductivity and the $(\Delta u_1-\Delta u_3)/\Delta u_1$. To evaluate these relationships, the preliminary analyses are carried out by using the FEM program CS-S (Coupled

Table 5.1.1, Conditions for finite element analysis

Parameter	Quantity	Remarks
Compression index, λ	0.11	dimensionless
Recompression index, κ	0.024	dimensionless
Hydraulic conductivity, k	5×10^{-9}	m/sec
Initial void ratio, e_o	1.0	dimensionless
Poisson's ratio, ν	0.3	dimensionless
Slope of critical line, M	1.16	dimensionless
Unit Wt. of soil, γ_t	1.8	t/m^3
Depth	20	m
Unit Wt. of water, γ_w	1.0	t/m^3

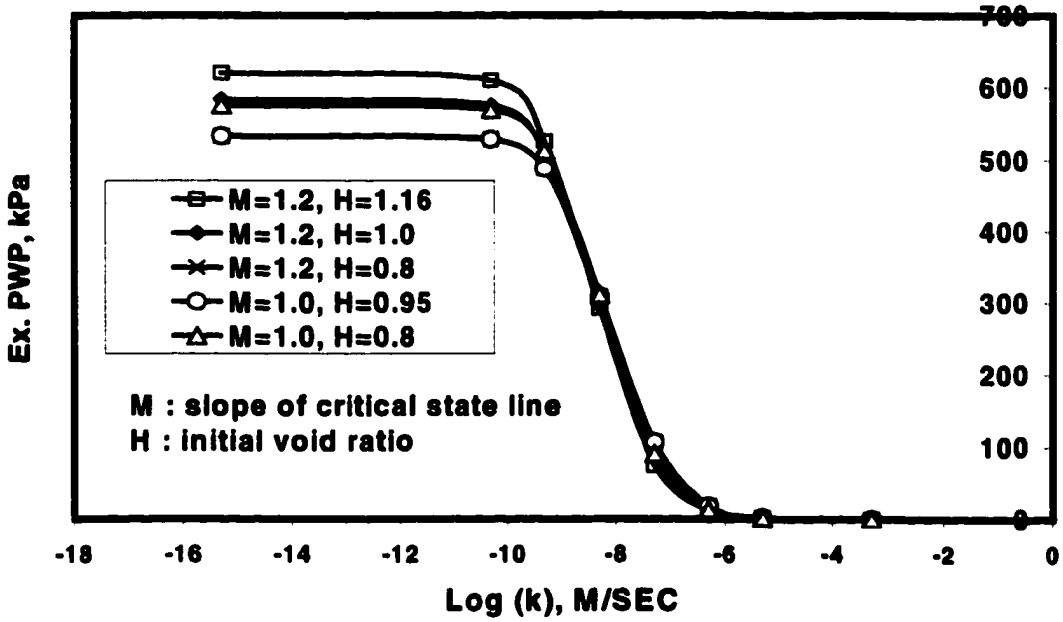

Figure 5.1.1, Predicted results of excess pore pressure and hydraulic conductivity (σ_v' = 200 kPa)

Systems – Soil) for various hydraulic conductivities and strength parameters. Figure 5.1.2 is the results for the condition as Table 5.1.1. From Figure 5.1.2, one can see the response is sensitive for the hydraulic conductivity. However, it is not sensitive to the other material parameters. Comparing Figure 5.1.2 to Figure 5.1.1, one can conclude that the effect of stress-strain parameters hardly exist in Figure 5.1.2. This is unexpected results.

When one considers that Figure 5.1.2 is essentially the simulation of the dissipation of the excess pore pressure between u_1 and u_3, one can understand the essential independency of Figure 5.1.2 to the stress strain parameter. For the uncoupled consolidation equations (2.8) and (2.9) shows that the excess pore pressure dissipation depends only on the hydraulic parameters such as the coefficient consolidation and drainage length. Coefficient of consolidation is the function of hydraulic conductivity, thus it is clear that the normalized pore pressure difference between u_1 and u_3 can be hardly the function of the stress-strain parameters.

This unexpected behavior of Figure 5.1.2 presents the advantage of the TPM. That is the TPM can be applied more versatile since it is free from stress-strain parameters. Figure 5.1.2 also presents that TPM can be applied for the lower range of hydraulic conductivity, such as 10^{-10} m/sec.

5.2 OPM (One Point Method)

5.2.1 Existing Data

Test results are collected from well- documented existing piezocone penetration tests. Test data for each case reflects the various site conditions, and consequently they vary considerably.

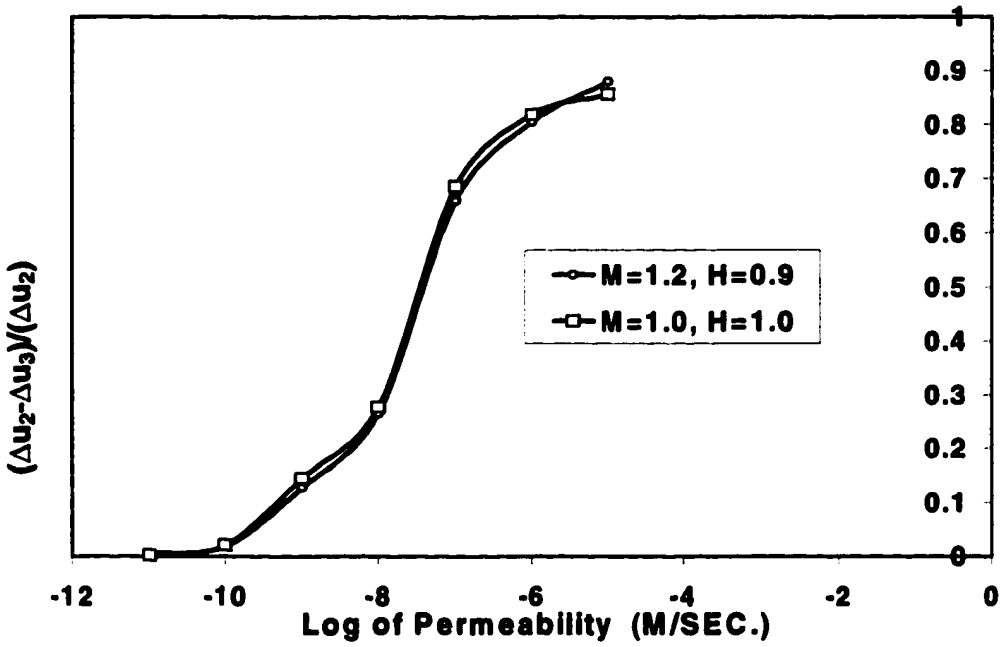

Figure 5.1.2, Predicted results of excess pore pressure and hydraulic conductivity for TPM ($\sigma_v' = 200$ kPa)

To compare the test results for similar conditions, the test results at the similar confining pressure (200 kPa) or at the equivalent depth (20m) were collected. A normalization technique also is used. Collected test data are normalized to the undrained shear strength 60 kPa, which is the shear strength of the specimen for the LSU calibration chamber test. This normalization is based on the fact that the induced excess pore pressure is proportional to the undrained shear strength from the Cavity Expansion Theory (Vesic, 1972).

$$\Delta u = s_u[0.817\alpha_f + 2\ln(R_p/r)] \qquad (5.2.1)$$

In equation (5.2.1) s_u is the undrained shear strength, α_f is Henkel's pore pressure parameter, R_p is the radius of the plastic zone, and r is the distance to the center of cavity.

The collected test results are shown in Table 5.1.2.

5.2.2 Calibration Chamber Test Data

LSU calibration chamber test results for u_1 location is shown in Table 5.2.1. In this section , only the results for u_1 location is presented and discussed. Fully detailed discussion is presented at the next section (section 5.3).

5.2.3 Comparison

The comparison of theoretical results, existing field data, and the calibration chamber test results is shown in Figure 5.2.1. Figure 5.2.1 shows the good agreement between the test data and predicted results. Considering the fact that these data are obtained by many different research groups in many different countries, the agreement is excellent. As discussed earlier, test data covers the wide range of soils which have the hydraulic conductivity range 10^{-9} m/sec to 10^{-6} m/sec.

Table 5.2.1, Cases of the cone penetration induced excess pore pressure and the hydraulic conductivity ($\sigma_v' = 200$ kPa)

Site or Description of Soil	Cohesion, (kPa)	Hydraulic conductivity k, (m/s)	Excess pore pressure,Δu (kPa)	Δu_{norm} (kPa)	OCR	Reference
Stjørdal (Norway)	83	5.2×10^{-8}	338	244	N.A.	Senneset et al (1988)
Glava Stjørdal (Norway)	90	6.3×10^{-10}	800	533	3 – 4	Sandven (1990)
Bakklandet Trondheim (Norway)	100	1.1×10^{-9}	800	480	1.7	Sandven (1990)
Valøya Trondheim (Norway)	125	1.0×10^{-9}	1250	600	2 – 3	Sandven (1990)
Halsen Stjørdal (Norway)	83	$(3-9)\times10^{-8}$	300 – 400	216 – 289	N.A.	Sandven (1990)
Norco(U.S.A)	50-60	2.7×10^{-11} - 5.0×10^{-10}	500 - 550	545 – 600	1 – 1.5	Tumay and Acar (1985)
Amherst (U.S.A)	71.8	$(1-2)\times10^{-9}$	450 - 500	376 – 417	1.3 – 3	Baligh and Levadoux (1986)
Pentre (U.K)	62.5	$(2-8)\times10^{-9}$	600	576	1.2 – 1.8	Powell and Quarterman (1997)
Bothkenner (U.K)	40-75	$(1.4\text{-}3)\times10^{-9}$	830 - 870	664 – 696	1.0 – 1.5	Lunne et al. (1989, 1997)
Quiou Sand (France)	N.A.	3×10^{-4}	10 - 15	10 – 15	1	Almeida et al. (1991) (Calibration Chamber Test)
Uniform Sand (Glass Bead)	N.A.	9×10^{-3}	0	0	1	Peterson (1991) Calibration Chamber Test)

Table 5.2.2, Summary of LSU calibration chamber test results

Site or Description of Soil	Cohe-sion, (kPa)	Hydraulic conductivity k, (m/s)	Excess pore pressure,Δu (kPa)	Δu_{norm} (kPa)	OCR	Remarks
K-50 (50% Kaolinite + 50% Sand)	60	8×10^{-9}	560 - 624	560 – 624	1	Kurup (1993)
K-33 (33% Kaolinite + 67% Sand)	85	2.1×10^{-8}	350-370	250-260	1.5	This Study

The soils of this range of hydraulic conductivity are clayey silts to fine sands. Thus it can be emphasized that this method is valid for soils of this hydraulic conductivity range. Since soils of hydraulic conductivity less than 10^{-9} m/sec are essentially classified as non-permeable soils and soils of hydraulic conductivity higher than 10^{-6} m/sec are essentially classified as free-drainage soils, therefore for the practical purposes this method is valid for most soils.

Comparing the results of Figure 5.2.1 with Elsworth (1993), one can see that the results of this study shows the better agreement with experimental data (Figure 5.2.2). Elsworth (1993) used the volumetric or linear dislocation scheme and linear-elastic model. However, this study used the updated Lagrangian reference frame with elasto-plastic large strain with micro-mechanical consideration. Due to more sophisticated model, the results from this study agree well with the experimental data. However, it also need to be pointed out that the computation time (cost) of this study is much higher than the Elsworth (1993) (Compare elasto-plastic incremental model with the linear elastic model.)

From Figure 5.2.1, one can also find another important phenomenon. Since the drainage condition is practically a fully undrained condition for the hydraulic conductivity of lower than 10^{-9} m/sec, therefore one can assume that the undrained cavity expansion theory is valid for these soils (as long as major concern is pore water pressure response). Also, for the soils of hydraulic conductivity higher than 10^{-6} m/sec, the drainage condition is practically a free drained condition, and therefore the drained cavity expansion theory is valid for these soils. For soils in-between these boundaries, the cavity expansion theory does not provide reliable results.

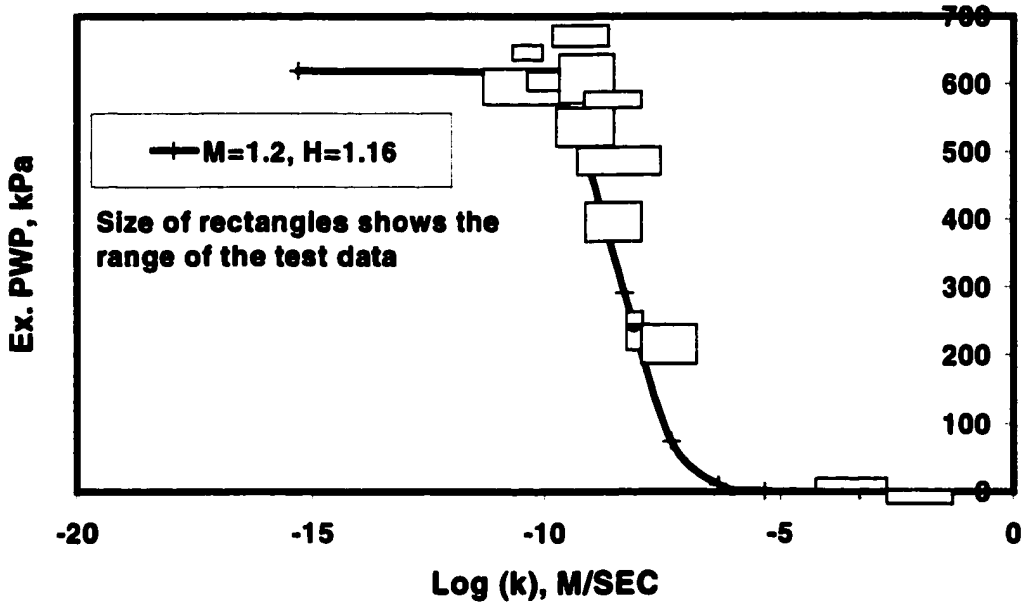

Figure 5.2.1, Comparison of test data and predicted results of the excess pore pressure and hydraulic conductivity (σ_v' = 200 kPa)

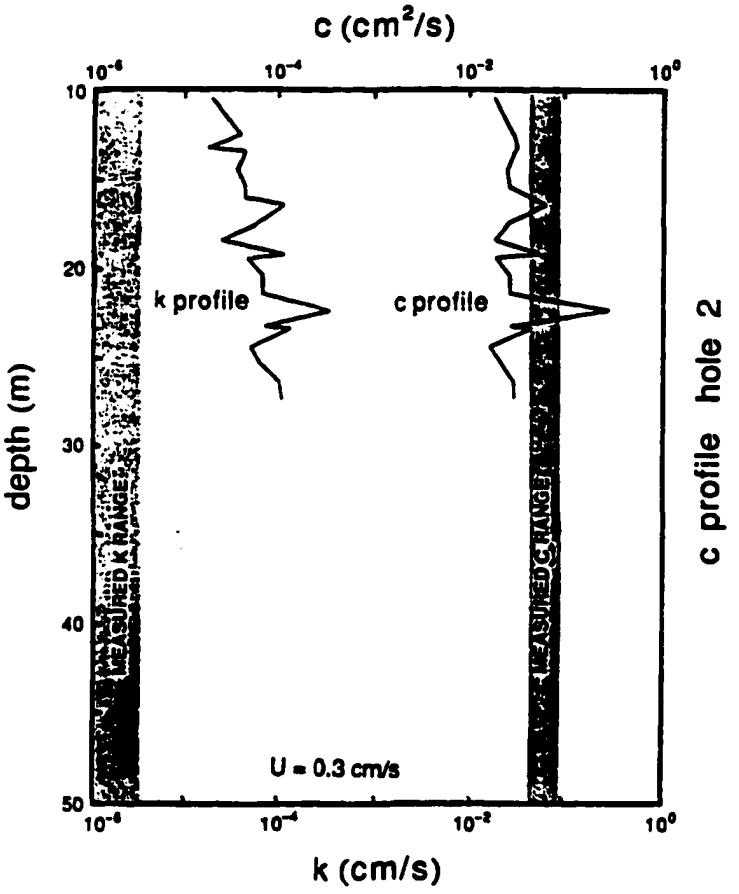

Figure 5.2.2, Elsworth (1993)'s prediction of hydraulic conductivity

This phenomenon can also be interpreted by the fact that simpler methods which do not take into account the partially drainage condition during cone penetration test can reasonably interpret the PCPT data outside these threshold hydraulic conductivities. However, within these threshold hydraulic conductivities, these methods may be far off from the correct solution.

Recalling the works of Senneset et al.(1988) and Elsworth (1993) that the undrained condition is essentially obtained and B_q is insensitive to hydraulic properties when B_q is larger than 0.4 or 0.5 as shown in Figure 5.2.3, one observes that this study presented similar results by demonstrating that the lower threshold hydraulic conductivity is about 10^{-9} m/sec, below which it is essentially an undrained condition for the cone penetration test.

5.2.4 Remarks

A new theoretical interpretation and experimental verification of the cone penetration induced excess pore pressure is carried out in this study. The large strain coupled theory of mixtures formulation using an updated Lagrangian reference frame is adopted in this work. Using this theory and the numerical simulation technique, the cone penetration induced excess pore pressure is predicted reliably and verified with the existing test data.

From this study, the following conclusions could be made:

The test data agreed well with the theoretically predicted results. Therefore, the results of this method can be used for the interpretation of the continuous pore pressure measurements, and can present the

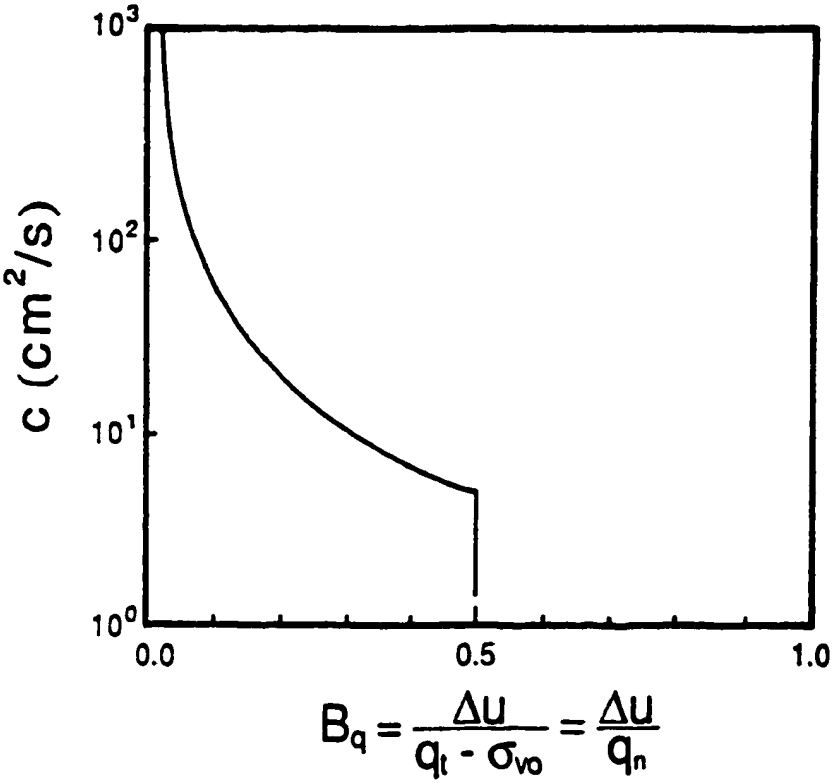

Figure 5.2.3, Variation of Bq (pore pressure ratio) with C (coefficient of consolidation) (after Elsworth, 1993)

continuous hydraulic conductivity profile of the soil under investigation.

Using the combination of data logger of the piezocone penetration test, this method can be used for the real time analysis for the hydraulic properties of the soil.

Two threshold hydraulic conductivities are obtained as 10^{-9} m/sec and 10^{-6} m/sec respectively for impermeable condition and free drainage condition. The coupled theory of mixtures should be used to predict the behavior of the soils within the hydraulic conductivity range of these threshold values. This is because the fully drained or fully undrained conditions are outside this threshold range.

This method is theoretically sound, and experimentally verified. Using this method, the efficiency of the piezocone penetration test can be increased significantly while the operating cost can be reduced substantially.

5.3 TPM (Two Points Method)

5.3.1 Existing Data

The collected field test results are shown in Table 5.4. The collected field test results are for various soils. Thus a normalization of the field test results is performed for the reference undrained shear strength of 60 kPa as for the case of section 5.2. Also, LSU calibration chamber test data is shown in Table 5.3.1.

5.2.2 Comparison

The field test data, calibration chamber test data, and the theoretical predicted results are shown in Figure 5.3.1. In Figure 5.3.1, the parameter $(\Delta u_2 - \Delta u_3) / \Delta u_2$ (Note that both Δu_2 and Δu_3 are normalized.) is used as the reference parameter for the quantification of the relationship between the excess pore pressure and hydraulic conductivity. This parameter is used due to the fact that the direct increment of pore pressure $(\Delta u_2 - \Delta u_3)$ is not a function of a single hydraulic conductivity value as discussed in Figure 3.9.4.

In Figure 5.3.1, the two solid lines represent the change of $(\Delta u_2 - \Delta u_3) / \Delta u_2$ with hydraulic conductivity, k for different values of M and H, respectively (where, M and H are the properties of Cam-Clay model). From the theoretically predicted lines in Figure 5.3.1, one can see that there is a clear relationship between the $(\Delta u_2 - \Delta u_3) / \Delta u_2$ and hydraulic conductivity in the hydraulic conductivity range from 10^{-10} to 10^{-6} m/sec. The soil with hydraulic conductivity smaller than 10^{-10} m/sec is a clayey soil with very low hydraulic conductivity and the soil with very low hydraulic conductivity and the soil with hydraulic conductivity higher than 10^{-6} m/sec is a sandy soil with very high hydraulic conductivity.

Considering that the hydraulic conductivity criteria in general for the clay liners for sanitary land fill is 10^{-9} m/sec and that for the free drainage materials for vertical drains and(or) horizontal drains is 10^{-5} m/sec, the curves in Figure 5.3.1 show that there is a clear relationship between the parameter $(\Delta u_2 - \Delta u_3) / \Delta u_2$ and hydraulic conductivity for most of the field soils. In Figure 5.3.1, the test results are indicated with rectangles instead of the points.

Table 5.3.1, Computational Results

Sites	Hydraulic conductivity, k (m/sec)		
	Coupled Consolidation	Uncoupled Consolidation	Lab. Test (vertical)
Bakklandet Trondheim (Norway)	2×10^{-8}	2.3×10^{-8}	$.11 \times 10^{-8}$
Pentre (U.K)	3×10^{-8}	1.2×10^{-8}	$(.2 - .8) \times 10^{-8}$
Bothkenner (U.K)	2×10^{-8}	6×10^{-9}	$(1.4\text{-}3) \times 10^{-9}$
Glava StjØrdal (Norway)	1.5×10^{-8}	1.5×10^{-8}	$.063 \times 10^{-8}$
LSU Calibration Chamber	1.3×10^{-8}	1.7×10^{-8}	$.74 \times 10^{-8}$

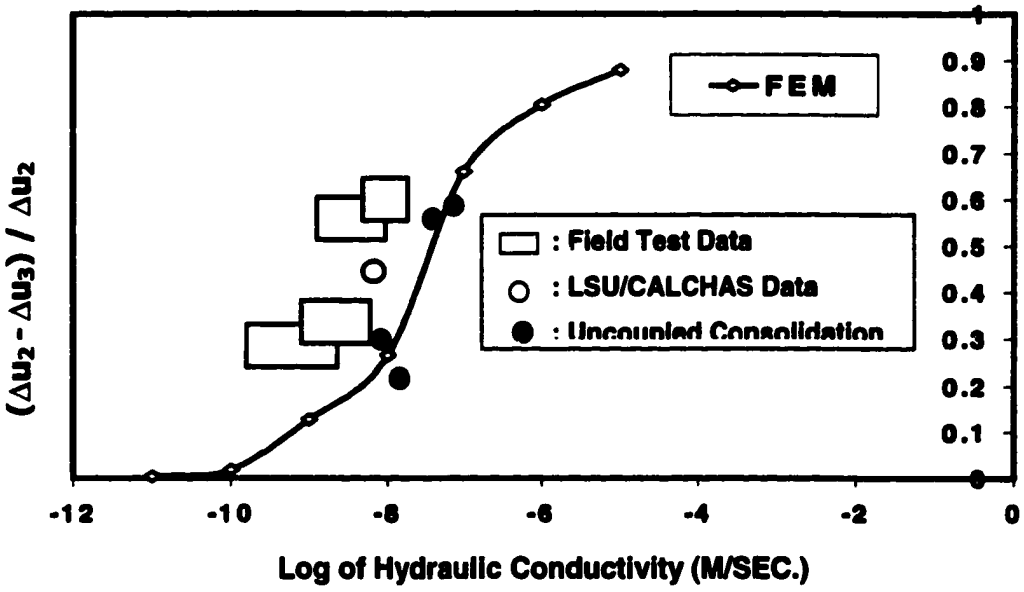

Figure 5.3.1, Change of pore pressure ratio [$(\Delta u_2 - \Delta u_3) / \Delta u_2$] with hydraulic conductivity

The rectangles reflect the transient variational nature of the measured pore pressures during the PCPT as shown in Figure 3.9.3. The center of the rectangles is the same as the values in Table 5.3.1. In Table 5.3.1, Δu_2 and Δu_3 values are taken from the mean Δu_2 and Δu_3 of the field measured pore pressure values.

It seems that the agreement between the test results and the theoretically predicted results is not quite good. The reason for this deviation is discussed in detail in the next section.

The solid and thick dots in Figure 5.3.1 represent the results from the uncoupled consolidation. The results from the uncoupled consolidation show a remarkably good agreement with the results obtained from the coupled consolidation. Considering its computational simplicity and implicit assumptions, these results are unexpected However, considering that the uncoupled consolidation theory does not take into account the pore pressure interactions around the cone penetrometer, the results of the uncoupled consolidation may deviate substantially in certain conditions, thus its usage should be limited for the initial approximation only.

Also, Figure 5.3.1 shows that the relation between the pore pressure ratio $(\Delta u_2 - \Delta u_3) / \Delta u_2$ and hydraulic conductivity is not clear for the zones where the hydraulic conductivity is higher than 10^{-6} m/sec or lower than 10^{-10} m/sec. However, the meaning of hydraulic conductivity for these soils is not really significant in most of the civil engineering structures. There is also the possibility of obtaining the hydraulic conductivity of these soils as shown in Table 5.3.2. Table 5.3.2 shows that the finite element analysis predicted excess pore pressures between Δu_2 and Δu_3 when Δu_3 is

measured eighty seconds after measuring Δu_2 (for miniature cones). Eighty seconds means that the distance between u_2 and u_3 is 160 cm for the typical regular size cone (10 cm^2 cross section).

This distance is not practically feasible for the typical regular size cone. However, for the miniature cone, which has a smaller cross section (assume 1 cm^2), the equivalent distance is reduced to 16 cm. This calculation is based on the radial consolidation concept as shown in equation (1). From equation (1), one can expect the following relationship such as:

$$t = (T_r r^2/c_r) \qquad (5.3.1)$$

In equation (5.3.1), t is the required time for a certain degree of consolidation, T_r is the time factor for a certain degree of consolidation, and r is the radius of cone, c_r is the coefficient of consolidation for radial direction.

Thus, by reducing the cross section of the cone penetrometer or increasing the distance between u_2 and u_3, one can obtain the hydraulic conductivity of the soil which is lower than 10^{-10} m/sec. Also, by increasing the cross section of the cone penetrometer or decreasing the distance between u_2 and u_3, one can obtain the hydraulic conductivity of the soil which is higher than 10^{-6} m/sec.

The "one point method" of previous section is applicable for soils with hydraulic conductivities in the range 10^{-9} m/sec to 10^{-6} m/sec. Figure 5.3.1 shows a wider range of application by using the proposed approach presented here, especially for lower hydraulic conductivity values. The one point method has its own advantages in that it can be used without the modification of the existing piezocone penetrometer which has a piezo-element at the u_1 position.

Table 5.3.2, Δu_2 and Δu_3 when Δu_3 is taken after enough time lag (80 sec.) for M=1.2 and H=0.9

Hydraulic conductivity (m/sec)	Δu_2 (kPa)	Δu_3 (kPa)
10^{-11}	431	425
10^{-10}	428	383
10^{-9}	403	253
10^{-8}	278	78
10^{-7}	112	8.2
10^{-6}	20	.8
10^{-5}	2.5	.1

However, the two points method has its advantage that it can be applied for a wider range of hydraulic conductivities. Thus, one can see these two methods are compensating each other's disadvantages and constitute a complete new method when used together.

Conclusively, the discussions in this study show the capability of the coupled theory of mixtures to predict the hydraulic conductivity of the soil utilizing the penetrating pore pressure from the PCPT. From this study, it is shown that the agreement with the test data is quite reasonable. Therefore, one can see the possibility of obtaining the continuous hydraulic conductivity profile, which was not possible in the past. Also, with the incorporation of the high speed processor, the continuous hydraulic conductivity profile can be obtained. Furthermore, the real time ("on the fly") continuous hydraulic conductivity profile is obtained with substantially reduced cost.

5.3.4 Remarks

A new theoretical interpretation and experimental verification of the two points cone penetration induced excess pore pressure is carried out in this study. The large strain coupled theory of mixtures formulation using an updated Lagrangian reference frame is adopted in this work. Using this theory and the numerical simulation, the multi (2) piezo-element cone penetration induced excess pore pressure is used to predict reliably the hydraulic conductivity of the soil.

From this study, the following conclusions could be made:

The theoretically predicted hydraulic conductivity from the two points method agrees reasonably well with the field test data. Therefore, the results of this two points

method can be used for the interpretation of the continuous pore pressure measurements, and can present the continuous hydraulic conductivity profile of the soil under investigation. Using the combination of the high speed processor, this method can be used for the real time continuous profile of the hydraulic conductivity of the soil.

Two threshold hydraulic conductivities are obtained as 10^{-10} m/sec and 10^{-6} m/sec respectively for the fully undrained drainage condition and the free drained condition. Beyond these threshold hydraulic conductivity, the difference of the pore pressure change ratio $[(\Delta u_2 - \Delta u_3) / \Delta u_2]$ is not sensitive to the change of the hydraulic conductivity. Thus the applicability of this method is not plausible. However, these threshold hydraulic conductivities are for the typical regular size of the cone with 10 cm^2 cross section. By changing the cone diameter and the distance between u_2 and u_3 positions, the threshold hydraulic conductivity can be moved outward. This is one of the advantages of the two points method compared to the one point method.

The results from the uncoupled consolidation agree remarkably well with the coupled consolidation for the conditions used in this study. However, uncoupled consolidation does not take into account the pore pressure interaction, and the coupling of the solid and pore water. The results using the uncoupled formulation should be used for initial approximation only. This study is carried out for the normally consolidated or lightly over consolidated soils. Thus future study for the over consolidated soils will widen the applicability of this method.

5.4 Evaluation of Calibration Chamber Test Results

5.4.1 Comparison

Calibration chamber test results are shown in Figure 5.4.1. Figure 5.4.1 is the combined representative results for u_1, u_2, u_3, and u_4 locations. Pore pressure response for u_1 location shows the typical results obtained in the piezocone penetration test. The steady state pore pressure is obtained about 2 seconds after the starting of the penetration. u_2 also showed a similar response. The absolute magnitude of u_2 is a little smaller but this is quite reasonable (Mayne, 1994).

The results of u_3 and u_4 showed the substantial initial drop of excess pore pressure and a gradual increase to the steady state condition. It is quite an unexpected behavior. The distance from the cone tip to the u_3 or u_4 location is 7 cm and 22 cm, respectively. This distance is roughly equivalent to 35 cm and 110 cm for the international reference size cones (10 cm^2 cross-section) for the pore pressure dissipation aspect.

Careful evaluation of the pore pressure at u_3 and u_4 locations present very meaningful phenomena. The steady state condition for the u_3 or u_4 are not obtained simultaneously as for the u_1 or u_2 locations. The steady state condition is essentially obtained in 2 stages. The first stage is obtained when u_1 indicates the steady state condition and u_3 and u_4 show a steady decreased pore pressure. The second stage of the steady state is obtained when u_1 maintains the steady state condition and u_3 and u_4 enter into the old locations of u_1 or u_2 and shows a steady increased pore pressure. The second stage of the steady state occurs because the u_3 or u_4 enters into the disturbed zone, which is initiated by the cone tip. This means that at the second stage,

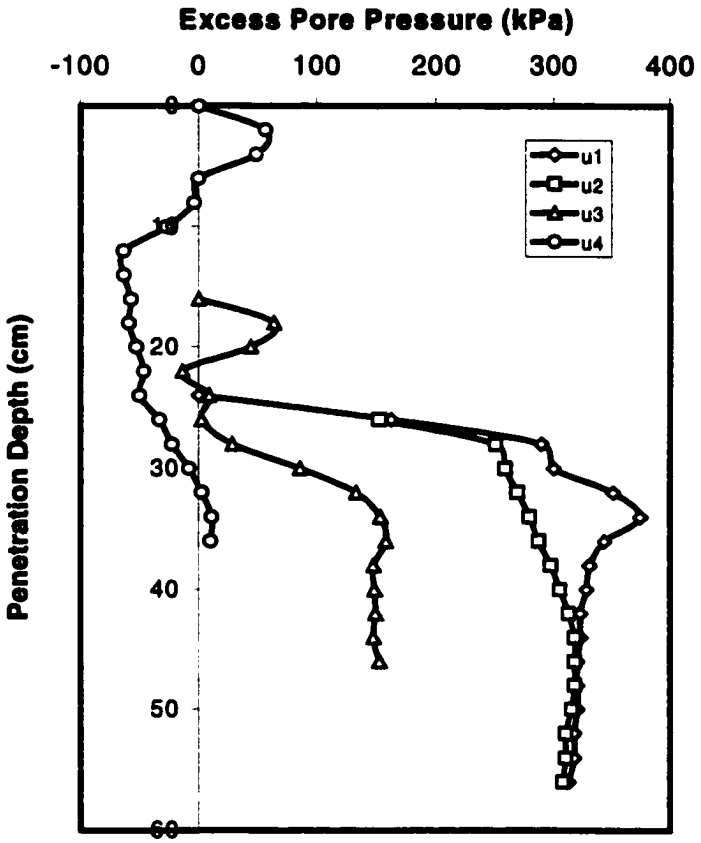

Figure 5.4.1, Combined penetration test results for u_1, u_2, u_3, and u_4 location

u_3 or u_4 enter into the new boundary condition which is completely different from their initial boundary condition. Initially there is no excess pore pressure at the surroundings of u_3 or u_4, but there is excess pore pressure at the new surrounding.

Independent from this study, Elsworth (1993) predicted the minimum penetration depth to obtain the steady state condition through a dislocation scheme. From Elsworth (1993), the minimum penetration depth for steady state condition is roughly 2 cm for the cone tip (varies with the hydraulic conductivity). However, that distance is roughly 20 cm for the cone shaft (also varies with the hydraulic conductivity, see Figure 5.4.2). Elsworth's (1993) findings do not exactly agree with the experimental results of this study. However, they show fair conceptual agreement with this test results.

From this discussion, one can see that for a better analysis of the cone penetration tests, a substantial amount of penetration is required especially for the analysis of the friction sleeve.

Figure 5.4.1 also shows the steady state pore pressure distribution which is high at the cone tip and low (gradual decrease) along the cone shaft. This trend agrees well with Levadoux and Baligh's (1986) experimental results and Whittle and Aubeny's (1991) and Elsworth's (1998) theoretical results.

Elsworth (1998) predicted the distribution of excess pore pressure along the cone body as shown in Figure 5.4.3. In Figure 5.4.3, the results from this study were also superimposed. The superimposed results showed the fair agreement with the Elsworth(1998). The governing equation of Figure 5.4.3 from Elsworth (1998) is as follows:

$$P_D = \frac{4 \cdot \Delta P}{U \cdot r} \frac{k_i}{\mu} \qquad (5.4.1)$$

In equation (5.4.1), P_D is the dimensionless pore pressure, ΔP is the excess pore pressure, U is the penetration speed of the cone, r is the radius of the cone, k_i is the intrinsic hydraulic conductivity, and μ is the dynamic viscosity of water. Equation (5.4.1) can be modified as follows:

$$P_D = \frac{4 \cdot \Delta P}{U \cdot r} \frac{1}{\mu} \left(\frac{k\mu}{\rho g}\right) = \frac{4 \cdot \Delta P}{U \cdot r} \frac{k}{\gamma_w} \qquad (5.4.2)$$

In equation (5.4.2), k = hydraulic conductivity in common meaning, γ_w is the unit weight of water. When one substitutes the hydraulic conductivity, unit weight of water and penetration speed, and geometry of cone, one obtains the following expression:

$$P_D = 5.25 \times 10^{-5} \cdot \Delta P \qquad (5.4.3)$$

From using equation (5.4.3), the prediction of excess pore pressure is made as shown in Table 5.4.1. The superposition of Table 5.4.1 with Elsworth (1998)'s results is shown in Figure 5.4.3.

Figure 5.4.4 shows the dissipation test results for all four piezometer locations. u_1 shows the typical dissipation curve and the computed hydraulic conductivity is about 2×10^{-8} m/sec (t_{50} method of Robertson et al., 1992). Considering that the measured hydraulic conductivity value in laboratory (constant head hydraulic conductivity for the triaxial specimen) is 2.1×10^{-8} m/sec, consequently the computed hydraulic conductivity is in very good agreement.

However, u_2 shows some deviation from the standard shape of the dissipation curve. u_3 and u_4 show large deviations from the standard dissipation curve and cannot

Table. 5.4.1, Calculation of dimensionless pore pressure

Location of Piezometer Tip	u_1	u_2	u_3	u_4
ΔP (g/cm^2)	3700	3100	2000	100
P_D	0.019	0.016	0.0078	0.000525
X_D	0.5	2	9.5	28.3

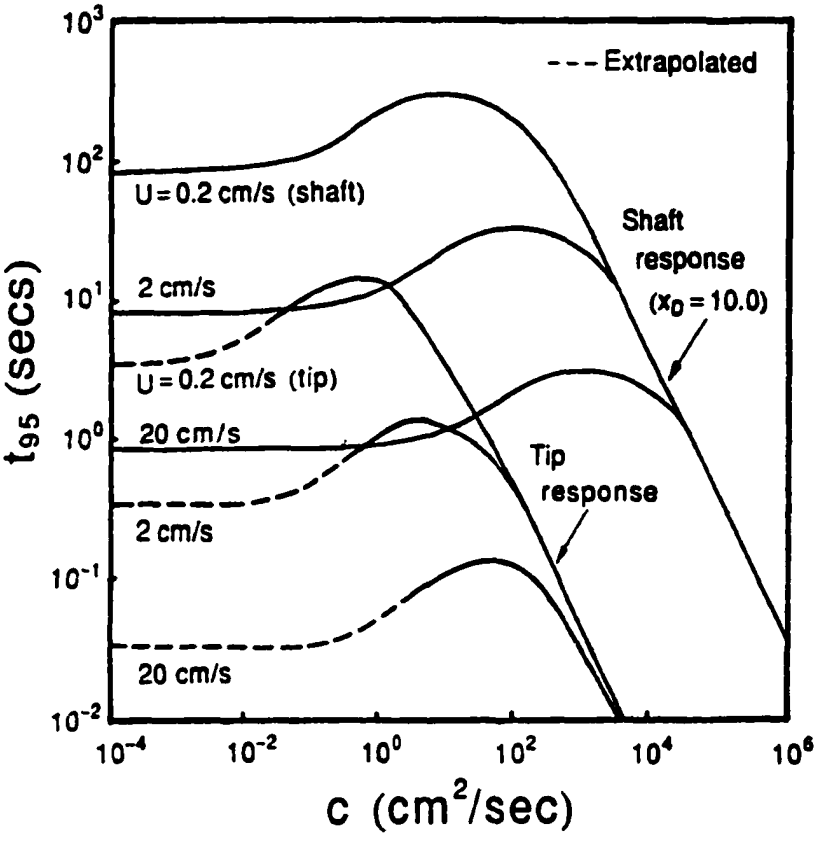

Figure 5.4.2, Minimum distance for steady state penetration (after Elsworth, 1993)

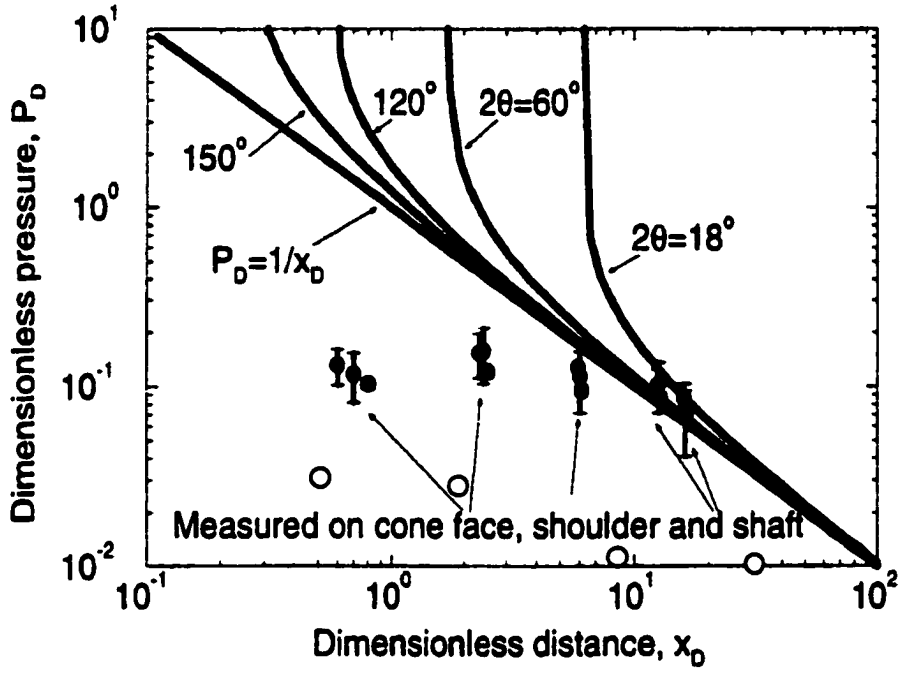

Figure 5.4.3, Distribution of excess pore pressure along cone shaft (Elsworth, 1998)
(Hollow circles are the results of this study)

be used for the computation of the hydraulic conductivity or the consolidation coefficient.

From Figure 5.4.1 and Figure 5.4.4, one can come to the following observations with respect to the pore pressure response of the penetrating cone.

For the u_1 location, the pore pressure response indicates a spherical cavity expansion type response, and it attains the steady state condition quite soon, and does not change because it maintains constant boundary condition. However, for u_2, u_3, and u_4 locations, it is not the case of a cylindrical cavity expansion. Through some mechanism, the negative pore pressure is generated at the cone shaft, and it approaches the initial steady state until it enters into the disturbed zone caused by the cone tip. In the new boundary condition, another steady state condition is reached. This new steady state is the equilibrium of the negative pore pressure that is generated by the cone shaft and the surrounding high pore pressure. Therefore, one can assume a small pore pressure near the cone shaft and a bigger pore pressure at the far end from the cone shaft. When the penetration of the cone stops, the interaction of the pore pressure starts in order to attain the pore pressure equalization. The high pore pressure from the far field flows into the near field of the cone shaft. Thus it shows an initial increase of the pore pressure response of the u_2, u_3 and u_4.

Considering the above discussion, one can explain the response of the u_1, u_2, u_3 and u_4. However, the dissipation curve for the cone shaft locations (u_2, u_3, u_4) essentially difficult to use for the evaluation of the hydraulic conductivity. The response of u_2 is somewhat close to u_1 since it is the closest to u_1. However, the above discussed pore pressure interaction is still there.

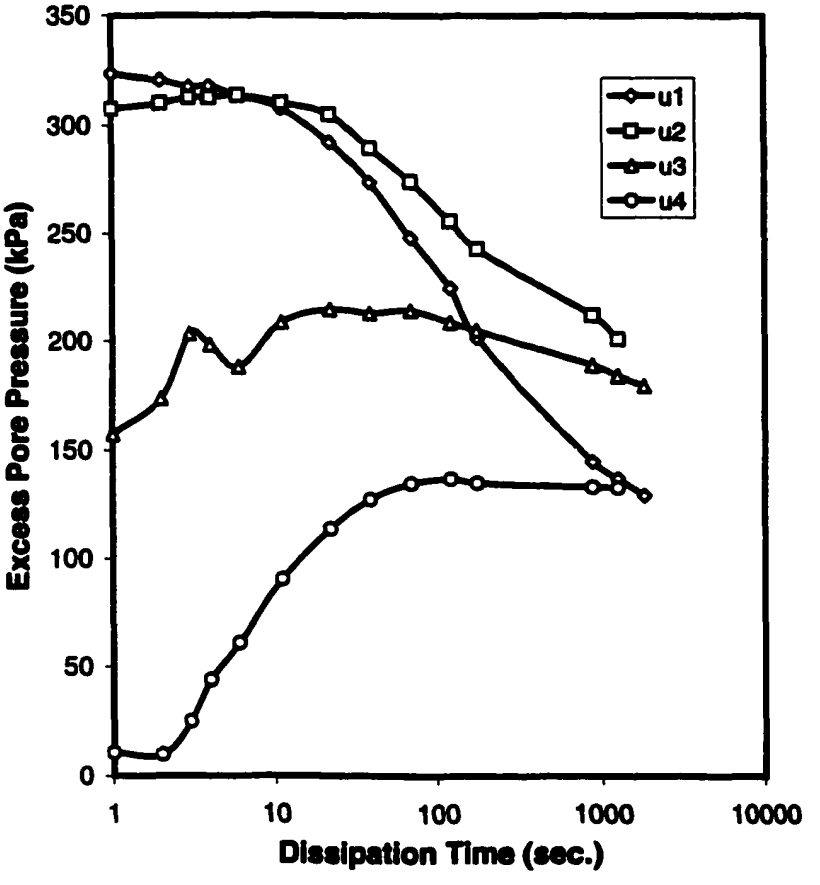

Figure 5.4.4, Dissipation Curves of u_1, u_2, u_3, and u_4 locations

5.4.2 Remarks

The primary purpose of this research is to obtain the relationship between the excess pore pressure from the cone penetration test and the hydraulic conductivity of the soil. Thus the author believes that with the improvement of the theoretical simulation technique, a better relationship could be obtained.

About the less good agreement between the predicted pore pressure response and the measured pore pressure response in Figure 5.3.1, the author believes that it is because of the numerical problem. Especially, the two stage steady state could not be incorporated in the finite element simulation. The author believes, the improvement of finite element simulation which includes the two stage steady state, the agreement is going to be improved. However, this improvement is not practically possible considering the computation time, and will be left as a future study.

5.5 Anisotropic Model vs Isotropic Model

5.5.1 Comparison

In this study, anisotropic Modified Cam Clay model (AMCCM) with plastic spin is derived. To see the effect of anisotropic model, a comparison was made between the results of the anisotropic model and isotropic model.

Figure 5.5.1 shows the excess pore pressure contours as obtained from the finite element analysis. Figures 5.5.1-a and 5.5.1-b show the results of AMCCM with the plastic spin and without the plastic spin, respectively. Figure 5.5.1-c shows the results of IMCCM with a mean principle stress that is the same as the vertical effective stress (hydrostatic stress condition). Figure 5.5.1-d shows the IMCCM with a mean principal stress that is same as Figure 5.5.1-a. The results of IMCCM with initial

anisotropic stress condition are shown in Figure 5.5.1-e. The initial confining condition is the same as in Figure 5.5.1-a. Figure 5.5.1-f shows the results of AMCCM with initial isotropic stress condition at which the mean principle stress is the same as the vertical effective stress.

In Figures 5.5.1-a and 5.5.1-b one can see that the spatial distributions of the excess pore pressures in both Figures are similar whether the plastic spin is incorporated or not. However, different maximum excess pore pressures are obtained in each case. This is due to the high concentration of micro-structural changes at the vicinity of the cone tip where the strains are extremely large. This behavior is shown indirectly in Figure 5.5.2 by the tensor component (N_{2133}) of the plastic spin. In the region of the cone face adjacent to the shoulder, one notes that most of the plastic spin activity occurs. This is also the region of maximum strain (Voyiadjis and Abu-Farsakh, 1997).

Comparison of Figure 5.5.1-a with Figure 5.5.1-c, Figure 5.5.1-d, and Figure 5.5.1-e shows the difference between the AMCCM and the IMCCM constitutive models. Figure 5.5.1-a, Figure 5.5.1-d, and Figure 5.5.1-e essentially have the same mean principle stress. The difference is the initial confining condition and the applied soil model. From Figure 5.5.1-a and Figure 5.5.1-d, one can see clearly that the pore pressure response of AMCCM is substantially higher than that of IMCCM (for the same mean principle stress). However, Figure 5.5.1-c shows that when one uses the confining pressure which is the same as the vertical effective stress, one obtains almost similar results with the AMCCM and the plastic spin. However, it should be noted that this agreement is mainly due to the higher mean confining pressure. Figure

5.5.1-e shows that even with an anisotropic initial confining condition, the response is not much different when the mean principle stress is the same. Figure 5.5.1-f shows that the combination of high initial mean principle stress (same as vertical effective stress) with AMCCM results in the highest pore pressure response.

From this discussions, one can see that the pore pressure response of cone penetration tests is substantially affected by the applied model and applied initial confining condition. However, one should acknowledge that the combination of anisotropic initial stress condition and AMCCM with plastic spin is the most realistic condition.

Figure 5.5.3 shows the variation of the cone penetrometer induced pore pressure with different hydraulic conductivity. It is noted that Figure 5.5.3 is for the case of ground depth 20 m (saturated) and the stiffness similar to the LSU calibration chamber test specimen (recompression index $\kappa = 0.024$, Poisson's ratio $\nu = 0.3$). For the different soils such stiffer soils, the back-bone curves in Figure 5.5.3 may be shifted up especially at lower hydraulic conductivity range. From Figure 5.5.3, one can know that the pore pressure response from the AMCCM (the one which considers both initial anisotropy and induced anisotropy) is closer to the experimental data than that from IMCCM. This condition (the one which considers both initial anisotropy and induced anisotropy) is more close to the true field condition, thus the results agree well with the anticipated results.

This behavior is quite rational considering the realistic behavior of soils as follows. For the IMCCM, the yield locus undergoes expansion only, and cannot incorporate the translation.

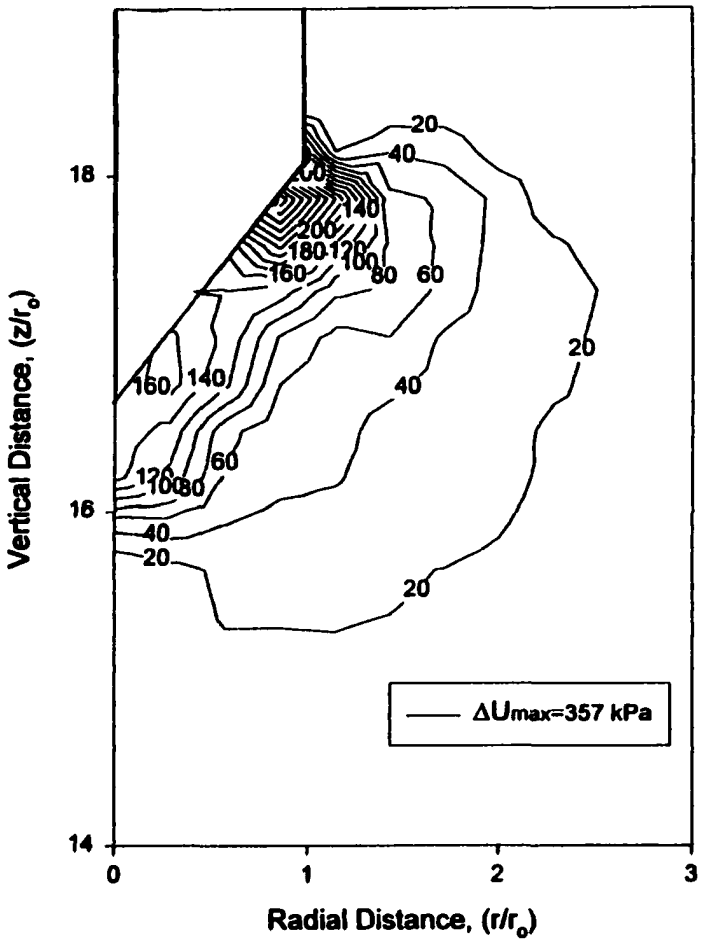

(a) AMCCM with Plastic Spin

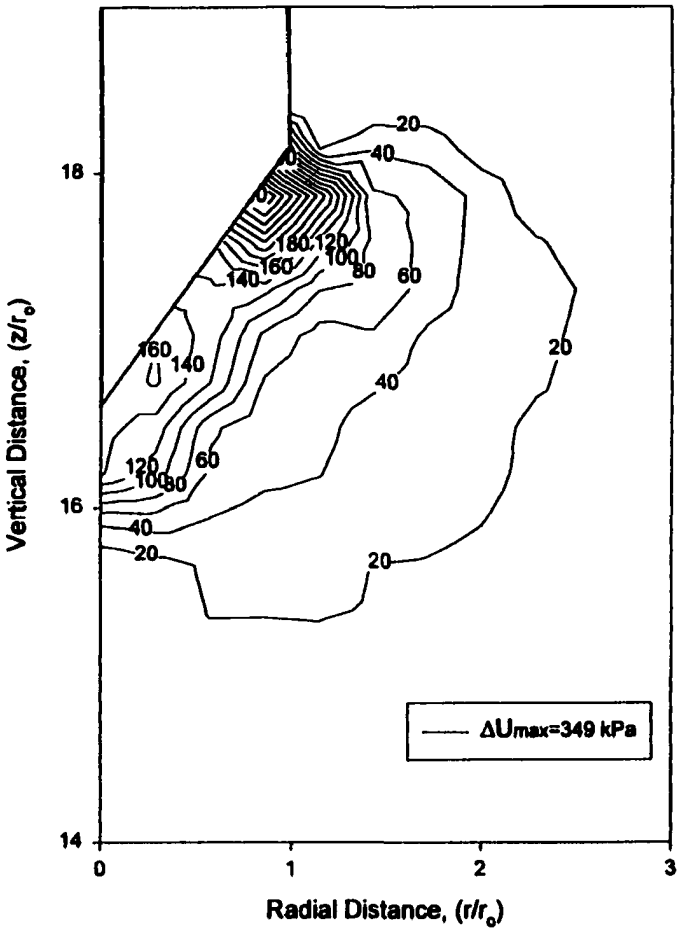

(b) AMCCM without Plastic Spin

Figure 5.5.1, Excess Pore Pressure Contours of AMCCM and IMCCM (figure continued)

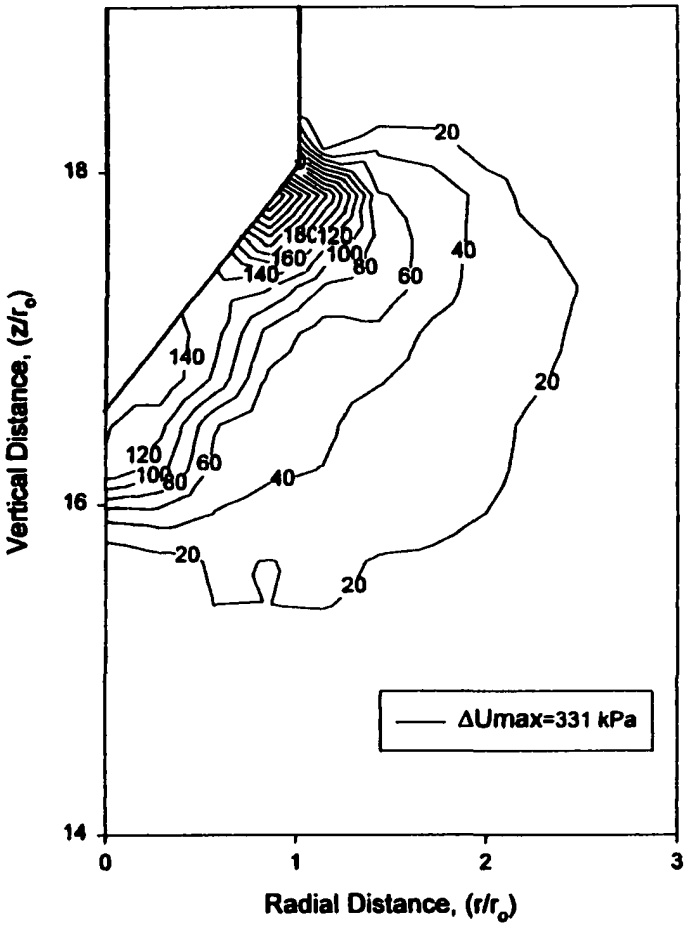

(c) IMCCM for mean principle stress same as vertical stress

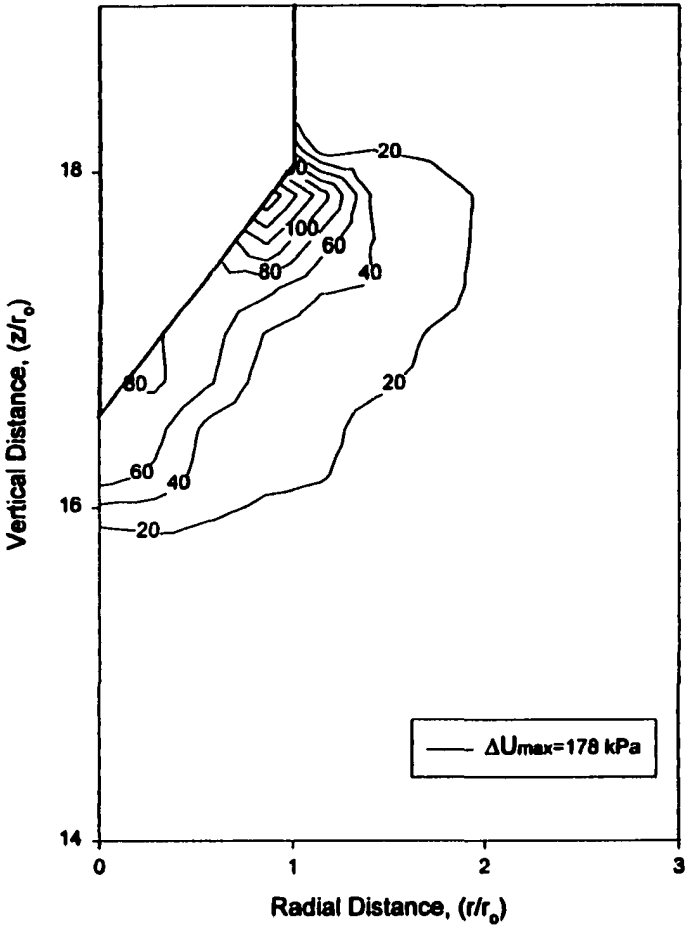

(d) IMCCM for same mean principle stress as (a)

(figure continued)

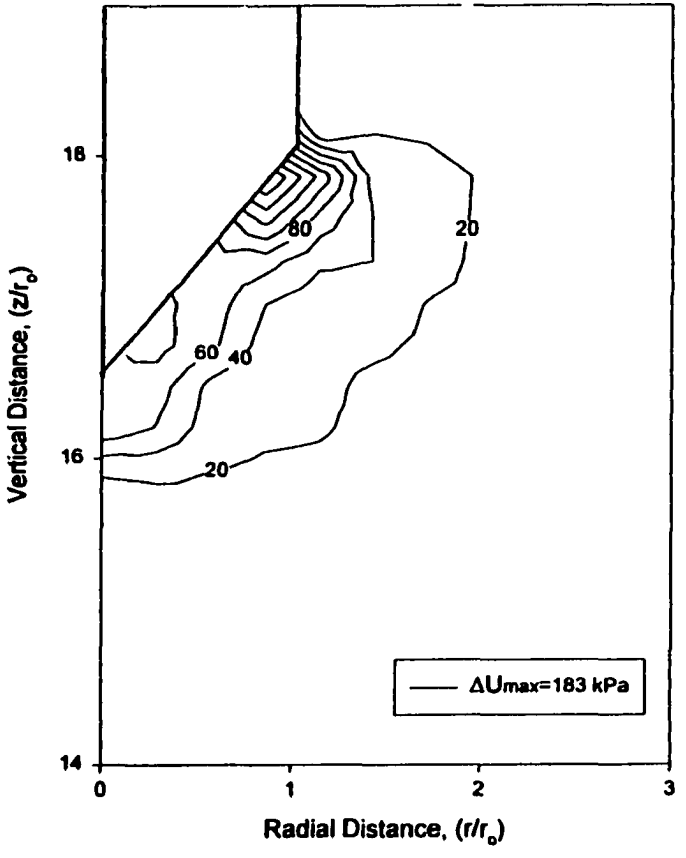

(e) IMCCM for same initial anisotropic stress condition as (a)

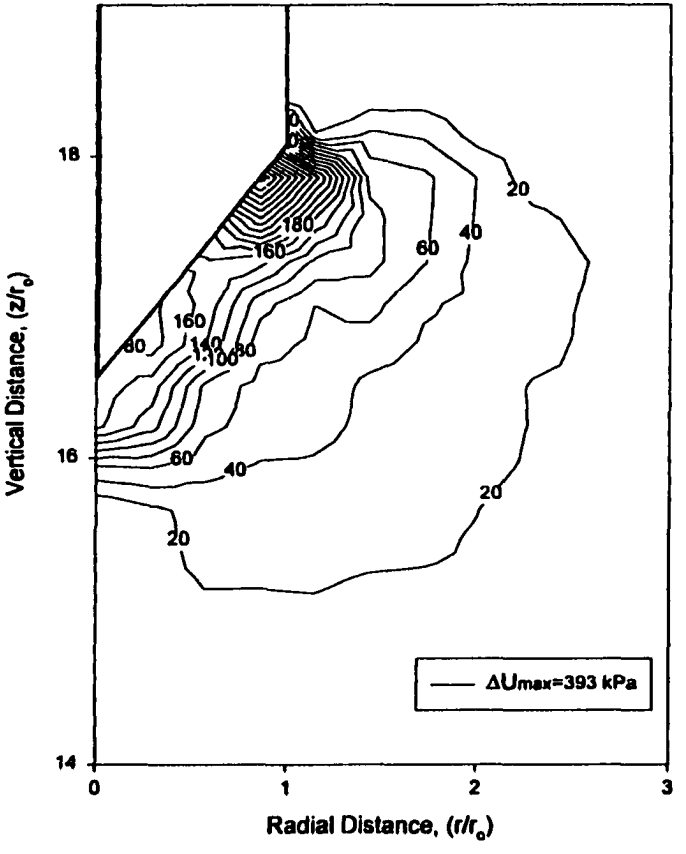

(f) AMCCM with initial isotropic stress condition as (b)

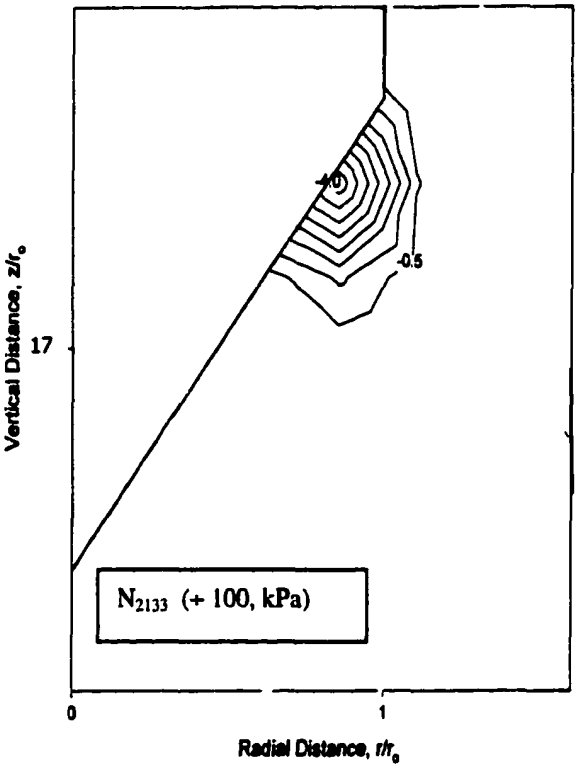

Figure 5.5.2, Contours of N_{2133} for Plastic Spin

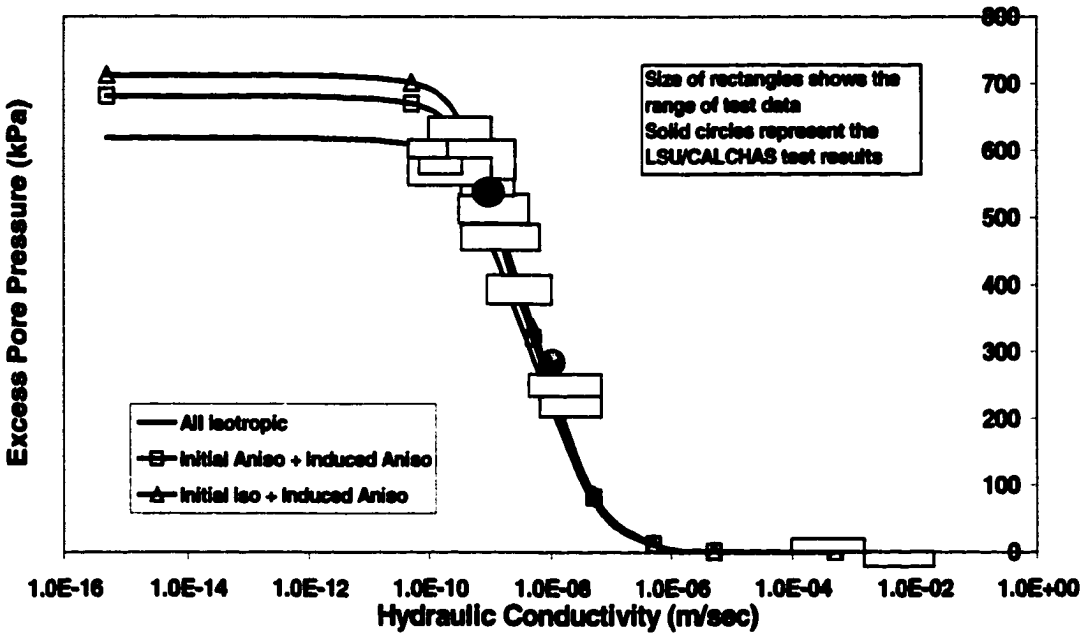

Figure 5.5.3, FEM results of pore pressure prediction of PCPT and experimental data

However, for real soils, the translation of the yield locus may occur because of the build up of internal stress (kinematic hardening). This translation of yield locus further moves up the yield locus for the normally consolidated soils (see the zone where P is larger than $P_o/2$ in Figure 1, and Figure 3), and results in the increased mean principal stress (increased P). The pore pressure of the soil is proportional to the stress level, therefore the translation of the yield locus causes the increased pore pressure. The incorporation of the kinematics of hardening for very large strain problems causes the stress oscillation behavior (Dafalias, 1983), thus the plastic spin is incorporated together with the back stress in order to alleviate such an inconsistency.

However, at the condition of initial isotropy and induced anisotropy, the corresponding pore pressure response is even bigger than the other two cases. This phenomenon is also predictable because of the fact that the initial isotropic condition assumes the hydrostatic confining condition That is the stresses are the same in all directions which is again equal to the major principal stress σ_1. Thus the resulting mean principal stress is bigger than the real mean principal stress. When one assumes $K_o = 0.5$, the initial principal stress P_o is equal to $(2/3)\sigma_1$ for the anisotropic(triaxial) conditions while P_o is equal to σ_1 for the isotropic condition.

From Figure 5.5.3, one notes the agreement between AMCCM and the experimental data is quite good, therefore better prediction of k could be made from the penetration pore pressure of the PCPT.

5.5.2 Remarks

From this investigation, it is concluded that the back stress causes the additional change of elasto-plastic stiffness.Also, the back stress allows the shift of the

yield locus, and ultimately the shift of the yield stress. In consquence, this back stress results in the increased pore pressure response. In other words, the isotropic model results in the pre-matured yielding of the material, and results in the lower yield stress and pore pressure.

When applied to the piezocone penetration test, the anisotropic model with plastic spin presents a closer pore pressure response to the experimental results. The need for the plastic spin is paramount only in the close vicinity of the cone tip where large strains and rotations occur. The rest of the region does not take advantage of the introduction of the plastic spin. However, the surface of the cone tip is where one measures the tip resistance and excess pore pressures which are affected by the presence of the plastic spin. Consequently, it is imperative to use the plastic spin when using the continuous intrusion piezocone penetration test for determining the hydraulic conductivity of soils 'on the fly'. The accuracy of the hydraulic conductivity depends mainly on the information obtained in the region adjacent to the cone tip.

CHAPTER 6. SUMMARY AND CONCLUSIONS

6.1 Summary

In this study, the coupled theory of mixtures (soil grains and pore water) with the large strain is used to predict the hydraulic conductivity of the soil from the excess pore pressure generated during the piezocone penetration test. An updated Lagrangian reference frame is used for a more rational modeling of the large strains. Formulation of the equations is based on the theory of mixtures for inelastic porous media proposed by Prevost (1980) and in an updated Lagrangian reference frame by Voyiadjis and Abu-Farsakh (1997). Typically, in analyzing the pore pressure response using the piezocone penetrometer, one inputs the soil properties such as the hydraulic conductivity, modulus, and other stress strain parameters and obtains the computed pore water pressures. However, in the proposed method, one inputs the measured pore pressure and other material properties and obtains the hydraulic conductivity.

The piezocone penetrometer is a type of electric cone penetrometer, which has the capability of characterizing the hydraulic properties of soils as well as the stress-strain characteristics of soils. Lots of research has been carried out in the design of the piezocone apparatus and interpretation of the test results. However, a number of pressing needs still exist in the design, test practice, and data interpretation of the piezocone penetration test (PCPT). Determination of the hydraulic conductivity from the PCPT is relatively convenient compared to other field hydraulic conductivity test methods. However, it is still time-consuming and needs improvement.

In order to obtain the hydraulic conductivity or the coefficient of consolidation of the soil from PCPT, the pore pressure response during a dissipation test is typically

used. The capability of dissipation tests is one of the major advantages of the PCPT because it can determine the hydraulic characteristics of the soils as well as the stress-strain characteristics. This method, however, requires the intermittent stopping of the advancement of the piezocone penetrometer at a specific depth for the dissipation test. This procedure consumes substantial time, and contributes to be the major drawback of the efficiency of the piezocone penetration test. Also, this method does not fully take into account the pore pressure interference between near and far fields which was pointed out by previous researchers (Kurup and Tumay, 1997).

Thus a new rational approach is proposed here. The proposed method utilizes the excess pore water pressure during the regular penetration of the piezocone penetrometer. By its nature, the pore pressure response around the cone tip is neither a fully drained nor a fully undrained condition. Since this is a partially drained condition; therefore, the excess pore pressure during the piezocone penetration is the function of the hydraulic conductivity of the soil as well as the function of stress strain properties. Inversely, the hydraulic conductivity of the soil can be predicted from the measured pore pressure response during the piezocone penetration test.

However, either the fully undrained condition for the cohesive soils, or the fully drained condition for the non-cohesive soils are assumed conventionally; and the effect of hydraulic conductivity on the pore pressure is disregarded. Thus, the coupled theory of multi-phase material (mixture of soil and water, in this case) is necessary for a more rational approach of the pore pressure response of the piezocone penetration test. In this work, elasto-plastic coupled equations for anisotropic stress conditions are formulated to describe the time-dependent deformation of saturated cohesive soils

(two-phase state). The formulation of these equation is based on the principle of virtual work and theory of mixtures for inelastic porous media proposed by Prevost (1980) and Voyiadjis and Abu-Farsakh (1998). The formulation for the anisotropic condition presented here is an extension of the Voyiadjis and Abu-Farsakh (1998) formulation for the isotropic condition.

Anisotropic stress condition is incorporated in the proposed model here by adapting the Dafalias (1987) anisotropic modified Cam Clay model. By adapting Dafalis' (1987) anisotropic model, the application becomes much simpler compared to other anisotropic models. The additionally required input parameter for anisotropic modified Cam Clay model is only the c and x parameters.

The anisotropic model which is used in this study is able to depict the initial anisotropy as well as the induced isotropy during deformation. This can depict the anisotropy change in soils during deformation induced by the penetration of the cone penetrometer. This capability is possible by adapting the evolution equation of the back stress.

The anisotropic models for large strains typically show an unstable stress strain relationship for very large strains. This behavior is typically called the oscillating behavior. The oscillating behavior is the result of the stress rate used for the micro-structural change. For example, there may be a condition that the shape of the soil element undergoes the rigid translation accompanied by microstructure change. When analyzed by the finite element method which does not incorporate the micro-structural change, the results will just show the rigid body rotation or translation. Also, the

results may be erroneous because its equilibrium state may be incorrect. This erroneous result causes the oscillating behavior.

To prevent this oscillating behavior, the plastic spin was used in the formulation. By plastic spin, the equilibrium equation is corrected internally, and correct solution is obtained.

This anisotropic soil model and plastic spin is incorporated in the FORTRAN program CS-S and numerical simulations were carried out for various soil parameters and conditions.

To verify the validity of the proposed study, the piezocone penetration test results were collected from around the world. Also, to avoid the deviation of the field data, the calibration chamber tests were carried out. Finally all three results were compared. For this test, a specially designed three piezo-element cone penetrometer was fabricated. Due to this three piezo-element cone penetrometer, the pore pressure response at the three locations of the penetrometer body were obtained during a single penetration. The efficiency of the penetration test is tripled in this case.

Finally, all three results (existing piezocone penetration tests, calibration chamber tests, and theoretical results) were compared and excellent agreement is obtained.

6.2 Conclusions

From this study, the following conclusions can be made:

1. With this method, the pore pressure dissipation tests are not required in order to obtain the hydraulic conductivity; thus, the efficiency of the Piezocone penetration test can be increased

significantly. It also allows one to obtain the continuous profile of the hydraulic conductivity.

2. This proposed method fully considers the pore pressure interaction between the near and far fields.

3. One point method (OPM) presents the applicable hydraulic conductivity range 10^{-9} m/sec to 10^{-6} m/sec. Also OPM can be used without the modification of current piezocone penetrometers which have the u_1 position porous element.

4. Two point method (TPM) presents the applicable hydraulic conductivity range 10^{-10} m/sec to 10^{-6} m/sec. TPM needs the modification of current piezocone penetrometers. It also needs the further refinement in the analysis algorithm, however, TPM has its own advantage that it primarily depends on the hydraulic conductivity rather than the stress strain properties.

5. The anisotropic soil model with the plastic spin showed better agreement with the test results than other models. Also, it should be noted that the anisotropic model should be used with the micro-mechanical considerations. Without micro-mechanical considerations, the anisotropic model gives erroneous results. This error is especially large when the induced strains are very large which is the case of the cone penetration test.

6. The three piezo-element penetrometer that is used in this study can be applied in the field piezocone penetrometer with the proper adjustment for the scaling factor.

7. The calibration chamber test results, existing field data, and the theoretically predicted results showed excellent agreement with each other, and shed promising light on the new method of determination of the hydraulic conductivity of soils from the continuous intrusion piezocone penetration test.

8. The back stress allows the shift of the yield locus, and ultimately the shift of the yield stress. In consequence, this back stress results in the increased pore pressure response.

9. The anisotropic model with plastic spin presents a closer pore pressure response to the experimental results. The need for the plastic spin is paramount only in the close vicinity of the cone tip where large strains and rotations occur. However, the surface of the cone tip is where one measures the tip resistance and excess pore pressures which are affected by the presence of the plastic spin. Consequently, it is imperative to use the plastic spin for the analysis of the piezocone penetration test.

6.3 Recommendations for Future Research

This study produced valuable results. However, the following recommendations are made for future research in order to address certain questions that have not been dealt with at the present time.

1. Modeling of Soil

. Piezocone penetration intrude into the ground with the speed of 2 cm/sec. Thus the process may be rate dependent. Therefore, for a more rigorous approach, the rate dependency in the soil model is desirable.

. Piezocone penetrates into the ground by brutforce penetration with relatively smooth surface. Thus the very high strain is concentrated along the penetrating cone body, and this will induce the high strain gradient around the cone penetrometer. Therefore, incorporation of the gradient theory is desirable for the modeling aspect.

. The plastic spin is a convenient method to take into account the micro-mechanical consideration. However, a more rigorous micro-mechanical approach is desirable.

2. Formulation

. For the application of this study to the more versatile soil conditions, such as unsaturated conditions, an extension of the theory of mixtures for three phase materials (air, water, solid) is desirable.

. Coupling with other phenomena is needed for application to some conditions like contaminant transport, chemical concentration, electrical potential difference etc.

3. Numerical Simulation

. For the full consideration of pore pressure interaction (two stage of steady state) along the cone shaft, long penetration needs to be

simulated. Since this long penetration is not feasible with the current computing capability, the development of new numerical schemes are desirable.

REFERENCES

Abu-Farsakh, M.Y., Voyiadjis, G.Z. and Tumay, M.T. (1998), "Numerical Analysis of the Miniature Piezocone Penetration Tests (PCPT) in Cohesive Soils," International Journal for Numerical and Analytical Methods in Geomechanics, Vol. 22, pp.791-818

Abu-Farsakh, Y. M (1997), "Coupled field equations for saturated soils and its application to piezocone penetration and shield tunneling," Ph. D. Dissertation, LSU, Baton Rouge, LA. 70808, 207p

Acar, Y.B. and Tumay, M.T. and Chan, A. (1982), "Interpretation of the dissipation of penetrometer pore pressures," Proc. Int. Symp. on Numerical Models in Geomechanics, Zurich, pp.353-358

Acar, Y.B. and Tumay, M.T. (1986), "Strain field around cones in steady penetration," J. of GE. Div., ASCE, Vol.112, pp.207-213, Feb. strain field

Al-Awkati, Z.A. (1975), "On problems of soil bearing capacity at depth," Ph. D. Dissertation, Duke Univ., Dept. of Civ. Engr.

Almeida , M.S.S., Jamiolkowski, M. and Peterson, R.W. (1991), "Preliminary results of CPT tests in calcarous Quiou sand," Calibration Chamber Testing, ed. An-Bin Huang, Elsvier, pp.41-54

Al-Tabba, A. (1994), "Consolidation with Radial Drainage: Observed and Predicted Behavior," XIII ICSMFE, New Delhi, pp.75-78

Al-Tabba, A. and Muir Wood, D. (1991), "Horizontal drainage during consolidation : insights gained from analyses of a simple problem," Geotechnique, Vol. 41, No. 4, pp.571-585

Alturi, N. (1984), "On constitutive relations at finite strain: hypo-elasticity and elasto-plasticity with isotropic or kinematic hardening," Computer Methods Appl. Mech. Engineering, 43, 137-171

Anandarajah, A. (1994), "Discrete Element Method for Simulating Behavior of Cohesive Soils," Journal of Geotechnical Engineering Div. ASCE. Vol.120, No.9, pp.1593-1613

Armstrong, P.J. and Frederick, C.O. (1966), "A mathematical representation of the multiaxial Bauschinger effect," CEGB Report RD/B/N/731, Berkerly Nuclear Laboratories

Baligh, M.M. (1975), "Theory of deep site static cone penetration resistance," Report No. R.75-76, MIT, Cambridge, Mass. 02139

Baligh, M.M. (1985), "Strain Path Method," J. of GE. Div. ASCE, Vol.111, No.9, pp.1108-1136

Baligh, M.M., Azzouz, A.S., Wissa, A.Z.E., Martin, R.T. and Morrison, M.J., (1981), "The piezocone penetrometer," ASCE, GE. Div. Symposium on Cone Penetration Testing and Experience, St. Louis, pp.247-263

Baligh, M.M., and Levadoux, J.N. (1980), "Pore pressure dissipation after cone penetration," MIT, Dept. of Civ. Engr. Report R.80-11. Cambridge, Mass. 02139, 367 p.

Baligh, M.M., and Levadoux, J.N. (1986), "Consolidation after undrained piezocone penetration, Part II: Interpretation," J. of GE. Div. ASCE, Vol. 112, No.7, July, pp.727-745

Baligh, M.M., Vivatrat, Y., and Ladd, C.C., (1980), "Cone penetration in soil profiling," J. of GE. Div. ASCE. Vol. 106, No. GT4, Apr. pp.447-461

Banerjee, P.K. and Yousif, N.B., (1986), "A plasticity model for the mechanical Behavior of anisotropically consolidated clay," Int. J. for Numerical analytical methods in geomechanics, Vol. 10, pp.521-541

Banerjee, P.K. and Fathallah, R. (1979), "An Eulerian Formulation of the Finite Element Method for Predicting the Stresses and Pore Water Pressures Around a Driven Pile," Proceedings of 3rd Int. Conf. Num. Method on Geomechanics, Aachen, West Germany, pp.1053-1060

Batdorf, S.B. and Budianski, B. (1949), "A Mathematical Theory of Plascitity Based on the Concept of Slip", National Advisory Committee for Aeronautics Technical Note, No. 1871, Washington, D.C. Apr.

Bathe, K.J. (1996), *Finite Element Procedures*, Prentice Hall, pp.485-641

Battaglio, M., Bruzzi, D., Jamiolkowski, M., Lancellotta, R. and Maniscalo, R. (1981), "Piezometer Probe Test in Cohesive Deposits," ASCE Cone Penetration Testing and Experience, Proceedings of a Session at ASCE National Convention, St. Louis, Missouri, USA, pp. 264-302

Battaglio, M., Bruzzi, D., Jamiolkowski, M. and Lancellotta, R. (1986), "Interpretation of CPT's and CPTU's – Undrained penetration of saturated clays," Proceedings of 4th Int. Geotechnical Seminar, Singapore, pp.129-143

Bazant, Z.P. and Kim, J-K. (1986), "Creep of anisotropic clay:Microplane model," J. of GE. ASCE, 112(4), pp.458-475

Bazant, Z.P. (1984), "Microplane Model for Strain Controlled Inelastic Behavior," Chap. 3, Mechanics of Engineering Materials, C.S. Desai and R.H. Gallagher, Eds. John Wiley & Sons, New York, NY, pp.45-59

Bazant, Z.P. and Oh, B.H. (1983), "Microplane Model for Fracture Analysis of Concrete Structures," Proceedings, Symposium of the Interaction of Non-nuclear Munitions with Structures," U.S. Airforce Academy, Colorado Springs, CO. May, pp.49-55

Bazant, Z.P. and Oh, B.H. (1985), "Microplane Model for Progressive Fracture of Concrete and Rock," Journal of Engineering Mechanics, ASCE, Vol.3, No.4, Apr. pp.559-582

Bazant, Z.P. and Prat, P.C. (1987), "Creep of anisotropic clays: New microplane model," J. of EM. ASCE, 113(7), pp.1050-1064

Begemann,K.K.S. (1965), "The friction jacket cone as an aide in determining the soil profile," Proceedings of 6th ICSMFE, Montreal, Vol.1

Biot, M.A. (1955), "Theory of elasticity and consolidation for a porous anisotropic solid," J. of Appl. Phys. Vol.26, pp.182-185

Biot, M.A. (1978), "New concepts and methods", Q. Appl. Math. 36, 19

Burland, J.B. (1965), "The Yielding and Dilation of Clay (Correspondence)", Geotechnique, Vol.15, pp.211-214

Campanella R.G. (1994) , Lecture Note, presented to Korean Geotechnical Society

Campanella, R.G. and Robertson, P.K., (1981), "Applied cone research," J. of GE. Div. ASCE, Symposium on Cone Penetration Testing and Experience, St. Louis, pp.343-362

Campanella, R.G., and Robertson, P.K., Gillespie, D.G. and Greig, J. (1985), "Recent development in in situ testing of soils," Proceedings XI ICSMFE, San Francisco, pp.849-854

Carol, I., Bazant, Z.P. and Prat, P.C. (1990), "New explicit microplane model for concrete: Theoretical aspects and unified implementation for constitutive verification and F.E. analysis," Report, E.T.S. Cannals I Ports-U.P.C.: Jordi girona, 31 – E-08034 Barcelona, Spain

Carter, J.P., Booker, J.R. and Small, J.C. (1979), "The analysis of finite elastoplastic consolidation," Int. J. for Num. and Analytical Methods in Geomechanics, pp.561-565

Carter, J.P., Small, J.C., and Booker, J.R. (1977), "A theory of finite elastic consolidation," J. of Solids Structures, Vol. 13, pp.467-478

Chan, A. (1982), "Analysis of Dissipation of Pore Pressure after Cone Penetration," M.S. thesis, Dept. of Civil and Environmental Engineering, LSU, LA 70803, 120 p.

Chen, W.F. (1975), *Limit Analysis and Soil Plasticity*, Elsvier, Amsterdam, Netherlands

Chen, W.F. and Mizuno, E. (1990), *Nonlinear Analysis in Soil Mechanics; Theory and Implementations*, Elsvier, New York, NY

Chen, B.S. and Mayne, P.W. (1994), "Profiling the Overconsolidation Ratio of Clays by Piezocone Tests," Report No. GIT-CEEGEO-94-1, August

Chopra, M.B. and Dargush, G.F. (1992), "Finite-Element Analysis of Time-Dependent Large-Deformation Problems," International Journal for Numerical and Analytical Methods for Geomechanics, Vol.16, pp.101-120

Clark, J.I. and Meyerhof, G.G. (1972), "The Behavior of Piles Driven in Clay. I. An Investigation of Soil Stress and Pore Water Pressure as Related to Soil Properties," Can. Geotech. J. Vol.9, pp.351-373

Cleary, M.P. (1977), "Fundamental Solutions for a fluid-saturated porous solid," Int. J. of Solid Structures, Vol.13, pp.785-806, Pergamon Press

Dafalias, Y.F. (1983), "Corotational rates for kinematic hardening at large plastic deformations, " Transactions of the ASME, J. of Applied Mechanics, pp.561-565

Dafalias, Y.F. and Aifantis, E.C. (1984), "On the origin of the plastic spin," MM report, No.8, MEEM, MTU, Houghton, Michigan

Dafalias, Y.F. (1985), "A missing link in the macroscopic constitutive formulation of large plastic deformations," In : Plasticity today (Sawczuk, A., Bianchi, G., eds.), pp.135-151, Symposium on Current trends and Results in Plasticity, CISM, Udine, Italy, Elsvier

Dafalias, Y.F. (1987), "An Anisotropic Critical State Clay Plasticity Model," Constitutive Laws for Engineering Materials: Theory and Applications, Eds. C.S. Desai et al. pp.513-521

Dafalias, Y. (1998), "Plastic Spin: Necessity or Redundancy?" Int. J. of Plasticity, Vol.14, No.9, pp.909-931

de Borst, R. and Vermeer, P.A. (1982), "Finite element analysis of static penetration test," Proceedings of 2nd European Symposium on Penetration Testing, Amsterdam

de Borst, R. and Vermeer, P.A. (1984), "Possibilities and Limitation of Finite Element for Limit Analysis," Geotechnique, Vol.34, No.2, pp.199-210

de Lima, D.C. (1990), "Development, Fabrication and Verification of the LSU In Situ Testing Calibration Chamber," Ph. D Dissertation, Louisiana State University, Baton Rouge, LA. 340 p.

de Lima, D.C. and Tumay, M.T. (1991), "Scale Effects in Cone Penetration Tests," Special Publication No.27, Proc., Geotechnical Engineering Congress, GT Div/ASCE, Boulder, CO. pp.38-51

de Lima, D.C. and Tumay, M.T. (1992), "Calibration and Implementation of Miniature Electric Cone Penetrometer and Development, Fabrication and Verification of the LSU In-situ Testing Calibration Chamber (LSU/CALCHAS)," LTRC/FHWA Report No. GE-92/08, 240p

de Ruiter, J. (1982), "The static cone penetration test: state-of-art report," Proceedings of the Second European Symposium on Penetration Testing, ESOPT II, Amsterdam, Vol. 2, pp.389-405

Dienes, J.K. (1979), "On the analysis of rotation and stress rate in deforming bodies," Acta Mechanica, 32, pp.217-232

DiMaggio, F.L. and Sandler, I.S. (1971), "Material Model for Granular Soils," Journal of Engineering Mechanics Div. ASCE, Vol.97, No.EM3, pp.935-950

Dobry, R. (1985), Presentation at the University of Texas at Austin

Dobry, R. Ng, T.-T., Petrakis, E. and Seridi, A. (1991), "General Model for Contact Law between Rough Spheres," J. of EM, Vol. 117, No.6, June, 1991, pp.1365-1381

Dobry, R. and Petrakis, E. (1991), "A Study of the Behavior and Micromechanical Modelling of Granlar Soil - Volume I : A Constitutive Relation for Granular Materials Based on the Contact Law between Two Spheres," Report to the US AFSOR, Department of Civil Engineering, RPI, Troy, NY

Durgunoglu, H.T., and Mitchell, J.K. (1975), "Static penetration resistance of soils: I-ANALYSIS," ASCE Specialty Conference on In situ Measurement of Soil Parameters, Raleigh, Vol. I

Elsworth, D. (1991), "Dislocation Analysis of Penetration in Saturated Porous Media," J. of EM. ASCE. Vol. 117, No.2, pp.391-408

Elsworth, D. (1992), "Pore-pressure response due to penetration through layered media," Int. J. for Numerical and Analytical Methods in Geomechanics, Vol.16, pp.45-64, John Wiley and Sons

Elsworth, D. (1993), "Analysis of Piezocone Dissipation Data Using Dislocation Methods," J. of GE. ASCE, Vol.119, No.10, pp.1601-1623

Elsworth, D. (1998), "Indentation of a sharp penetrometer in a poroelastic medium", Int. J. of Solids Structures, Vol. 35, No. 34-35, pp.4895-4904

Envi (1996), Envi web page, http://www.envi.se

Foott, R. and Ladd, C.C. (1977), "Behavior of Atchafalaya levees during construction," Geotechnique, Vol. 27, No.2, pp.137-160

Gibson , R.E., (Discussion of Wilson, G.) (1950), "The bearing capacity of screw piles and screw-crete cylinders," J. of Institution of Civil Engineers, Vol.34, No.4, p.382

Gibson, R.E. and Gilbert, A. and Schiffman, R.L. (1990), "On Cryer's problem with large displacements and variable permeability," Geotechnique, Vol.40, No.4, pp.627-631

Gibson, R.E., England, G.L. and Hussey, M.J.L. (1967), "The theory of one-dimensional consolidation of saturated clays, I Finite non-linear consolidation of thin homogeneous layers," Geotechnique, Vol. 17, pp.261-273

Gibson, R.E., Schiffman, R,L. and Cargill, K.W. (1981), "The theory of one-dimensional consolidation of saturated clays, II Finite non-linear consolidation of thick homogeneous layers," Canadian geotechnical J. Vol.18, pp.280-293

Green, A.E. and McInnis, B.C. (1967), "Generalized hypo-elasticity," Proc. Rou. Soc. Edinburgh, A57, Part III, pp.220-230

Green, A.E. and Naghdi, P.M. (1965), "A general theory of an elastic-plastic continuum," Arch. Rational Mech. Anal. 18, pp.251-281

Gupta, R.C. (1991), "Finite strain analysis for deep cone penetration," J. of GE. Div. ASCE. Vol.117, No.10, pp.1610-1630

Gupta, R.C. and Davidson, J.L. (1986), "Piezoprobe determination of the coefficient of consolidation," Soils and Foundation, Vol.26, No.3, pp.12-22

Henkel, D.J. and Wade, N.H. (1966), "Plane strain on a saturated remolded clay," J. of Soil Mechanics and Foundations, ASCE, Vol. 92, No.6

Houlsby,G. and Teh, C.I. (1988), "Analysis of piezocone in clay, " Proc. ISOPT I, Vol. 2, A.A. Balkema, Rotterdam, Netherlands, pp.777-783

Houlsby, G.T. and Wroth, P. (1982), "Determination of undrained strengths by cone penetration tests," Proceedings of 2nd European Symposium on Penetration Testing (ESOPT II), Amsterdam

Huang, A.B., Holtz, R.D. and Chameau, J.L. (1988), "A Calibration Chamber for Cohesive Soils," ASTM Geotechnical Testing Journal, Vol.11, No.1, pp.30-35

Jamiolkowski, M., Ladd, C.C., Germaine, J.T. and Lancellotta, R. (1985), "New Development in Field and Laboratory Testing of Soils," Proceedings of 11th ICSMFE, San Fransisco, pp.57-153

Janbu, N. and Senneset, K. (1974), "Effective Stress Interpretation of the In Situ State Penetration Tests," ESOPT, June 5-7, Also, handout for geotechnical seminar at Louisiana State University by Senneset (1998)

Johnson, G.C. and Bammann, D.J. (1984), "A discussion of stress rates in finite deformation problems," Int. J. of Solids Structures, 20, pp.725-737

Jones, G.A. and Rust, E.A.(1982), "Piezometer penetration using CUPT," Proceedings of the Second European Symposium on Penetration Testing, ESOPT II, Amsterdam, Vol. 2, pp.607-613

Jones, G.A. and Rust, E.A. (1993), "Estimating coefficient of consolidation from piezocone tests:[1] Discussion," Can. Geotech. J. Vol. 30, pp.723-724

Juran, I. and Tumay, M.T. (1989), "Soil Stratification Using the Dual Pore-Pressure Piezocone Tests," Proceedings of the European Symposium on Penetration Testing, ESOPT-I, Stockholm, Sweden, Vol.2.2, pp.181-195

Kabir, M.G. and Lutenegger A.J. (1990), "In situ estimation of the coefficient of consolidation," Can. Geotech. J. Vol. 27, pp.58-67 (Case Study)

Kaufman, R.I. and Weaver, F.J. (1967), "Stability of Atchafalaya Levees," J. of SMFE, ASCE, Vol.93, No.SM4, pp.157-176

Kiousis, P.D. (1985), "Large Strain Theory as Applied to Penetration Mechanism in Soils," Ph. D. Dissertation, Louisiana State University, Baton Rouge, LA 70803

Kiousis, P.D. and Voyiadjis, G.Z. (1985), "Lagrangian Continuum Theory for Saturated Porous Media," Journal of Engineering Mechanics Div., ASCE, Vol.111, No.10, pp.1277-1288

Kiousis, P.D., Voyiadjis, G.Z. and Tumay, M.T. (1988), "A large strain theory and its application in the analysis of the cone penetration mechanism," International J. for Numerical and Analytical Methods in Geomechanics, Vol..12, No.1, pp.45-60

Kiousis, P.D., Voyiadjis, G.Z. and Tumay, M.T.,(1986), "A large strain theory for the two dimensional problems in geomechanics," Int. J. for Numerical and Analytical Methods in Geomechnics, Vol. 10, pp.17-39

Konrad, J.M., and Law, K.T., (1987), "Undrained shear strength from piezocone tests," Canadian Geotechnical J. Vol.14, pp.392-405

Krizek, R.J. and Sheeran, D.E. (1970), "Slurry Preparation and Characteristics of Samples Consolidated in Slurry Consolidometer," Technical Report No. 2, Contract No. DACW39-70-C-0053, U.S. Army Corps of Engineers, Waterways Experiment Station, Vicksburg, pp.1-5

Kratochvil, J. (1971), "Finite-strain theory of crystalline elastic-inelastic material", J. of Appl. Phys. 42, pp.1104-1108

Kurup, P.U. (1993), "Calibration chamber studies of miniature piezocone penetration tests in cohesive soil specimen," Ph. D. Dissertation, Louisiana State University, Baton Rouge, LA. 70808, 234p

Kurup, P.U. and Tumay, M.T. (1998), "Calibration of a miniature cone penetrometer for highway applications," in press, Transportation Research Record, National Research Council; (also presented at "Calibration of In Situ test Methods for Transportation Related Structures Design," Session of the 77th Meeting, Transportation Research Board , January, 11-15, Washington, D.C.

Kurup, P.U. and Tumay, M.T. (1997), "A numerical model for the analysis of piezocone dissipation curves," Proceedings International Symposium on Numerical Models in Geomechanics (NUMOG VI), Montreal, Canada, July, 2-4, pp.353-358

Kurup, P.U., Voyiadjis, G.Z. and Tumay, M.T. (1994), "Calibration chamber studies of Piezocone Test in Cohesive Soils," J. of GE. ASCE, Vol.120, No.1, pp.81-107

Lacasse, S. and Lunne, T. (1982), "Penetration Tests in Two Norwegian Clays," Proceedings of the 2nd European Symposium on Penetration Testing, Amsterdam, Vol. II, pp.607-613

Ladanyi, B. (1963), "Expansion of a Cavity in a Saturated Clay Medium," Journal of Soil Mechanics and Foundation Engineering Div., ASCE, Vol.90, No. SM4, pp.127-161

Ladanyi, B. and Eden, W.J. (1969), "Use of Deep Penetration Test in Sensitive Clays," 7th ICSMFE, Mexico, pp.225-230

Lee, E.H. (1993), "Interaction between Physical Mechanism and Structure of Continuum Theories," Large Deformations of Soilds: Physical Basis and Mathematical Modelling , edited by J. Gittus, J. Zarka, and S. Nemat-Nasser, Elsvier, pp.143-161

Lee, E.H., Mallett, R.L. and Wertheimer, T.B. (1983), "Stress analysis for anisotropic hardening in finite-deformation plasticity," Transactions of the ASME, J. of Applied Mechanics, Vol.50, pp.554-560

Levadoux, J.N. and Baligh, M.M. (1980), "Pore Pressure during Cone Penetration in Clays," MIT Dept. of Civil Engineering Report No. R80-15, 310 p

Levadoux, J.N. and Baligh, M.M. (1986), "Consolidation after undrained piezocone penetrometer, I: Prediction," J. of GE. Div. ASCE, Vol.112, No.7, pp.707-725

Lim, B.S. (1999), "Determination of Consolidation Characteristics in Fine Grained Soils Evaluated by Piezo Cone Tests," Ph. D. Dissertation, Louisiana State University, Baton Rouge, LA 70808, (expected at 1999)

Loret, B. (1983), "On the effects of plastic rotation in the finite deformation of anisotropic elastoplastic materials. Mechanics of Materials, 2, pp.287-304

Lunne, T. and Kleven, A., (1981), "Role of CPT in north sea foundation engineering," J. of GE. Div. ASCE, Symposium on Cone Penetration Testing and Experience, St. Louis, pp.49-75

Lunne, T., Christoffersen, H.P. and Tjelta, T.H. (1985), "Engineering use of piezocone data in North sea clays," Proceedings XI ICSMFE, San Francisco, Vol.2, pp.907-912

Lunne, T., Lacasse, S. and Rad, N.S. (1989), "General report/Discussion session 2 : SPT, CPT, pressuremeter testing and recent developments in in-situ testing – Part 1 : All tests except SPT," XII ICSMFE, Rio de Janeiro, Vol.4, pp.2339-2403

Lunne, T., Robertson, P.K. and Powell, J.J.M. (1997), *Cone Penetrating Testing*, Blackie Academic & Professional, pp.1-7, 172-190

Manassero, M. (1994), "Hydraulic Conductivity Assessment of Slurry Walls Using Piezocone Test," J. of GE. ASCE, Vol.120, No.10, pp.1725-1746

Mandel, J. (1971), "Plasticite classque et viscoplasticite," Courses ad Lectures No. 97, International Center for Mechanical Sciences, Udine, Sprinejer, NY

Massarch, K.R. and Broms, B.B. (1981), "Pile driving in clay slopes," Proceedings of ICSMFE, Stockholm, pp.469-474

Mayne, P.W. (1991), "Determination of OCR in clays by piezocone tests using cavity expansion and critical state concepts," Soils and Foundations, Vol.31, No.2, pp.65-76

Mayne, P.W. (1992), "In-situ determination of clay stress history by piezocone," Proceedings of the Wroth Memorial Symposium, St. Catherine's College, Oxford, 27th-29th, July, pp.361-372

Mayne, P.W. (1992), "Interpretation of overconsolidation ratio from in situ tests in Recent clay deposits in Singapore and Malaysia:[1] Discussion," Can. Geotech. J. Vol. 29, pp. 166-167

Mayne, P.W. (1996), "Development of a Seismic Piezocone Pressuremeter for Evaluating the In-Situ G/Gmax Degradation Characteristics of Soils," Geosystems web page, http://www.geosystems.gatech.edu

Mayne, P.W. and Chen, B.S.Y. (1994), "Preliminary calibration of PCPT-OCR model for clays," XIII ICSMFE, New Delhi

Mayne, P.W. and Kulahwy, F. H. (1990), "Observations on the development of pore water stresses during piezocone penetration in clays," Can. Geotech. J. Vol.27, pp.418-428

Mayne, P.W. and Kulhawy, F.H. (1992), "Effects of Lateral Stress on CPT Penetration Pore Pressure," Discussion, J. of GE. ASCE. Vol.118, No.10, pp.1167-1169

Meyerhof, G.G. (1961), "The ultimate bearing capacity of wedge shaped foundations," Proceedings of 5th ICSMFE, Paris, Vol.2

Mindlin, R.D. and Deresiecwicz (1953), "Elastic spheres in contact tunder varying oblique forces," J. of Appl. Mech. ASME, Vol. 20, pp.327-344

Muromachi, T. (1981), "Cone penetration testing in Japan," ASCE, GE Div. Symposium on Cone Penetration Testing and Experience, St. Louis, pp.76-107

Nagtegaal, J.C. and de Jong, J.E. (1982), "Some aspects of non-isotropic workhardening in finite strain plasticity," In : Plasticity of metals at finite strain : theory, experiment and computation (Lee, E.H, Mallet, R.L., eds.), pp.65-102, The

Division of Applied Mech., Stanford Univ., Stanford, CA, and Dept. of Mech. Engrg., Aeronautical Eng. And Mech., R.P.I. Troy, New York

Onat, E.T. (1984), "Shear flow of kinematically hardening rigid-plastic materials," In:Mechanics of material behavior (Dvorak, G.J., Shield, R.T., eds.), Elsvier, pp.311-323

Pande, G.N. and Sharma, K.G. (1980), "A micro-structural model for soils under cyclic loading," Proc. Int. Symp. On Numerical Models in Geomechanics, R. Dungar, G.N. Pande, and G.A. Studer, eds., A.A. Balkema Publishers, pp.218-226

Pande, G.N, and Sharma, K.G. (1983), "Multilaminate model of clays-A numerical evaluation of the influence of rotation of principal axes," Int. Journal for Analytical Methods for Geomechanics, 7, pp.397-418

Pande, G.N. and Xiong, W. (1982), "An improved multi-laminate model of jointed rock masses," Proc. 1st Int. Symp. on Numerical Models in Geomechanics, R. Dungar, G.N. Pande, andG.A. Studer, eds., A.A. Balkema Publishers, pp.218-226

Paulun, J.E. and Percherski, R.B. (1985), "Study of corotational rates for kinematic hardening in finite deformation plasticity," Arch. Mech. 37, (6), pp.661-677

Perzyna, P. (1966), "Fundamental Problems in Viscoplasticity," J. of GE, ASCE, Vol. 104, No. GT8, pp. 1075-1090

Peterson, R.W. (1991), "Penetration resistance of fine cohesionless materials," Calibration Chamber Testing, ed. An-Bin Huang, Elsvier, pp.215-328

Petrakis, E. Dobry R., Van Laak P., Liu L. and Kotsanopoulos P. (1991), "An Experimental Investigation of Yield Surfaces in Granular Media," Constitutive laws for Engineering Materials,

Petrakis, E., Dobry, R. and Ng, T.-T. (1991), "A Study of the Behavior and Micromechanical Modelling of Granular Soil - Volume III: A Numerical Investigation of the Behavior of Granular Media Using Nonlinear Discrete Element Simulations," Report to the US AFSOR, Department of Civil Engineering, RPI, Troy, NY. 12180

Powell, J.J.M. and Quarterman, R.S.T. (1997), "A Study of piezocone dissipation tests in soft clays for consolidation properties," under preparation, (excerpted from Lunne, Robertson, Powell (1997))

Prager, W. (1961), *Introduction to mechanics of continua*, New York: Ginn and Company

Prat, P.C. and Bazant, Z.P. (1989), "Microplane model for triaxial deformation of soils," Proc. 3rd Int. Symp. on Numerical Models in Geomechanics (NU-MOG III), Elsevier, pp.139-146

Prat, P.C. and Bazant, Z.P. (1990), "Microplane model for triaxial deformation for saturated cohesive soils," J. of GE. ASCE, 117(6), pp.891-912

Prevost, J.H. (1980), "Mechanics of continuous porous media," Int. J. of Eng. Sci. Vol. 18, pp.787-800

Prevost, J.H., (1981), "Consolidation of an elastic porous media," J. of the EM. Div. ASCE, Vol. 107, No. EM1, pp.169-186

Randolph, M.F, Carter, J.P. and Wroth, C.P. (1979), "Driven piles in clay – the effects of installation and subsequent consolidation," Geotechnique, Vol.29, No.4, pp.361-393

Randolph, M.F. and Wroth, C.P. (1970), "An analytical solution for the consolidation around a driven pile," Int. J. of Numerical and Analytical Methods in Geomechanics, Vol. 3, pp.217-229

Robertson, P.K., Sully, J.P., Woeller, D.J., Lunne, T., Powell, J.J.M. and Gillespie, D.G. (1992), "Estimating coefficient of consolidation from piezocone test," Can. Geotech. J. Vol. 29, pp.539-550

Robertson, P.K., Campanella, R.G., Gillespie, D. and Grieg, J. (1986), "Use of piezometer cone data," Proceedings of In situ '86, ASCE, Specialty Conference, Blacksburg, Virginia

Roy, M., Blanchet, R., Tavenas, F. and La Rochelle, P. (1981), "Behavior of a sensitive clay during pile driving," Can. Geotech. J. Vol.18, pp.67-86

Roy, M., Tremblay, M., Tavenas, F. and La Rochelle, P. (1982), "Development of pore pressures in quasi-static penetration tests in sensitive clay," Can. Geotech. J. Vol.19, pp.124-138

Roy, M., Tremblay, M., Tavenas, F. and La Rochelle, P. (1982), "Development of quasi-static piezocone apparatus," Can. Geotech. J. Vol.19, pp.180-188

Sandven, R. (1990), "Strength and Deformation Properties of Fine Grained Soils Obtained from Piezocone Tests," Ph. D dissertation, Institute for Geoteknikk, Trondheim, Norway

Sandven, R., Senneset, K. and Janbu, N. (1988), "Interpretation of piezocone tests in cohesive soils," Proceedings ISOPT 1, Vol.2, pp.939-954, Orlando, Florida, pp.939-953

Schiffman, R.L. (1980), "Finite and infinitesimal strain consolidation," J. of GE Div. ASCE, Vol. 106, No. GT2, pp.203-207

Schnaid, F. and Houlsby, G.T. (1991), "An assessment of chamber size effects in the calibration of in situ tests in sand," Geotechnique, Vol.3, pp.437-445

Schofield, A.N. and Wroth, C.P. (1968), *Critical State Soil Mechanics*, McGraw Hill, London

Scott, R.F. (1990), "Radial consolidation of a phase-change soil," Geotechnique, Vol.40, No.2, pp.211-221

Senneset, K. (1974), "Penetration testing in Norway," State-of-the-art report, ESOPT, June 5-7

Senneset, K. and Janbu, N. (1982), "Strength and deformation parameters from cone penetration tests," Proceedings ESOPT, Amsterdam, pp.863-870

Senneset, K. and Janbu, N. (1984), "Shear strength measured with piezometer cones," Proceedings, ESOPT II, Amsterdam, Vol. 2, pp.41-54

Senneset, K. and Janbu, N. (1984), "Shear strength parameters obtained from static cone penetration tests," ASTM STP, No. 883, pp.41-54

Senneset, K., Sandven, R., Lunne, T., By, T. and Amundsen, T. (1988), "Piezocone tests in silty soils," Proceedings ISOPT 1, Vol.2, pp.955-966

Senneset, K. Sandven, R. and Janby, N. (1989), "Evaluation of Soil Parameters from Piezocone Tests," Transportation Research Record 1235, National Research Council, Washington D.C. 1989, 14p.

Sills, G.C. (1975), "Some conditions under which Biot's equation of consolidation reduce to Terzaghi's equation," Geotechnique, Vol.25, No.1, pp.129-132

Sivakumar, S.M. (1993), "A Non-Proportional Cyclic Plasticity Model for Metals with Ratchetting Effect," Ph. D. Dissertation, Louisiana State University, Baton Rouge, LA. 70803

Smits, F.P. (1982), "Penetration pore pressure measured with piezometer cones," Proceedings, ESOPT II, Amsterdam, Vol. 2, pp.877-881

Soderberg, L.O. (1962), "Consolidation theory applied to foundation pile time effects," Geotechnique, Vol.12, pp.217-225

Song, C.R., Paek, S.H. and Oh, D.Y. (1992), "Assessment of consolidation characteristics by field instrumentation," Proceedings of Korean Geotechnical Society (KGS) Fall '92 National Conference, pp. 121-130

Steenfelt, J.S., Randolph, M.F., Wroth, C.P. (1981), "Instrumented Model Piles Jacked into Clay," 10th, ICSMFE, Stockholm, pp.857-864

Sully, J.P., Campanella, R.G., and Robertson, P.K. (1988), "Interpretation of penetration pore pressure to evaluate stress history in clay," Proceedings ISOPT 1, Vol.2, pp.993-999

Taylor, G.I. (1938), "Plastic strain in metals," J. Inst. Metals, 62, pp.307-324

Teh, C.I. and Houlsby, G.T. (1991), "An analytical study of the cone penetration test in clay," Geotechnique, Vol. 41, No.1, pp.17-34

Terzaghi, K. (1943), Theoretical Soil Mechanics, John Wiley and Sons, pp.265-296

Torstensson, B.A. (1975), "Pore pressure sounding instrument," Proceedings, ASCE, Spec. Conf. On In situ Measurement of Soil Properties, Vol. II, Raleigh, N.C. pp.48-54

Torstensson, B.A. (1977), "The pore pressure probe," Paper 34, Geotech. Meeting, Norwegian Geotech. Soc., Oslo, Norway. Pp. 34.1-34.15

Truesdell, C, (1955), "Hypo-elasticity," J. of Rational Mech. Anal. 4, pp.83-133

Tumay, M.T. and Acar, Y.B. (1985), "Pore pressures in piezocone penetration test (PCPT) in soft cohesive soils," Special Technical Publication No. 833, Strength Testing of Marine Sediments : Laboratory and In situ Measurements, ASTM, Nov. pp.72-82

Tumay, M.T., Acar, Y.B., Cekirge M. H. and Ramesh, N. (1985), "Flow field around cones in steady penetration," J. of GE. Div. ASCE, Vol.111, No.2, Feb. pp. 193-205

Tumay, M.T., Boggess, R.L. and Acar, Y., (1981), "Subsurface investigation with piezocone penetrometer," ASCE Spec. Publ., pp.325-342

Tumay, M.T. and de Lima, D.C. (1992), "Calibration and implementation of miniature electric cone penetrometer and development, Fabrication and verification of LSU In-situ testing calibration chamber (LSU/CALCHAS)," LTRC/FHWA Report No. GE-92/08

Tumay, M.T. and Kurup, P. (1997), "Calibration and implementation of miniature electric cone penetrometers for road and highway design and construction control," Report No. 305, U.S. Department of Transportation, FHWA, Dec. 91p

Tumay, M.T. and Kurup, P. (1999), "A Continuous Intrusion Miniature Cone Penetration Applications," Report, FHWA/LA.88/311, 60p

Tumay, M.T., Kurup, P. and Boggess, R.L. (1998), "A Continuous intrusion electronic miniature cone penetration tests systems for site characterization," in press, proceedings, International Conference on Site Characterization, '98, Atlanta, GA, April 19-22

van der Berg, P. (1993), "Cone penetration in layered media, an ALE finite element formulation," XIII J. of ICSMFE, pp. 1957-1962

Vesic, A.S. (1972), "Expansion of cavities in infinite soil mass," J. of Soil Mechanics and Foundation Div. ASCE, Vol.98, pp.265-290

Voyiadjis, G.Z. and Abu-Farsakh, Y. M. (1997), "Coupled theory of mixtures for clayey soils", Computer and Geotechnics, Vo.20, No.3-4, pp.195-222

Voyiadjis, G.Z. (1988), "Degradation of Elastic Modulus in Elastoplastic Coupling with Finite Strains," International Journal of Plasticity, Vol.4, pp.335-353

Voyiadjis, G.Z., Abu-Farsakh, M.Y. and Tumay, M.T. (1998), "Soil deformations around the piezocone using the coupled theory of mixtures," *Poromechanics a Tribute to Maurice A. Biot*, Proceedings of the Biot Conference on Poromechanics, Louvain-Neuve/Belgium/14-16, Sept, pp.531-536

Voyiadjis, G.Z. and Foroozesh, M. (1990), "Anisotropic distortional yield model," Journal of Applied Mechanics, ASCE, Vol.57, pp.537-547

Voyiadjis, G.Z. and Kattan, P.I. (1989), "Eulerian constitutive model for finite deformation plasticity with anisotropic hardening," Mechanics of Materials, Vol.7, No.4, pp.279-293

Voyiadjis, G.Z. and Kattan, P.I. (1990), "A generalized Eulerian two-surface cyclic plasticity model for finite strains," Acta Mechanica, Vol.81, pp.143-162

Voyiadjis, G.Z. and Kattan, P.I. (1991), "Phenomenological evolution equations for the backstress and spin tensors," Acta Mechanica, Vol.88, pp.91-111

Voyiadjis, G.Z., Kurup, P.U. and Tumay, M.T. (1993), "Preparation of large size cohesive specimens for calibration chamber testing," GTJODJ, Vol.16, pp.339-349

Voyiadjis, G.Z., Kuruup, P.U. and Tumay, M.T. (1994), "Determination of Soil Properties from Laboratory Piezocone Penetration Tests," XIII ICSMFE, New Delhi, pp.303-308

Voyiadjis, G.Z., thiagarajan, G. and Petrakis, E. (1992), "Anisotropic distortional yield model for granular media," Microstructural characterization in constitutive modeling of metals and granular media, ASME-MD32, pp.119-134

Voyiadjis, G.Z., Thiagarajan, G. and Petrakis, E. (1995), "Constitutive modeling for granular media using an anisotropic distortional yield model," Acta Mechanica, 110, pp.151-171

Whittle, A.J. and Aubeny, C.P. (1991), "Pore pressure fields around piezocone penetrometers installed in clay," Proceedings of the 7th International Conference on Computer Methods and Advances in Geomechanics, Cairns, 1, Balkema Pub., Rotterdam, pp.285-290

Wissa, A.E.Z., Martin, R.R. and Galanger, J.E., (1975) "The piezometer probe," Proceedings of ASCE Spec. Conf. on In situ Measurement of Soil Properties, Raleigh, N.C. pp.536-545

Withers, N.J., Howie, J. Hughes, J.M.O. and Robertson, P.K. (1989), "Performance and analysis of cone pressuremeter tests in sands," Geotechnique, Vol.39, No.3, pp.433-454

Yu, H.S. and Houlsby, G.T. (1991), "Finite Cavity Expansion in Dilatant Soils :loading analysis," Discussions of Geotechnique, Vol.42, No.4, pp.649-654

Zhang. Z. and Tumay, M.T. (1999), "Statistical to Fuzzy Approach Toward CPT Soil Classification," Journal of Geotechnical and Geoenvironmental Engineering, Mar. pp. 179-186

Zbib, H.M. (1993), "On the mechanics of large inelastic deformations: kinematics and constitutive modeling," Acta Mechanica, 96, pp.119-138

Zbib, H.M. and Aifantis, E.C. (1987), "The Concept of relative spin and its implications to large deformation theories, Part I: hyperelasticity and vertex-type plasticity," MM Report No.13, MEEM, Michigan Technical University, Houghton, Michigan

Zbib, H.M. and Aifantis, E.C. (1988a), "One the Concept of Relative and Plastic Spins and its Implications to Large Deformation Theories, Part I: Hypoelasticity and Vertex-type Plasticity," Acta Mechanica, Vol.75, pp.15-33

Zbib, H.M. and Aifantis, E.C. (1988b), "On the Concept of Relative and Plastic Spins and its Implications to Large Deformation Theories, Part II: Anisotropic Hardening Plasticity," Acta Mechanica, Vol.75, pp.35-56

Zienkiewicz, O.C. and Pande, G.N. (1977), "Time-dependent multi-laminate model of rocks-A numerical study of deformation andfailure of rock masses," J. of Numerical and Analytical Methods for Geomechanics, 1, 219-247

Zuidberg, H.M., Schaap, L.H.J. and Beringen, F. (1982), "A penetrometer for simultaneous measurement of cone resistance, sleeve friction and dynamic pore pressure," Proceedings, ESOPT II, Amsterdam, Proceedings, Vol. 2, pp.963-970

VITA

Chung Rak Song was born in Young-Joo, Korea, on March 20, 1961. He obtained the Bachelor degree from Yonsei University, Seoul, Korea, at 1984. During his undergraduate program in Yonsei University, he was qualified as the first class civil engineer in Korea at 1983. He obtained the master of science degree from The University of Texas at Austin in soil dynamics at 1986. He served in the Korean military forces, which is a duty of all Korean male, from 1987 to 1988. He worked in many national and international projects while working for the Daewoo Engineering Company in Korea from 1988 to 1996 as a design and field engineer. He obtained PE (professional engineer) qualification at 1993. He published thirty-five articles and one book. He was an invited lecturer for the Korean Geotechnical Society in geotechnical instrumentation area. In August 1996, he joined the graduate program at Louisiana State University and is currently a candidate for the degree of Doctor of Philosophy in Civil Engineering.

DOCTORAL EXAMINATION AND DISSERTATION REPORT

Candidate: Chung Rak Song

Major Field: Civil Engineering

Title of Dissertation: Computational Approach for Determination of The Hydraulic Conductivity of Soils Using Continuous Intrusion Piezocone Penetration Test

Approved:

Major Professor and Chairman

Dean of the Graduate School

EXAMINING COMMITTEE:

CO-CHAIR

Date of Examination:

Aug. 25th, 1999